NASA CONTRACTOR REPORT

NASA CR-275

EFFECT OF MECHANICAL STRAIN ON p-n JUNCTIONS

by J. J. Wortman

Prepared under Contract No. NASr-222 *by*
RESEARCH TRIANGLE INSTITUTE
Durham, N. C.
for

NATIONAL AERONAUTICS AND SPACE ADMINISTRATION • WASHINGTON, D. C. • AUGUST 1965

NASA CR-275

EFFECT OF MECHANICAL STRAIN ON p-n JUNCTIONS

By J. J. Wortman

Prepared under Contract No. NASr-222 by
RESEARCH TRIANGLE INSTITUTE
Durham, N.C.

for

NATIONAL AERONAUTICS AND SPACE ADMINISTRATION

For sale by the Clearinghouse for Federal Scientific and Technical Information
Springfield, Virginia 22151 – Price $4.00

EFFECT OF MECHANICAL

STRAIN ON p-n

JUNCTIONS

Jimmie J. Wortman

ABSTRACT

A theory is developed for the effect of mechanical strain on the electrical characteristics of germanium and silicon p-n junction devices. The model is based on the deformation potential theory of semiconductors which accounts for strain-induced changes in the energy band structure. Changes in the minority carrier densities are found to cause the major changes in the electrical characteristics. The changes in the energy structure and hence the minority carrier densities are shown to depend upon the type of stress applied, with anisotropic stresses causing larger changes than hydrostatic stresses. Equations which are based on the energy changes are developed for the current-voltage characteristics of diodes and transistors under stress.

The results of an experimental investigation are reported. Experiments were carried out on mesa diodes, planar diodes and transistors. The theory is compared with the experimental data and is found to be in good agreement.

ACKNOWLEDGMENTS

The author wishes to thank Dr. R. M. Burger for his guidance and encouragement during the course of this work. He wishes to express his appreciation to Dr. J. R. Hauser for his many helpful discussions and contributions. Thanks are due H. L. Honbarrier and R. R. Stockard for their assistance in the experimental program.

The author is also grateful to the National Aeronautics and Space Administration, Office of Advanced Research and Technology, Washington, D. C., for sponsoring the major portion of this effort under contract No. NASr-222.

Jimmie J. Wortman

CONTENTS

CONTENTS (Con'd.)

LIST OF FIGURES

LIST OF FIGURES (Con'd.)

LIST OF FIGURES (Con'd.)

LIST OF TABLES

LIST OF SYMBOLS

a	lattice spacing (cm)
α	dimensionless band parameter
α	grounded base current gain
A_b	total area minus stressed area on base side of e-b junction (cm^2)
A_e	total area minus stressed area on emitter side of e-b junction (cm^2)
A_{sn}	stressed areas at the edge of the depletion region on the n side of the junction (cm^2)
A_{sp}	stressed area at the edge of the depletion region on the p side of the junction (cm^2)
A_T	total junction area (cm^2)
B_b	stressed area on base side divided by total e-b junction area
B_e	stressed area on emitter side divided by total e-b junction area
c_{ij}, s_{ij}	stiffness, compliance coefficient (cm^2/dyne), (dyne/cm^2)
c.p.	cyclic permutation
δ	energy separation of the "heavy" and "light" hole bands from the split-off band
δ_{ij}	Kronecker delta
Δ_1	energy band in k-space
Δ_2'	energy band in k-space
ΔE	constant (0.5 ev)
ΔE_g	change in the energy gap (ev)
D_p, D_n	hole, electron diffusion coefficient (cm^2/sec)

D_u	deformation potential coefficient (ev)
D_d	deformation potential coefficient (ev)
D'_u	deformation potential coefficient (ev)
E	energy (ev)
E_{ci}	energy of conduction band edge (ev)
E_F	energy of the Fermi level (ev)
E_g	energy gap (ev)
E_i	intrinsic Fermi level (ev)
$E(\bar{k})$	energy as a function of $\bar{k}$ (ev)
E_o	energy under zero strain conditions (ev)
E_t	energy of trap (ev)
E_{V1}	energy of the heavy hole band (ev)
E_{V2}	energy of the light hole band (ev)
E_{V3}	energy of the split-off hole band (ev)
e	hydrostatic strain
e_b	strain on base side of e-b junction
e_e	strain on emitter side of e-b junction
e_n, e_p	position dependent strains at the edge of the depletion region on the n and p sides of the junction
e_s	strain components referred to the crystal axes
$\Gamma'_{25}(j=3/2)$	valence band edge point; "heavy" and "light" holes
$\Gamma'_{25}(j=1/2)$	valence band edge point; split-off band
$\gamma_\nu(e)$	ratio of minority carrier density with strain to that without strain
$\hbar$	Planck's constant ($[6.624/2\pi] \times 10^{-27}$ erg·sec)

H	Hamiltonian (ev)
H_o	Hamiltonian under zero strain (ev)
I	total current (amp)
I_b	base current (amp)
I_{bs}	base current in the stressed region (amp)
I_c	collector current (amp)
I_n	electron current (amp)
I_{no}	electron current under zero strain (amp)
I_p	hole current (amp)
I_{po}	hole current under zero strain (amp)
I_{ne}	electron component of emitter current (amp)
I_{pe}	hole component of emitter current (amp)
I_s	reverse saturation current (amp)
$I_U(e)$	generation-recombination current (amp)
$I_U(o)$	generation-recombination current with zero applied strain (amps)
J_I	"ideal" current density (amp/cm^2)
J_U	generation-recombination current density (amp/cm^2)
$J_U(o)$	generation-recombination current density (amp/cm^2)
J_x, J_y, J_z, J	angular momentum matrices
k	Boltzmann's constant (8.62×10^{-5} ev/°K)
$\bar{k}$	wave vector (cm^{-1})
κ_x	distance of band edge point in k-space as measured from X_1 point, $\kappa_x = -[2\pi a^{-1} - \kappa_x]$, (cm^{-1})

K_1, K_2, K_3	constants
ℓ, m, n	direction cosines
L_p, L_n	hole, electron diffusion length (cm)
m_c	effective mass (gm)
m^*_{ij}	components of effective mass tensor (gm)
$m_{\parallel}$	electron effective mass in parallel direction (gm)
$m_{\perp}$	electron effective mass in transverse direction (gm)
m_o	electron rest mass (9.109×10^{-28} gm)
μ_n	electron mobility (cm^2/volt·sec)
μ_p	hole mobility (cm^2/volt·sec)
m_{V1}	effective mass of heavy holes (gm)
m_{V2}	effective mass of light holes (gm)
m_{V3}	effective mass of split-off band holes (gm)
m^*_V	density of states effective mass of holes (gm)
n	electron density or concentration (cm^{-3})
n_i	intrinsic carrier density (cm^{-3})
n_{io}	zero strain intrinsic carrier density (cm^{-3})
n_p	density of electrons in p-type material (cm^{-3})
n_{po}	zero strain density of electrons in p-type material (cm^{-3})
N	band parameter
p	hole density or concentration (cm^{-3})
p_1, n_1	hole, electron density (cm^{-3})
p_n	density of holes in n-type material (cm^{-3})
p_{no}	zero strain density of holes in n-type material (cm^{-3})
q	electronic charge on an electron (1.602×10^{-19} coul)

R	spreading resistance (ohm)
ρ	resistivity (ohm-cm)
σ	stress ($dyne/cm^2$)
σ	conductivity ($ohm^{-1} \cdot cm^{-1}$)
T	absolute temperature (°K)
ϑ	constant depending on the device (dimensionless)
τ	lifetime (sec)
τ_{no}	lifetime of electrons injected into highly p-type material (sec)
τ_{po}	lifetime of holes injected into highly n-type material (sec)
U	steady state recombination rate (sec^{-1})
V	band parameter
ν	number of conduction minima
V_a	applied voltage (volt)
V_{cb}	collector-base voltage (volt)
V_{eb}	emitter-base voltage (volt)
V_o	built-in junction potential (volt)
W	width of space charge region (cm)
W_n, W_p, W_d	widths of the n, p and depletion region (cm)
$[]_d$	deformation potential coefficient (ev)
$[]_s$	deformation potential coefficient (ev)
$[]_u$	deformation potential coefficient (ev)
$[]'_u$	deformation potential coefficient (ev)

Chapter I

INTRODUCTION

It has been known for some time that large mechanical stresses ($\sim 10^8$ - 10^{11} dynes/cm^2) have a significant effect upon the electrical characteristics of p-n junction devices. Early work treated the effect of hydrostatic pressure upon diodes [1]. It was found that the major effect of a hydrostatic pressure is to change the band gap of the semiconductor. Recent experimental investigations have shown that anisotropic stress has a larger effect upon p-n junction characteristics than does hydrostatic pressure and, in addition, the effects are considerably different [2,3,4,5,6,7,8,9,10]. For example, in Ge diodes hydrostatic pressure causes the reverse saturation current to decrease while anisotropic stress causes it to increase.

A model based upon purely hydrostatic effects is not adequate to explain the experimental results for anisotropic stress conditions. It has been suggested that the phenomenon could result from the creation of generation-recombination levels as a consequence of strain [6]. Another model has been proposed in which the phenomenon is attributed to strain induced changes in the minority carrier lifetime [7]. None of these theories are able to explain the many facets of the phenomenon.

It is the purpose of this work to show that the phenomenon is explained by strain-induced changes in the energy band structure of the

semiconductor. A theoretical model is developed which is based on the distortion of the energy band structure under a general strain condition. Analytical expressions are developed for the current and voltages as a function of a general elastic strain for diodes and transistors. Experimental measurements have been made on a variety of silicon p-n junction devices. These results and the results of other workers in the field are compared with the theory. The theory is in good qualitative agreement with the experimental results.

Chapter II

ENERGY BAND STRUCTURE AND DEFORMATION POTENTIAL THEORY OF Ge AND Si

2.1 Energy Band Structure

Germanium and silicon form single crystals with the diamond cubic structure. The periodicity and the binding energy of the atoms in the crystal lattice impose certain quantum mechanical restrictions on the energy that electrons in the crystal can have [11]. As is the case for all semiconductors, germanium and silicon each have a forbidden energy range (energy gap) separating the valence levels and the conduction levels. It is this energy gap that gives semiconductors the desirable electrical properties which they possess. As will be discussed later, a mechanical deformation of the crystal lattice changes the forbidden gap and thereby changes the electrical properties of the semiconductor.

It is convenient, from quantum mechanical considerations, to describe the energy bands in terms of momentum space (k-space). The energy bands of germanium and silicon are functions of position in k-space. The maximum valence levels and the minimum conduction levels are of interest here since it is these levels that determine the energy gap. The following is a discussion of the unstrained energy structure of Ge and Si. The maximum valence levels occur at k = (000) and the minimum conduction levels occur in the <111> and <100> directions for germanium and silicon respectively.

Figures 1 and 2 are sketches of the band structure of germanium and silicon as a function of $\bar{k}$ for the <111> and <100> directions [12]. The notation used to indicate energy surfaces and k-space points are those adapted from group theory [13].

Germanium has eight conduction minima which lie in the <111> directions and are located at the L_1 point, $k = \Pi a^{-1}(111)$, where a is the lattice spacing. Silicon has six conduction minima which occur in the <100> directions and are located at $k \approx 1.7\Pi a^{-1}(100)$ which is approximately 85% of the distance from k = (000) to $k = 2\Pi a^{-1}(100)$ or the X_1 point. The conduction electrons are located at these conduction minima. The name "many valley" semiconductor is sometimes given to germanium and silicon and is derived from the fact that they have conduction minima in more than one k-space direction. Using this model, n-type Ge is a <111> valley material and n-type silicon is a <100> valley material.

The maximum valence levels, Γ'_{25}, for both germanium and silicon are located at k = (000) and are assigned an energy value of zero for convenience. The Γ'_{25} level is degenerate in energy. Figure 3 shows an expanded view of the levels in Si [14]. As can be seen, there is a slight separation in energy of these bands at k = (000) which results from the two angular momentum quantum numbers j = 3/2 and j = 1/2. The $\Gamma'_{25}(j = 3/2)$ level is itself degenerate at k = (000) and is slightly split for $k \neq (000)$ due to spin orbit coupling. Electron spin resonance experiments have shown that for the $\Gamma'_{25}(j = 3/2)$ level the upper of the bands is slightly different in shape from that of the lower band and as a result the effective masses are different for the two. The upper band gives rise to the so-called "heavy" holes and the lower band the "light" holes. In non-degenerate material the $\Gamma'_{25}(j = 1/2)$ level is usually neglected when performing hole population

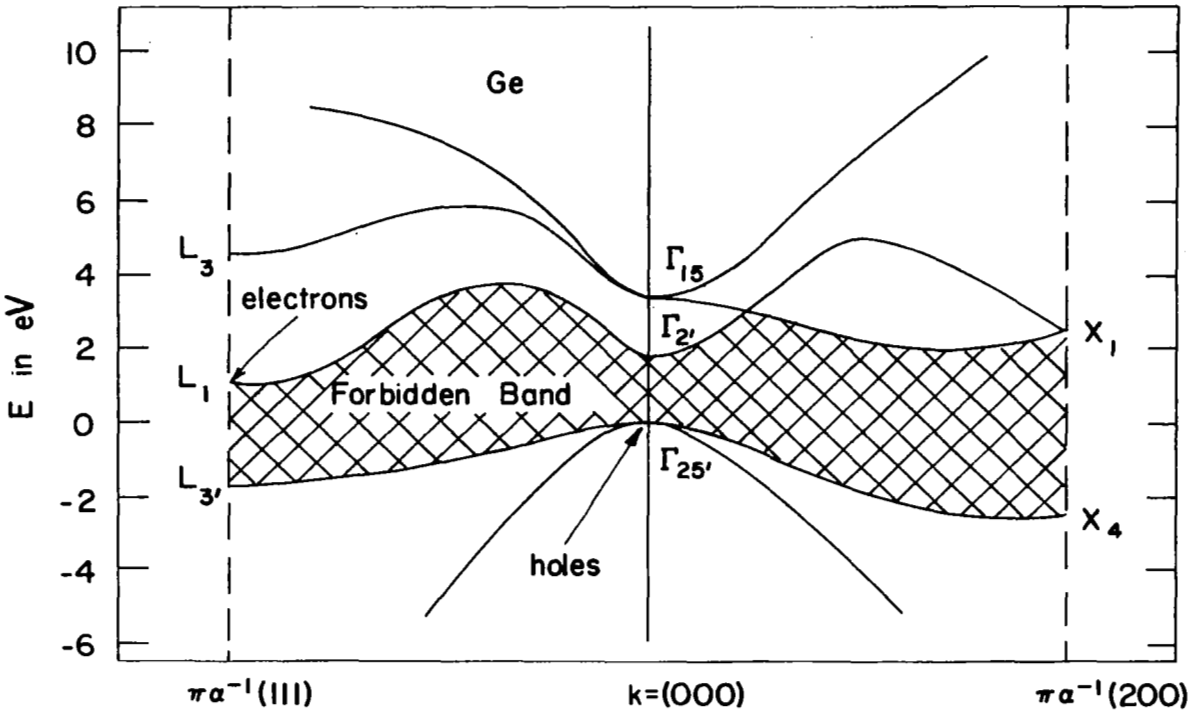

Fig. 1. Energy Band Structure of Germanium for the <111> and <100> Directions in k-space.

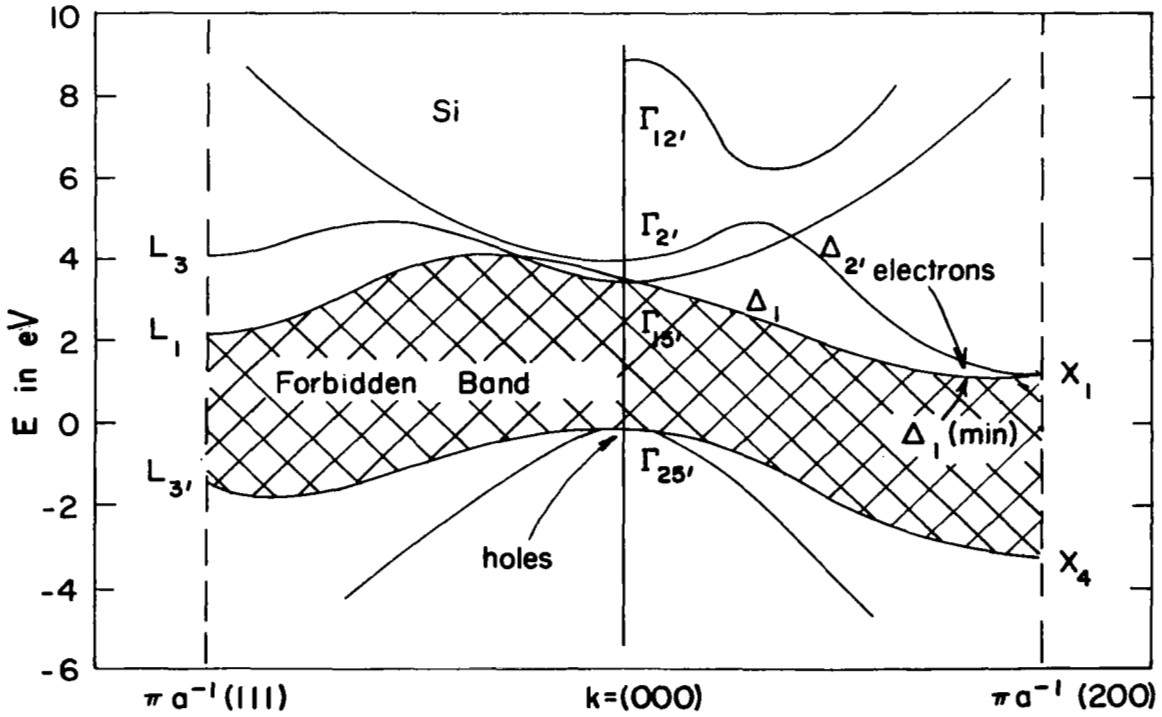

Fig. 2. Energy Band Structure of Silicon for the <111> and <100> Directions in k-space.

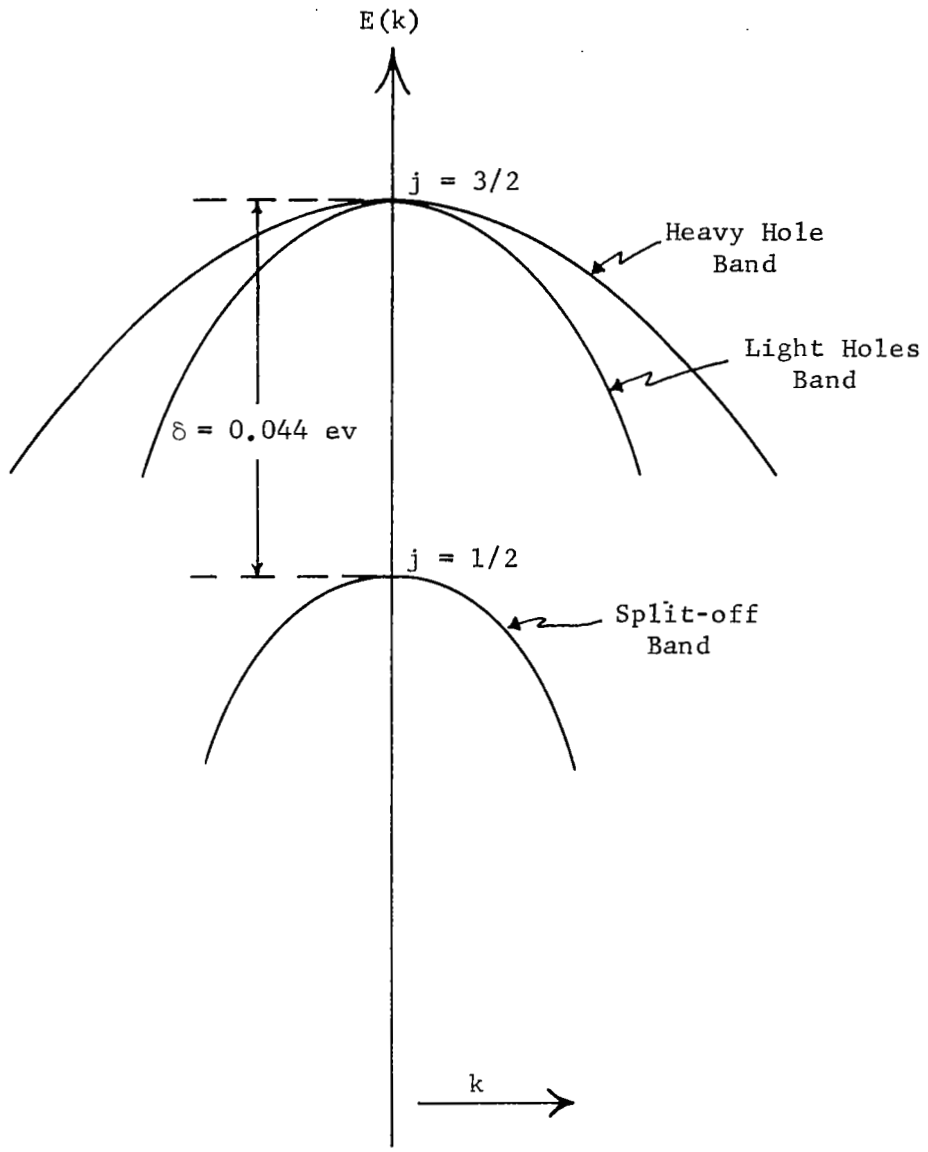

Fig. 3. The Valence Bands of Silicon near $\bar{k} = 0$.

calculations since it is separated in energy from the j = 3/2 bands. This assumption is quite good for germanium while in some cases it may not be a good assumption for silicon.

The points in k-space where the conduction band minima and valence band maxima occur are called band edge points. In the case of the conduction bands for germanium and silicon, if one translates the origin in k-space to the band edge points, constant energy surfaces are found to be ellipsoids

of revolution about the band edge points. Figure 4 is a sketch of the multi-valley energy surfaces for n-type silicon.

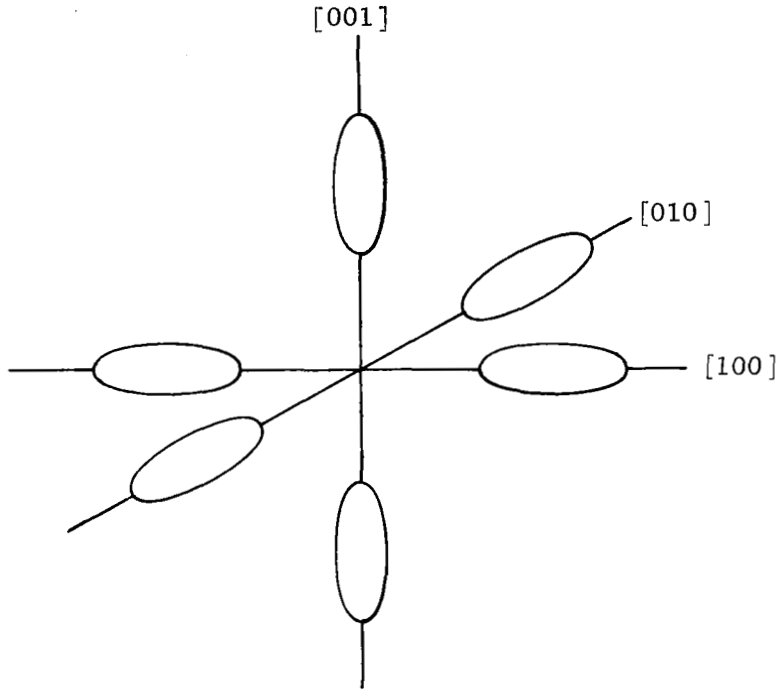

Fig. 4. Multi-valley Energy Surfaces for the Conduction Band of n-type Silicon.

Constant energy surfaces in the valence band are much more complicated due to the degeneracy. Early workers in the field assumed that the surfaces were spherical. Of late, experiment and theory have shown that the surfaces are warped spheres. Figure 5 is a sketch of the cross-section of energy surfaces a constant distance below the origin for silicon. As shown, the heavy and light hole surfaces are quite different.

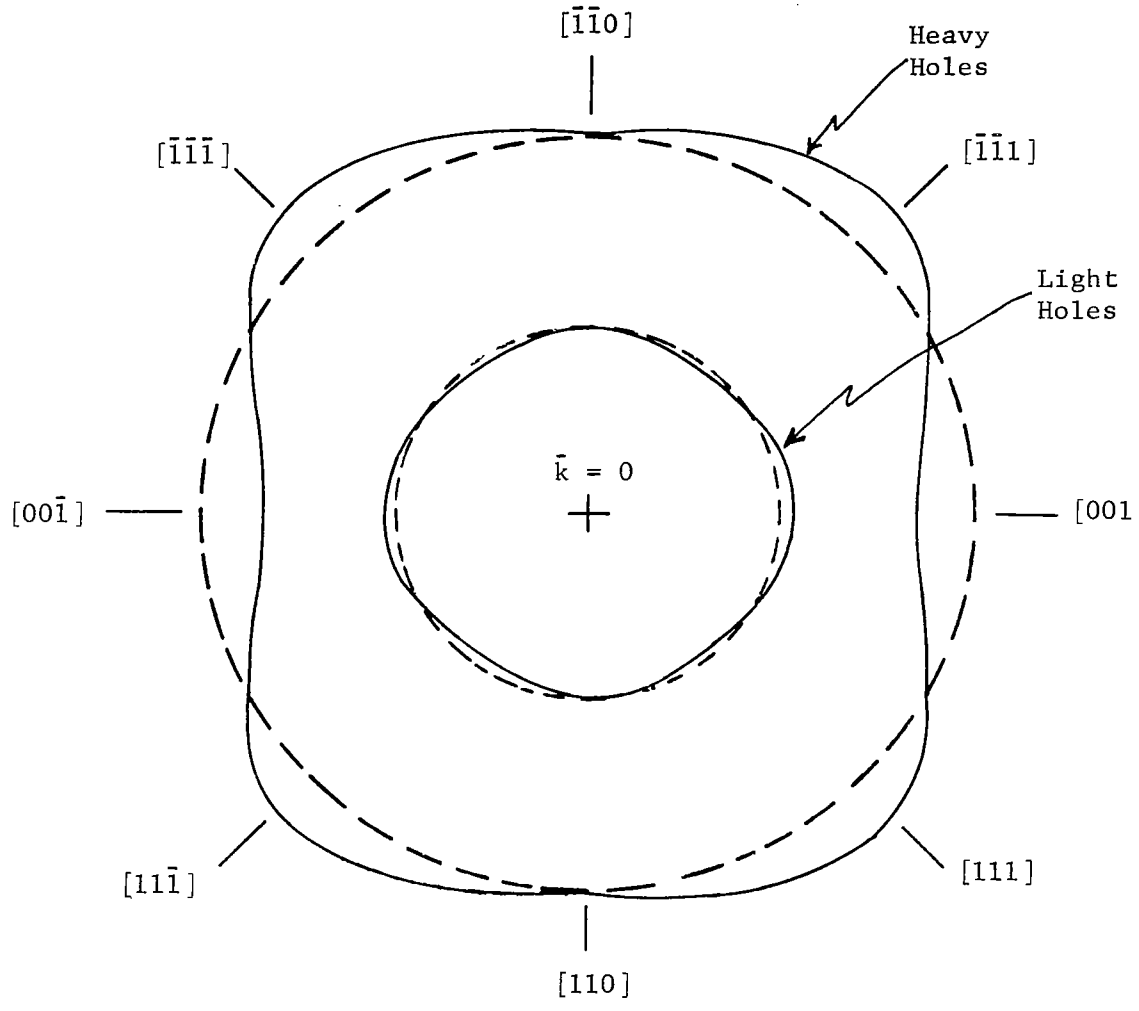

Fig. 5. Cross-section of the Valence Band Energy Surfaces a Constant Distance Below the Origin.

2.2 Deformation Potential Theory

As one might expect, if the crystal is mechanically deformed the periodicity of the lattice will be altered and hence the energy bands will change. Bardeen and Shockley first introduced deformation potential theory in 1950 to explain mobility [15]. In 1955, Herring and Vogt [16] expanded the Bardeen-Shockley theory in formulating their transport theory of

many-valley semiconductors. The deformation potential coefficients, []'s as introduced by Herring and Vogt are defined by

$$E = E_o + \sum_{s=1}^{6} []_s \, e_s \tag{2.1}$$

where E is the energy at the band edge point, E_o is the unstrained energy, and e_s are the strain components indexed in the usual manner (see Appendix A) and referred to the crystallographic axes. Equation 2.1 has since been found to apply in general only for the conduction band of germanium. The discussion to follow considers in some detail the effect of a general strain on the conduction and valence bands of germanium and silicon.

2.2.1 Valence Bands of Ge and Si

Kleiner and Roth [17] have derived the Hamiltonian, H, from symmetry considerations which includes the effect of a homogeneous strain $e_s (s = 1,2,\ldots 6)$, on the valence band edge:

$$H = H_o + D_d(e_1 + e_2 + e_3) + \frac{2}{3} D_u[(J_x^2 - \frac{1}{3} J^2) e_1 + c.p.] + \frac{2}{3} D_u'[\frac{1}{2}(J_y J_z + J_z J_y) e_4 + c.p.] \tag{2.2}$$

where the D's are the deformation potential coefficients, the J's are the 4×4 angular momentum matrices of the hole for $j = 3/2$, and H_o is the zero strain Hamiltonian; D_d is the shift per unit dilatation of the band edge, while $2 D_u$ is the splitting of the band edge induced by uniaxial shear strain along the [001] axis, $2D_u'$ gives the splitting similarly for the [111] axis. Finally, "c.p." means cyclic permutations of x, y, and z referring to the crystallographic axes.

For a Cartesian coordinate system, the conventional representation for the angular momenta for j = 3/2 are [18]

$$J_x = \frac{1}{2}\begin{pmatrix} 0 & \sqrt{3} & 0 & 0 \\ \sqrt{3} & 0 & 2 & 0 \\ 0 & 2 & 0 & \sqrt{3} \\ 0 & 0 & \sqrt{3} & 0 \end{pmatrix}, \quad J_y = \frac{1}{2}\begin{pmatrix} 0 & -\sqrt{3}i & 0 & 0 \\ \sqrt{3}i & 0 & -2i & 0 \\ 0 & 2i & 0 & -\sqrt{3}i \\ 0 & 0 & \sqrt{3}i & 0 \end{pmatrix},$$

$$J_3 = \frac{1}{2}\begin{pmatrix} 3 & 0 & 0 & 0 \\ 0 & 1 & 0 & 0 \\ 0 & 0 & -1 & 0 \\ 0 & 0 & 0 & -3 \end{pmatrix}, \quad J^2 = \frac{15}{4}\begin{pmatrix} 1 & 0 & 0 & 0 \\ 0 & 1 & 0 & 0 \\ 0 & 0 & 1 & 0 \\ 0 & 0 & 0 & 1 \end{pmatrix}. \tag{2.3}$$

Substituting Eq. (2.3) into (2.2) gives

$$H - H_o = \begin{pmatrix} R_1 + R_2 & R_5 - iR_4 & R_3 - iR_6 & 0 \\ R_5 + iR_4 & R_1 - R_2 & 0 & R_3 - iR_6 \\ R_3 + iR_6 & 0 & R_1 - R_2 & -R_5 + iR_4 \\ 0 & R_3 - iR_6 & -R_5 - iR_4 & R_1 + R_2 \end{pmatrix}, \tag{2.4}$$

where

$$\begin{aligned} R_1 &= D_d(e_1 + e_2 + e_3); \\ R_2 &= \tfrac{2}{3} D_u(e_3 - \tfrac{1}{2}[e_1 + e_2]); \\ R_3 &= \tfrac{2}{3} D_u(\tfrac{1}{2}\sqrt{3})(e_1 - e_2); \\ R_6 &= \tfrac{2}{3} D'_u(\tfrac{1}{2}\sqrt{3})\, e_6; \\ R_5 &= \tfrac{2}{3} D'_u(\tfrac{1}{2}\sqrt{3})\, e_5; \\ R_4 &= \tfrac{2}{3} D'_u(\tfrac{1}{2}\sqrt{3})\, e_4. \end{aligned}$$

The allowed energy levels are found by determining the eigenvalues of the Hamiltonian (diagonalizing the Hamiltonian). Mathematically this is done by subtracting the energy, E, from each of the diagonal elements of the Hamiltonian and equating the determinate of the new matrix to zero, i.e. $H - \delta_{ij} E = 0$. Diagonalizing the Hamiltonian for the energy gives

$$E = E_o + R_1 \pm (R_2^2 + R_3^2 + R_4^2 + R_5^2 + R_6^2)^{1/2}$$

or (2.5)

$$\Delta E = E - E_o = D_d(e_1 + e_2 + e_3) \pm \{(\tfrac{2}{3} D_u)^2 (e_1^2 + e_2^2 + e_3^2 - e_1e_2 - e_1e_3 - e_2e_3) + (\tfrac{2}{3} D_u')^2 (e_4^2 + e_5^2 + e_6^2)\}^{1/2} .$$

From Eq. (2.5) it is seen that there is not only a shift of the level due to D_d but also a splitting of the level, due to D_u and D_u', which removes the degeneracy. The separation in energy is twice the square root term of Eq. (2.5). If the net strains multiplying D_u are compressional strains then the + sign of Eq. (2.5) corresponds to the heavy hole band and the - sign corresponds to the light hole band. If the strain is tensional then the ordering of the bands is reversed. For convenience of notation, let the heavy hole band be E_{v1} and the light hole band be E_{v2}. From Eq. (2.5) the changes in these levels for <u>compressional</u> strain are

$$\Delta E_{v1} = D_d e + \{(\tfrac{2}{3} D_u)^2 (e_1^2 + e_2^2 + e_3^2 - e_1e_2 - e_1e_3 - e_2e_3) + (\tfrac{2}{3} D_u')^2 (e_4^2 + e_5^2 + e_6^2)\}^{1/2} \quad (2.6a)$$

and

$$\Delta E_{v2} = D_d\, e - \{(\tfrac{2}{3} D_u)^2 (e_1^2 + e_2^2 + e_3^2 - e_1e_2 - e_1e_3 - e_2e_3) + (\tfrac{2}{3} D'_u)^2 (e_4^2 + e_5^2 + e_6^2)\}^{1/2} \quad . \tag{2.6b}$$

For the sake of completeness the change in the split-off band $\Gamma'_{25}(j = 3/2)$, E_{v3}, is $\Delta E_{v3} = D_d\, e$. Figure 6 is a sketch of the bands for a compressional strain.

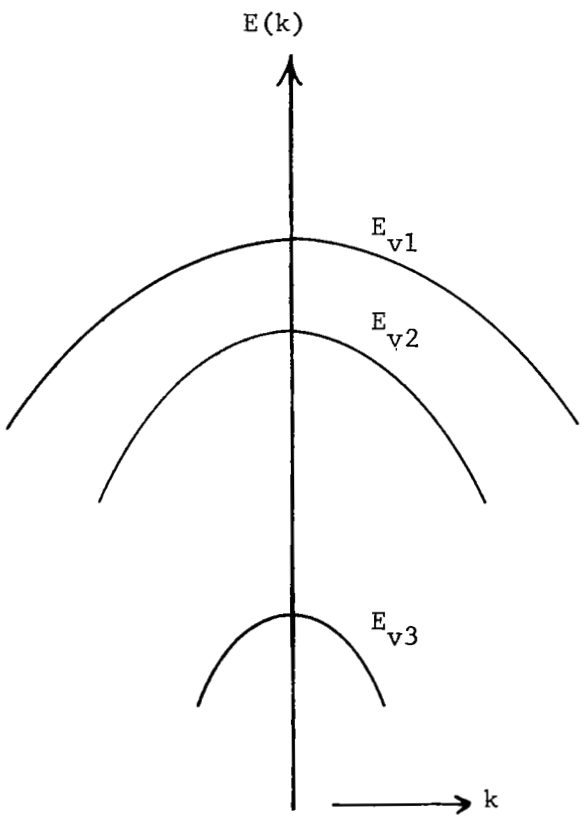

Fig. 6. The Split Valence Bands of Silicon for a Compressional Stress.

2.2.2 Conduction Band of Ge

The effect of strain on the conduction band of Ge has already been mentioned in Sect. 2.2. For the band edge point at $k = \pi a^{-1}(111)$ the shift in energy is

$$\Delta E_{c1} = \sum_{s=1}^{6} [\,]_s \, e_s \,, \tag{2.1}$$

where E_{c1} is used to denote the conduction minimum at $k = \pi a^{-1}(111)$. Symmetry restrictions on the deformation potentials reduce the number of constants to two for germanium, $[\,]_u$ and $[\,]_d$ [16]. Equation (2.1) reduces to

$$\Delta E_{c1} = ([\,]_d + \tfrac{1}{3}[\,]_u)\, e + \tfrac{1}{6}[\,]_u(e_4 + e_5 + e_6) \,, \tag{2.7}$$

where $e = e_1 + e_2 + e_3$. The other seven band edge points in the <111> directions can be obtained by symmetry and will be stated in complete form later.

2.2.3 Conduction Band of Si

The effects of strain on the conduction band minima of silicon are considerably more complicated, due mainly to the fact that the minima are not located at highly symmetrical points in k-space. Strain can have the effect of shifting the band edge point in k-space. Hensel and Hasegawa [19,20] have derived the Hamiltonian as a function of the wave vector $\bar{k}$ and strain e_s for the band edge point lying along the [100] axis. The Hamiltonian is given by

$$H = \begin{bmatrix} (\hbar V \kappa_x + \frac{\hbar^2}{2m_{\|}} \kappa_x^2 + \frac{1}{2m_{\perp}}(k_y^2 + k_z^2) + []_d e + []_u e_1) & []'_u e_4 + N k_y k_z \\ []'_u e_4 + N k_y k_z & (-\hbar V \kappa_x + \frac{\hbar^2}{2m_{\|}} \kappa_x^2 + \frac{1}{2m_{\perp}}(k_y^2 + k_z^2) + []_d e + []_u e_1) \end{bmatrix} \quad (2.8)$$

where $m_{\|}$ and $m_{\perp}$ are the effective masses along the [100] and its transverse directions respectively, V and N are band parameters, κ_x is the [100] component of the wave vector $\bar{k}$ as measured from the symmetry point $X_1(\kappa_x = -[2\Pi a^{-1} - k_x])$ and $[]'_u$ is an additional deformation potential coefficient introduced as a result of symmetry analysis.

Diagonalizing the Hamiltonian and setting $k_y = k_z = 0$ (Eq. 2.8) gives

$$E = \frac{\hbar^2}{2m_{\|}} \kappa_x^2 + []_d e + []_u e_1 \pm [\hbar^2 v^2 \kappa_x^2 + ([]'_u e_4)^2]^{1/2} \quad (2.9)$$

In order to get some feel for the significance of this equation, let the strain be zero. Equation (2.9) then reduces to

$$E = \frac{\hbar^2}{2m_{\|}} \kappa_x^2 \pm \hbar V \kappa_x . \quad (2.10)$$

This now describes the unstrained energy as a function of κ_x. Referring to Fig. 2, this describes the energy bands Δ_1 and Δ'_2 where the positive sign of Eq. (2.10) corresponds to the Δ'_2 band and the negative sign corresponds to the Δ_1 band. The band edge point κ_o is found by differentiating Eq. (2.10) with respect to κ_x and equating the result to zero, i.e. the normal procedure for determining the stationary points of a function. Performing

this operation gives

$$\hbar \kappa_o = - m_{\|} |V| . \tag{2.11}$$

The band edge point under zero strain conditions is $k_o = 0.85(2\pi a^{-1})$. Solving for κ_o gives

$$\kappa_o = - 0.15(2\pi a^{-1}) . \tag{2.12}$$

The energy value separating the two levels (Δ_1 and Δ_2') at the point κ_o as determined by the plus and minus sign of Eq. (2.10) is

$$\Delta E = 2m_{\|} V^2 . \tag{2.13}$$

Returning to Eq. (2.9), the same procedure as that just illustrated can be used to determine the conduction band minimum and the band edge point for a general strain. Taking the derivative of Eq. (2.9) with respect to κ_x and equating the result to zero gives

$$\hbar^2 (\kappa_x)^2_{min} = m_{\|} V^2 - \frac{([]'_u e_4)^2}{V^2} , \tag{2.14}$$

or

$$\hbar^2 (\kappa_x)^2_{min} = \hbar^2 \kappa_o^2 - \frac{([]'_u e_4)^2}{V^2} , \tag{2.15}$$

where $(\kappa_x)_{min}$ is the band edge point under strain. The band edge point, $(\kappa_x)_{min}$, is a function of the shear deformation potential coefficient $[]'_u$ and of the shear strain e_4. Hensel, et. al. [19] have given estimated values of ΔE as 0.5 ev and $[]'_u$ as 5.7 ev. Figure 7 is a plot of $(\kappa_x)_{min}$ as a function of e_4 and has been calculated using the above values of ΔE and $[]'_u$, where $(k_x)_{min} = - [2\pi a^{-1} - (\kappa_x)_{min}]$. Note that $(k_x)_{min}$ increases

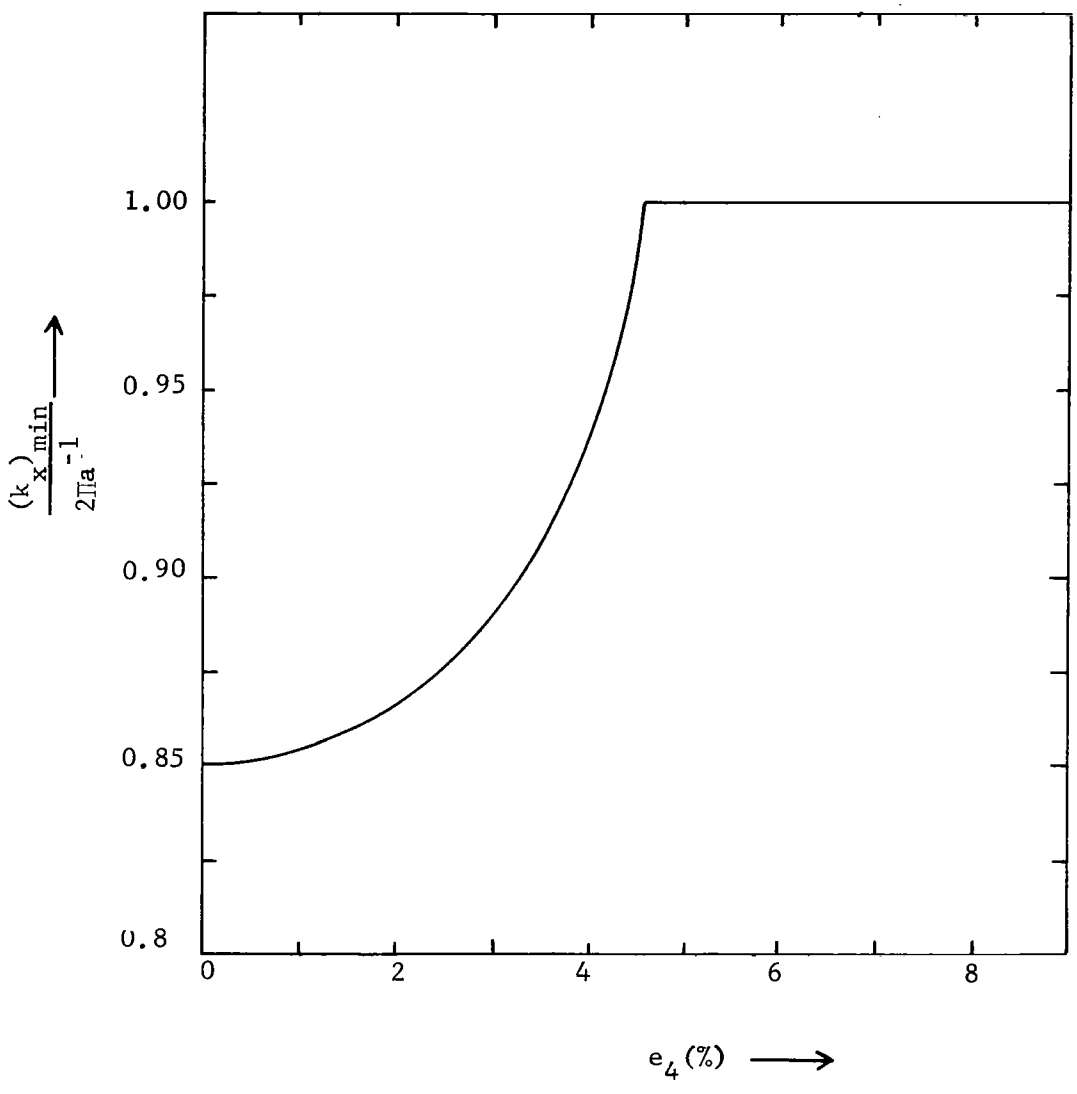

Fig. 7. Variation of the Band Edge Point as Measured from the Origin in the [100]-direction with Respect to the Shear Strain e_4.

with shear strain until it reaches the symmetry point X_1 where it assumes a value of $2\pi a^{-1}$ for larger strains. Once $(k_x)_{min}$ reaches X_1 it can no longer increase due to symmetry restrictions, i.e. $(\kappa_x)^2_{min}$ must be greater than or equal to zero otherwise $(\kappa_x)_{min}$ would be imaginary. The strain level at which $(\kappa_x)_{min} = 0$ is

$$\left|e_4\right| = \frac{\Delta E}{2[]'_u} \tag{2.16}$$

where the bars indicate the absolute magnitude.

Substituting Eq. (2.15) into Eq. (2.9) and evaluating at the band edge point gives

$$E = \frac{\Delta E}{4} - \frac{([]'_u\ e_4)^2}{\Delta E} + []_d\ e + []_u\ e_1 \pm \frac{\Delta E}{2} \cdot \tag{2.17}$$

The positive and negative signs of Eq. (2.17) give the energy of the Δ'_2 and Δ_1 bands respectively at the band edge point as a function of strain. In order to reduce the notation, let E_{ci} be the energy of the conduction band minimum where i = 1, 2, 3. Here 1, 2, 3 represent the [100], [010], [001] directions respectively. The [100] valley minimum is then

$$E_{c1} = -\frac{\Delta E}{4} + []_u\ e_1 + []_d\ e - \frac{([]'_u\ e_4)^2}{\Delta E} \tag{2.18}$$

The above equation is good for strains less than that required to shift the band edge point to X_1, i.e. $\left|e_4\right| \leq \Delta E/(2[]'_u)$. For strain above the critical value $(\kappa_x)_{min}$ is equal to zero. In this case the energy is obtained directly from Eq. (2.9) and is

$$E_{c1} = []_d\ e + []_u\ e_1 - \left|[]'_u\ e_4\right| \cdot \tag{2.19}$$

The magnitude of the energy is not important here but rather the change in the energy with strain. The change in E_{c1} with strain is as follows:

$$\Delta E_{c1} = \begin{cases} []_d\, e + []_u\, e_1 - ([]'_u\, e_4)^2/\Delta E; & |e_4| \le \Delta E/(2[]'_u) \\ []_d\, e + []_u\, e_1 + \frac{\Delta E}{4} - []'_u\, e_4\ ; & |e_4| > \Delta E/(2[]'_u). \end{cases} \tag{2.20}$$

2.2.4 Deformation Potential Coefficients

The deformation potential coefficients have been calculated theoretically by Kleinman, et. al [21, 22, 23]. His calculations are for pure (no impurities) Ge and Si and are based upon a knowledge of the electronic wave functions. Many of the coefficients have been calculated from data taken from piezoresistance and cyclotron resonance experiments. Table I lists both experimental and theoretical values of the coefficients.

There is good reason to believe that the deformation potentials change with doping and type of impurity. Mason and Bateman [24, 25] and Csavinsky and Einspruch [26] have measured the change in the elastic constants of Si for doped samples using ultrasonic pulse techniques. They have been able to estimate the deformation potentials from their measurements, and they find that the shear deformation potential (D'_u) increases with increased doping. Table II shows the results of their measurements. As shown in Table II, it may be possible that D'_u varies considerably. This large uncertainty will, of course, be reflected in later calculations of junction parameters.

Table I

Deformation Potential Coefficients (ev/unit dilation) for Ge and Si. (Kleinman's theoretical values are shown in brackets.)

	Si	Ge
D_d	[-2.09]	[-2.09]
D_u	2.04[a], [3.74]	3.15[b], [3.74]
D'_u	2.68[a], [4.23]	6.06[b], [3.6]
$[]_d$	[-4.99]	[-10.16]
$[]_u$	11[c], 8.3[d], [9.57]	19.2[e], [11.4]
$[]'_u$	5.7[f]	
$D_d - ([]_d + \frac{1}{3}[]_u)$	-1.44[g], [-0.30]	4.82[g], [4.27]

a. J. C. Hensel and G. Feher, Phys. Rev. 129, 1041 (1963).

b. J. J. Hall, Phys. Rev. 128, 68 (1962).

c. D. K. Wilson and G. Feher, Phys. Rev. 124, 1068 (1961).

d. J. E. Aubrey, W. Gubler, T. Henningsen and S. H. Koenig, Phys. Rev. 130, 1667 (1963).

e. H. Fritzche, Phys. Rev. 115, 336 (1959).

f. J. C. Hensel and H. Hasegawa, paper presented at the International Conference on the Physics of Semiconductors, Paris, July 1964, and private communications.

g. W. Paul, J. Phys. Chem. Solids 8, 196 (1959).

Table II

Values of the Shear Deformation Potential Coefficient D_u' for Boron Doped Si as a Function of Doping Concentration

Concentration (cm^{-3})	D_u'(ev)
1.4×10^{16}	8.5[b]
2.5×10^{18}	30[a]
3.2×10^{18}	5.8[b]
1.0×10^{19}	13[c]
1.1×10^{20}	11.8[b]

a. W. P. Mason and T. B. Bateman, "Ultrasonic Attenuation and Velocity Changes in Doped n-type Germanium and p-type Silicon and their use in Determining an Intrinsic Electron and Hole Scattering Time", Phys. Rev. Letters 10, 151, 1 March 1963.

b. P. Csavinsky and Norman G. Einspruch, "Effect of Doping on the Elastic Constants of Silicon", Phys. Rev. 132, 2434 (1963).

c. W. P. Mason and T. B. Bateman, "Ultrasonic Wave Propagation in Doped n-Germanium and p-Silicon", Phys. Rev. 134, A1387 (1964).

2.2.5 Summary

The effects of strain on the conduction minima and valence maxima of Ge and Si have been treated. These calculations have been based on the deformation potential theory of semiconductors. By way of summary, the following equations were obtained which can be used for calculating the change in energy of the valence and conduction band edge points with compressional strain:

Valence Band of Ge and Si

$$\Delta E_{v1} = D_d\, e + \{(\tfrac{2}{3} D_u)^2 (e_1^2 + e_2^2 + e_3^2 - e_1e_2 - e_1e_3 - e_2e_3) + (\tfrac{2}{3} D'_u)^2 (e_4^2 + e_5^2 + e_6^2)\}^{1/2} \tag{2.21}$$

$$\Delta E_{v2} = D_d\, e - \{(\tfrac{2}{3} D_u)^2 (e_1^2 + e_2^2 + e_3^2 - e_1e_2 - e_1e_3 - e_2e_3) + (\tfrac{2}{3} D'_u)^2 (e_4^2 + e_5^2 + e_6^2)\}^{1/2} \tag{2.22}$$

where E_{v1} is the "heavy" hole band and E_{v2} is the "light" hole band.

Conduction Band of Ge

$$\Delta E_{c1} = ([]_d + \tfrac{1}{3}[]_u)\, e + \tfrac{1}{6}[]_u(e_4 + e_5 + e_6)\ , \tag{2.23}$$

$$\Delta E_{c2} = ([]_d + \tfrac{1}{3}[]_u)\, e + \tfrac{1}{6}[]_u(e_4 - e_5 - e_6)\ , \tag{2.24}$$

$$\Delta E_{c3} = ([]_d + \tfrac{1}{3}[]_u)\, e + \tfrac{1}{6}[]_u(-e_4 + e_5 - e_6)\ , \tag{2.25}$$

$$\Delta E_{c4} = ([]_d + \tfrac{1}{3}[]_u)\, e + \tfrac{1}{6}[]_u(-e_4 - e_5 + e_6)\ , \tag{2.26}$$

where E_{c1} is the conduction minimum in the [111] and $[\bar{1}\bar{1}\bar{1}]$ directions, E_{c2} is the minimum in the $[1\bar{1}\bar{1}]$ and $[\bar{1}11]$ directions, E_{c3} is the minimum in the $[1\bar{1}1]$ and $[\bar{1}1\bar{1}]$ directions, E_{c4} is the minimum in the $[11\bar{1}]$ and $[\bar{1}\bar{1}1]$ directions.

Conduction Band of Si

$$\Delta E_{c1} = \begin{cases} []_d\, e + []_u\, e_1 - ([]'_u\, e_4)^2/\Delta E; & |e_4| \le \Delta E/(2[]'_u) \\ []_d\, e + []_u\, e_1 + \dfrac{\Delta E}{4} - []'_u\, e_4\ ; & |e_4| > \Delta E/(2[]'_u) \end{cases} \tag{2.27}$$

$$\Delta E_{c2} = \begin{cases} []_d\, e + []_u\, e_2 - ([]'_u\, e_5)^2/\Delta E; & |e_5| \leq \Delta E/2([]'_u) \\ []_d\, e + []_u\, e_2 + \frac{\Delta E}{4} - []'_u\, e_5\ ; & |e_5| > \Delta E/2([]'_u) \end{cases} \tag{2.28}$$

$$\Delta E_{c3} = \begin{cases} []_d\, e + []_u\, e_3 - ([]'_u\, e_6)^2/\Delta E; & |e_6| \leq \Delta E/(2[]'_u) \\ []_d\, e + []_u\, e_3 + \frac{\Delta E}{4} - []'_u\, e_6\ ; & |e_6| > \Delta E/(2[]'_u) \end{cases} \tag{2.29}$$

where E_{c1} is the conduction minimum in the [100] and [$\bar{1}$00] directions, E_{c2} is the conduction minimum in the [010] and [0$\bar{1}$0] directions, E_{c3} is the minimum in the [001] and [00$\bar{1}$] directions.

Referring to the set of Eqs. (2.23), (2.24), (2.25), (2.26) and to the set (2.27), (2.28), (2.29) it is seen that for a general strain some of the conduction minima increase in energy while others decrease. This means that electrons will populate the lowest minima and depopulate the higher minima. Likewise the valence levels shift relative to each other as shown by Eqs. (2.21) and (2.22). Again the holes will populate the higher energy level. The band gap E_g is defined as the difference in energy between the lowest conduction minimum and the highest valence maximum. For hydrostatic pressure all of the conduction levels shift the same amount. Likewise the valence levels shift together. The shift of E_g with strain is then simply the change in the conduction levels minus the change in the valence levels.

Chapter III

EFFECT OF STRAIN ON JUNCTION PARAMETERS

3.1 Carrier Concentration

Changes in the energy levels, as discussed in Chapter II, cause changes in the carrier concentrations. For non-degenerate material for which Maxwell-Boltzmann statistics apply, the density of electrons n associated with an ellipsoidal energy surface at a band edge point is [27]

$$n = 2(2\pi kT/\hbar^2)^{3/2} m_c^{3/2} \exp[-(E_c - E_F)/kT] \tag{3.1}$$

where m_c is the effective mass of the energy surface, E_c is the energy of the band edge point, and E_F is the Fermi level. If there are ν ellipsoidal energy minima in k-space, the density of conduction electrons is

$$n = 2\left(\frac{2\pi kT}{\hbar^2}\right)^{3/2} \{m_{c1}^{3/2} \exp\left[-\frac{(E_{c1} - E_F)}{kT}\right] + m_{c2}^{3/2} \exp\left[-\frac{(E_{c2} - E_F)}{kT}\right] + \cdots + m_{c\nu}^{3/2} \exp\left[-\frac{E_{c\nu} - E_F}{kT}\right]\} . \tag{3.2}$$

The conduction band of Si has six energy minima in the <100> directions in k-space with equal effective masses while Ge has eight minima in the <111> directions with equal effective masses. Pairs of energy minima are always affected in the same manner by stress so that only three minima need be

considered for Si ([100], [010], and [001] directions) and four for Ge ([111], $[1\bar{1}\bar{1}]$, $[\bar{1}1\bar{1}]$, and $[11\bar{1}]$ directions). Referring to Eq. (3.2), the density of electrons depends on the effective mass, the energy of the particular conduction levels and the Fermi energy of the crystal. The effects of strain on the conduction minima have already been treated. It should be noted that the energy terms enter into the density relationship as an exponential while the effective mass enters as a 3/2 power. The effective mass m_c may change slightly with strain; however, for the present discussion it will be assumed that it remains constant. The validity of this assumption is discussed in detail in Appendix B.

Assuming then that m_c is constant and is the same for each energy minimum, the density of electrons under strained conditions for both Si and Ge can be written as

$$n = n_o \exp[\frac{\Delta E_F}{kT}] \frac{1}{\nu} \{\exp[-\frac{\Delta E_{c1}}{kT}] + \cdots + \exp[-\frac{\Delta E_{c\nu}}{kT}]\} \qquad (3.3)$$

where $\nu = 3$ for Si and 4 for Ge, n_o is the electron density in the unstrained condition, ΔE_F is the change in Fermi level, and the ΔE_c's are the changes in the energy minima of the conduction levels under strain.

The equation for the hole density differs slightly from that for electrons due to the degeneracy of the valence band levels at k = (000). The hole density, p, is

$$p = 2(\frac{2\pi kT}{\hbar^2})^{3/2} \{m_{v1}^{3/2} \exp[-\frac{(E_F - E_{v1})}{kT}] + m_{v2}^{3/2} \exp[-\frac{(E_F - E_{v2})}{kT}] + m_{v3}^{3/2} \exp[-\frac{(E_F - E_{v3})}{kT}]\} \qquad (3.4)$$

where E_{v1} and E_{v2} are the energies of the $\Gamma'_{25}(j = 3/2)$ levels (heavy and light hole bands) and E_{v3} is the energy of the $j = 1/2$ level. It will be assumed here that the $j = 1/2$ level can be neglected compared to the $j = 3/2$ level because it has a smaller effective mass and is lower in energy. The third term in Eq. (3.4) is thereby neglected. (This is a good assumption for Ge while for silicon the error in p will be less than 20%.)

In the unstrained case E_{v1} and E_{v2} are equal so that an effective mass m_v^* can be defined for the combination of the two levels as follows

$$m_v^* = [m_{v1}^{3/2} + m_{v2}^{3/2}]^{2/3} . \tag{3.5}$$

This is the normal hole effective mass. Again it will be assumed that the effective mass of the individual levels do not change with strain (see Appendix B). The hole density under strain becomes

$$p = p_o \left\{ \frac{m_{v1}^{3/2}}{(m_v^*)^{3/2}} \exp\left[-\frac{\Delta E_F - \Delta E_{v1}}{kT}\right] + \frac{m_{v2}^{3/2}}{(m_v^*)^{3/2}} \exp\left[-\frac{\Delta E_F - \Delta E_{v2}}{kT}\right] \right\} \tag{3.6}$$

where p_o is the hole density with zero strain.

Equations (3.3) and (3.6) are valid for either p- or n-type material. In non-degenerate n-type material, with zero applied stress, the electron density is approximately equal to the net donor density. Likewise, in non-degenerate p-type material the hole density is approximately equal to the net acceptor density. The effects of strain on impurity states in Ge and Si are not completely known. For hydrostatic stress, experiment has shown that the changes in impurity ionization energy are negligible compared with band gap changes [28]. Hall has

shown that ionization energy decreases with strain for large <111> uniaxial stresses in Al and In doped Ge [29]. Kohm [30] has also given a theoretical discussion in which it is suggested that the change in ionization energy is second order for shear strains. It will be assumed that shifts in ionization energy of impurities can be neglected and that the majority carrier concentration is independent of strain.

Since both the valence and conduction bands shift with strain, the Fermi level must also shift. This can be seen for p-type material by setting Eq. (3.6) equal to the acceptor density N_a. Since the ionization energy has been assumed to be independent of stress, the hole density remains constant, and

$$\exp[\frac{\Delta E_F}{kT}] = \frac{m_{v1}^{3/2}}{(m_v^*)^{3/2}} \exp[\frac{\Delta E_{v1}}{kT}] + \frac{m_{v2}^{3/2}}{(m_v^*)^{3/2}} \exp[\frac{\Delta E_{v2}}{kT}] \tag{3.7}$$

Substituting Eq. (3.7) into Eq. (3.3) and solving for the minority carrier concentration gives

$$n_p/n_{po} = (1/\nu) \left\{ \frac{m_{v1}^{3/2}}{(m_v^*)^{3/2}} \exp[\frac{\Delta E_{v1}}{kT}] + \frac{m_{v2}^{3/2}}{(m_v^*)^{3/2}} \exp[\frac{\Delta E_{v2}}{kT}] \right\} \times \left\{ \exp[-\frac{\Delta E_{c1}}{kT}] + \cdots + \exp[-\frac{\Delta E_{c\nu}}{kT}] \right\} \tag{3.8}$$

where n_p is the minority carrier concentration with strain and n_{po} is the unstrained minority carrier concentration. If a similar calculation is made for n-type material, it is found that the same expression results for p_n/p_{no} so that the minority carrier density can be written in general as

$$\gamma_\nu(e) = \frac{p_n}{p_{no}} = \frac{n_p}{n_{po}} = (1/\nu)\left\{\frac{m_{v1}^{3/2}}{(m_v^*)^{3/2}}\exp[\frac{\Delta E_{v1}}{kT}] + \frac{m_{v2}^{3/2}}{(m_v^*)^{3/2}}\exp[\frac{\Delta E_{v2}}{kT}]\right\} \times \left\{\exp[-\frac{\Delta E_{c1}}{kT}] + \cdots + \exp[-\frac{\Delta E_{c\nu}}{kT}]\right\} \tag{3.9}$$

The factor $\gamma_\nu(e)$ gives the ratio of minority carrier density under strain to minority carrier density with zero applied strain. For hydrostatic stress Eq. (3.9) reduces to

$$\gamma_\nu(e) = \exp(-\frac{\Delta E_g}{kT}) \tag{3.10}$$

Figures 8 and 9 are plots of $\gamma_\nu(e)$ for Si and Ge respectively as a function of uniaxial compression stresses for several orientations. The uniaxial stresses were calculated as shown in Appendix A. The experimental values of the deformation potentials as shown in Table I and II were used in the calculations. Note in Figs. 8 and 9 that hydrostatic stress causes the minority carrier concentration for Ge to decrease while it causes the minority carrier concentration of Si to increase. Also $\gamma_\nu(e)$ is more sensitive to <100> uniaxial stresses in Si while <111> uniaxial stresses cause larger changes in Ge.

The above treatment of the effect of strain on carrier concentration is based on two assumptions (1) no change in effective mass with strain and (2) no change in ionization energy with strain.

The pn product ($pn = n_i^2$) is an important parameter in semiconductor theory because at equilibrium it remains constant with position in p-n junction devices. It does however change with strain. This can be seen by forming the pn product from Eqs. (3.3) and (3.6)

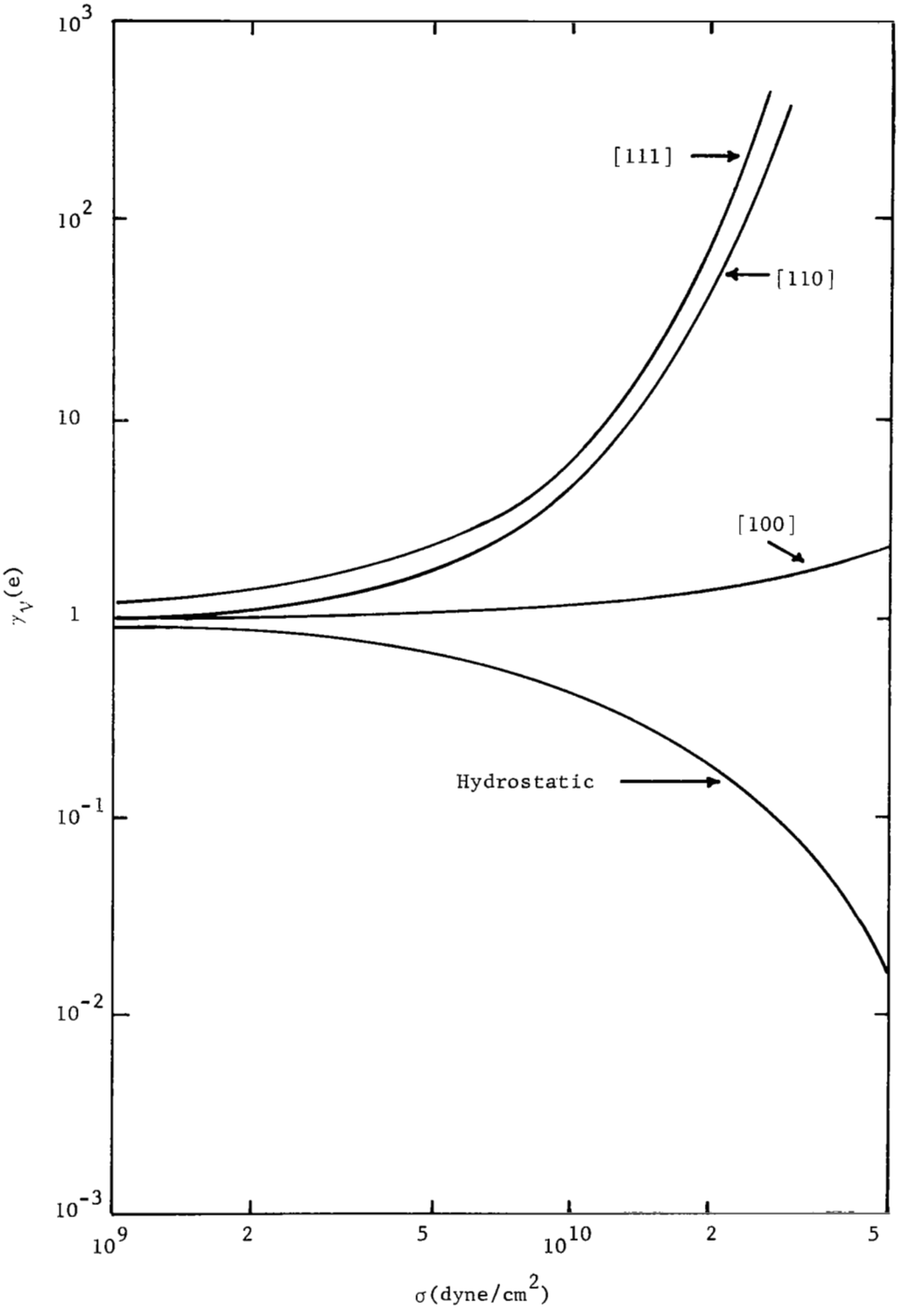

Fig. 8. Ratio of Stressed to Unstressed Minority Carrier Density for Ge as a Function of Stress for Hydrostatic, [100], [110], and [111] Uniaxial Stress.

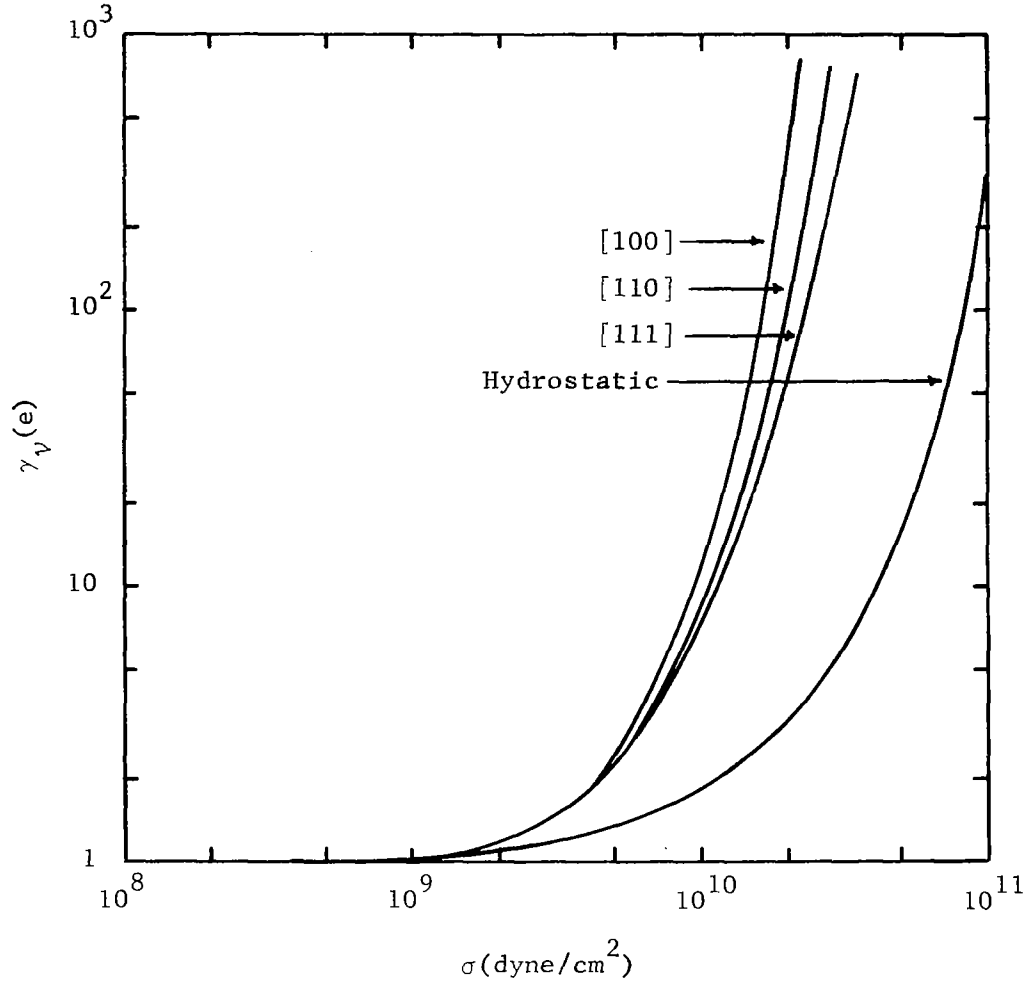

Fig. 9. Ratio of Stressed to Unstressed Minority Carrier Density, $\gamma_\nu(e)$, for Si as a Function of [100], [110], [111] and Hydrostatic Stress.

$$n_i^2 = pn = p_o n_o \gamma_\nu(e) \ . \tag{3.11}$$

Rewriting Eq. (3.11) gives

$$n_i^2 = n_{io}^2 \gamma_\nu(e) \tag{3.12}$$

where n_i is the intrinsic carrier concentration under strain and n_{io} is the intrinsic carrier concentration with zero strain.

3.2 Effect of Strain on the "Ideal" Current Components of p-n Junctions

This section discusses the "ideal" or diffusion currents in p-n junctions as predicted by the Shockley model. Generation-recombination currents are discussed in the following section. The p-n junction model to be discussed is shown in Fig. 10, where A_T is the total junction area, A_{sn} and A_{sp} are the stressed areas at the edges of the depletion region on the n and p sides respectively, W_n, W_p, and W_d are the respective widths of the n region, p region, and depletion region. The hole and electron currents are

$$I_p = \frac{qA_T D_p p_n}{L_p} \coth\left(\frac{W_n}{L_p}\right) \left\{\exp\left[\frac{qV_a}{kT}\right] - 1\right\} \tag{3.13}$$

$$I_n = \frac{qA_T D_n n_p}{L_n} \coth\left(\frac{W_p}{L_n}\right) \left\{\exp\left[\frac{qV_a}{kT}\right] - 1\right\} \tag{3.14}$$

where D_p and D_n are the hole and electron diffusion coefficient, L_p and L_n are the hole and electron diffusion lengths, p_n and n_p are the equilibrium minority carrier densities at the edges of the depletion region on the n and p sides of the junction respectively, and V_a is the junction voltage.

Under stress there are two regions of the junction which must be considered. The current in the unstressed area is given by replacing A_T with $A_T - A_{sn}$ in Eq. (3.13) and $A_T - A_{sp}$ in Eq. (3.14). The current through the stressed areas will be modified by the stress induced changes in the parameters. As shown in Figs. 8 and 9, the minority carrier concentrations change by several orders of magnitude for large strains. It is assumed here that changes in the other parameters are negligible compared to changes in minority carrier densities. This assumption is discussed in Appendix C.

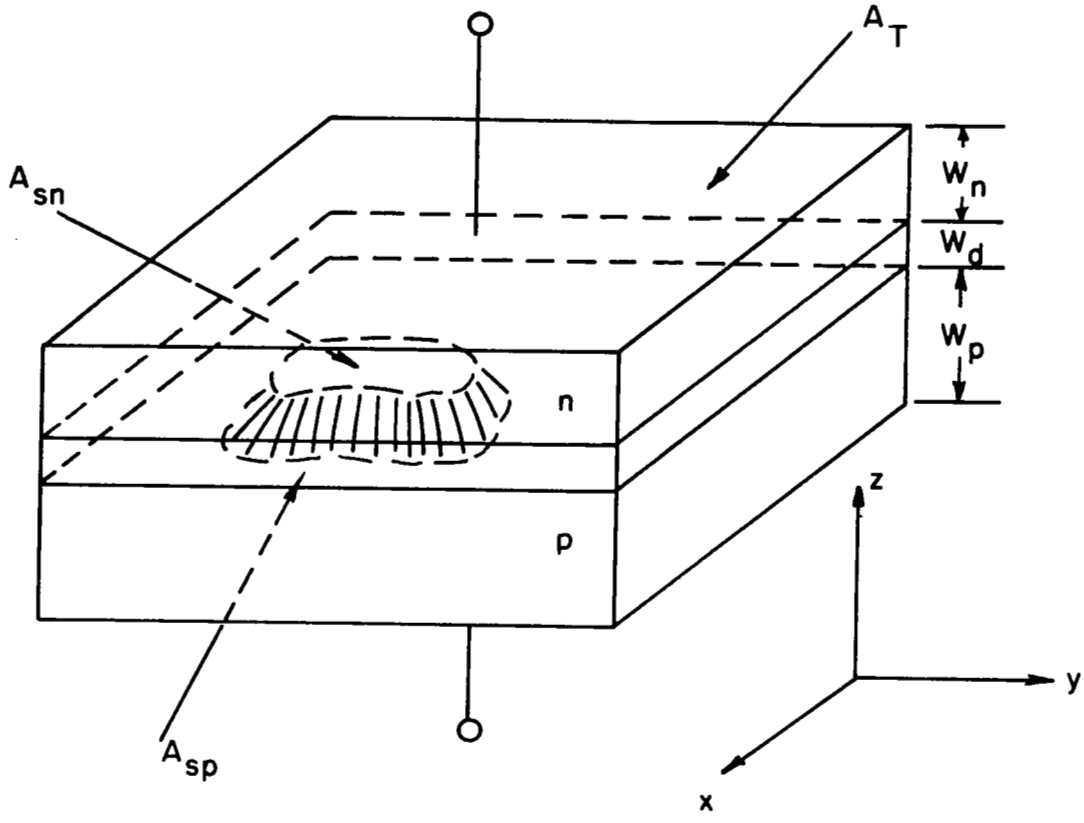

Fig. 10. Stressed p-n Junction Model.

Taking into account the stressed and unstressed regions, the equation for the "ideal" component of diode current can be written:

$$I_s = \frac{I_I}{\exp[\frac{qV}{kT}] - 1}$$

$$= I_{po}\{\frac{A_T - A_{sn}}{A_T} + \frac{1}{A_T}\int_{A_{sn}} \gamma_\nu(e_n)\, dx\, dy\} \qquad (3.15)$$

$$+ I_{no}\{\frac{A_T - A_{sp}}{A_T} + \frac{1}{A_T}\int_{A_{sp}} \gamma_\nu(e_p)\, dx\, dy\}\ ,$$

where I_I is the "ideal" diode current, I_s is the reverse saturation current, e_n and e_p are the position dependent strains at the edges of the depletion region on the n and p sides respectively, and

$$I_{po} = \frac{qA_T D_p p_{no}}{L_p} \coth\left(\frac{W_n}{L_p}\right) ,$$
$$I_{no} = \frac{qA_T D_n n_{po}}{L_n} \coth\left(\frac{W_p}{L_n}\right) . \qquad (3.16)$$

Defining an effective ratio of minority carrier densities as,

$$\bar{\gamma}_\nu(e) \equiv \frac{1}{A_s} \int_{A_s} \gamma_\nu(e)\, dxdy ,$$

Eq. (3.15) reduces to

$$I_s = I_{po}\left\{\frac{A_T - A_{sn}}{A_T} + \frac{A_{sn}}{A_T}\bar{\gamma}_\nu(e_n)\right\} + I_{no}\left\{\frac{A_T - A_{sp}}{A_T} + \frac{A_{sp}}{A_T}\bar{\gamma}_\nu(e_p)\right\} . \qquad (3.17)$$

Two special cases are of interest. The first occurs when the stress is symmetric across the junction, so that $A_{sn} = A_{sp} = A_s$, and $\bar{\gamma}_\nu(e_p) = \bar{\gamma}_\nu(e_n) = \bar{\gamma}_\nu(e)$. Then

$$I_s = [I_{po} + I_{no}]\left[\frac{A_T - A_s}{A_T} + \frac{A_s}{A_T}\bar{\gamma}_\nu(e)\right] . \qquad (3.18)$$

or

$$I_s = I_{so}\left[\frac{A_T - A_s}{A_T} + \frac{A_s}{A_T}\bar{\gamma}_\nu(e)\right] , \qquad (3.19)$$

where I_{so} is the unstrained saturation current.

For hydrostatic pressure the stressed area is equal to the total area and $\gamma_\nu(e) = \exp[-\frac{\Delta E_g}{kT}]$. The reverse saturation current is then

$$I_s = I_{so} \exp[-\frac{\Delta E_g}{kT}] \tag{3.20}$$

For $\frac{\Delta E_g}{kT} \ll 1$, this may be written as

$$\frac{\Delta I_s}{I_s} \approx -[\frac{\Delta E_g}{kT}] \tag{3.21}$$

where ΔI_s is the change in saturation current for a change in band gap of ΔE_g. This equation agrees with the results obtained by Hall, et. al. [31].

The dependence, on temperature, of the current through a stressed diode can be described. Referring to Eqs. (3.16) and (3.17), $\bar{\gamma}_\nu(e_n)$ and $\bar{\gamma}_\nu(e_p)$ as well as the diffusion coefficient, the diffusion lengths, and the minority carrier densities are temperature dependent. For small temperature variations near room temperature, only the changes in carrier density, $\bar{\gamma}_\nu(e_n)$ and $\bar{\gamma}_\nu(e_p)$ need be considered. The carrier densities p_n and n_p are proportional to $\exp[-\frac{E_g}{kT}]$ [32]. For large strains, $\bar{\gamma}_\nu(e) \propto \exp[-\frac{\Delta E_g}{kT}]$ where ΔE_g is of course strain dependent. For the case where the stress is symmetric across the junction and

$$\frac{A_s}{A_T} \bar{\gamma}_\nu(e) >> \frac{A_T - A_s}{A_T}$$

(valid at high stress or when the entire junction is stressed),

$$I \propto \{\exp[\frac{qV}{kT}] - 1\} \exp[-\frac{E_g}{kT}] \exp[-\frac{\Delta E_g}{kT}] . \tag{3.22}$$

If $\frac{qV}{kT} >> 1$

$$\frac{\partial \ell n I}{\partial T} = \frac{1}{kT^2} [E_g + \Delta E_g - qV] , \tag{3.23}$$

and when $\frac{qV}{kT} \ll -1$,

$$\frac{\partial \ell nI}{\partial T} = \frac{1}{kT^2}[E_g + \Delta E_g] \ . \qquad (3.24)$$

As shown in the above equations the slope of ℓnI vs T depends upon the stress through ΔE_g. ΔE_g is negative for uniaxial compressive stresses. Therefore the slope of ℓn I vs T decreases with increasing stress.

The effect of a large stress applied to a small area of a p-n junction is to cause the "ideal" or diffusion current through the small area to increase. For high stress levels the current through the stressed area can become much larger than that through the unstressed area, hence the total diode current is essentially that flowing in the stressed area.

3.3 Effect of Strain on the Space Charge Generation-Recombination Current in p-n Junctions

Space charge generation-recombination current can be important in p-n junctions (particularly in silicon) [33]. This current adds to the "ideal" or diffusion current which is predicted by the Shockley theory. Mechanical strain can cause a change in generation-recombination currents in two ways. First, strain can cause the generation-recombination current to increase by simply increasing the number of generation-recombination centers located in or near the space charge region of a p-n junction. The second way strain can change the generation-recombination current is to shift the relative position of the energy of the trap levels with respect to the conduction and valence levels.

Rindner, et. al. [5,6] have suggested that the first effect, creation of trap centers by strain, is in fact the underlying mechanism responsible for large changes observed in the electrical characteristics of p-n junction

devices when subjected to strains. They argue that the trap levels result as a consequence of dislocations introduced in the crystal by strain. As to whether or not dislocations can be caused by strain, at room temperature, is subject to controversy [34,35]. If dislocations are created by strain they would be expected to remain when the strain is removed--not reversible.

Rindner and Tramposch [34] have performed experiments on germanium in which a diamond needle was used to indent the sample at and below room temperature. The sample was then annealed and etched to exhibit the presence of dislocations. After etching, the samples did in fact contain dislocations in the vicinity of the indention. Craig and Pugh [35] have performed similar experiments on germanium with the exception of the annealing cycle. They found that no dislocations were formed. They conclude that Rindner and Tramposch actually introduced the dislocations during the annealing cycle. It is the opinion of this author that Craig and Pugh are correct in their findings and that the creation of generation-recombination levels with strain is negligible. Even if it were possible to produce the generation-recombination centers, a model based on this effect will not begin to explain the many facets of the phenomenon that have been observed.

The second aspect of generation-recombination currents (change in the relative position of the trap energy with respect to the conduction and valence bands) can be important. The following discussion treats this problem. Hauser [36] has derived an approximate theoretical expression for the current for a single trap level located in the forbidden band. A review of Dr. Hauser's work is given in Appendix E. The space charge generation-recombination current, J_U, is given by:

$$J_U = \frac{qn_i^2 W[\exp\{qV_a/kT\} - 1]}{(\tau_{no}p_1 + \tau_{po}n_1)\left(1 + \frac{[\tau_{no} + \tau_{po}]\, n_i \exp\{qV_a/kT\}}{[\tau_{no}p_1 + \tau_{po}n_1]}\right)} \tag{3.25}$$

where W is the width of the space charge region, V_a is the applied voltage, τ_{no} is the lifetime for electrons injected into highly p-type material, and τ_{po} is the lifetime for holes injected into highly n-type material. The hole and electron densities p_1 and n_1 are given by [33]

$$p_1 = n_i \exp(E_t - E_i)/kT \tag{3.26}$$

$$n_1 = n_i \exp(E_i - E_t)/kT \tag{3.27}$$

where E_t is the energy of the trap level and E_i is the energy of the intrinsic Fermi level. The width of the space charge region, W, is a function of the applied voltage. For a step junction the width is

$$W = W_o(1 - V_a/V_o)^{1/2} , \tag{3.28}$$

where W_o is the width with zero applied voltage and V_o is the built-in junction potential.

To see how the generation-recombination current changes with mechanical strain, each parameter in Eq. (3.25) is analyzed. The intrinsic carrier density has already been discussed in Sect. 3.1. Again it will be assumed that τ_{no} and τ_{po} are strain independent (see Appendix C). The built-in potential is related to the intrinsic carrier concentration by

$$V_o \propto \ell n\left(\frac{N_a N_d}{n_i^2}\right) \tag{3.29}$$

Since changes in V_o are logarithmically related to changes in n_i^2, it will be assumed that V_o and hence W are independent of strain when compared to changes in n_i.

This leaves only p_1 and n_1 to be discussed. They are related to the energy of the trap level as shown by Eqs. (3.26) and (3.27). Unfortunately there is no information available on the effect of strain on E_t. In the absence of this information it is not possible to predict how J_U varies with strain in the reverse biased and low forward biased regions.

For large forward biases J_U is independent of p_1 and n_1. For this case J_U is given by (see Appendix E):

$$J_U = \frac{qn_i W}{\tau_{no} + \tau_{po}} \exp\{qV_a/2kT\} \tag{3.30}$$

Substituting Eq. (3.12) into Eq. (3.30) one finds

$$J_U(e) = J_U(o) \sqrt{\gamma_v(e)} , \tag{3.31}$$

or

$$\frac{I_U(e)}{I_U(o)} = \sqrt{\gamma_v(e)} , \tag{3.32}$$

where $J_U(o)$ is the unstrained generation-recombination current. As shown by the above equations, the generation-recombination current is not as strain sensitive as the ideal current.

Taking into account the stressed and unstressed regions as was done for the "ideal" current, the generation-recombination current is

$$I_U = \left[\frac{A_T - A_s}{A_T} + \frac{A_s}{A_T} \sqrt{\bar{\gamma}_v(e)}\right] I_U(o) . \tag{3.33}$$

It should be noted that it is the strain <u>in the junction</u> that is important here as opposed to the strain at the edge of the depletion region in the ideal current.

3.4 Effect of Stress on Transistor Characteristics

A p-n-p junction transistor model is considered. The equations for the electron and hole components of emitter current are [32]

$$I_{pe} = p_n\{K_1[\exp(\frac{qV_{eb}}{kT}) - 1] + K_2[\exp(-\frac{qV_{cb}}{kT}) - 1]\} \tag{3.34}$$

and

$$I_{ne} = n_p K_3\left\{\exp[\frac{qV_{eb}}{kT}] - 1\right\} \tag{3.35}$$

where K_1, K_2, and K_3 are functions of the device dimensions and material constants, n_p and p_n are the minority carrier densities in the emitter and base respectively, V_{eb} is the emitter-base voltage, and V_{cb} is the collector-base voltage. The minority carrier densities are shown explicitly to indicate the dependence of I_{pe} and I_{ne} on stress. Under normal forward bias transistor operation, $qV_{eb}/kT \gg 1$ and $qV_{cb}/kT \gg 1$. Using these restrictions, the emitter currents under stress conditions similar to those discussed for the p-n junction are

$$I_{pe} \approx I_{po}\{A_b + B_b\,\overline{\gamma}_\nu(e_b)\}\exp\frac{qV_{eb}}{kT}\,, \tag{3.36}$$

$$I_{ne} \approx I_{no}\{A_e + B_e\,\overline{\gamma}_\nu(e_e)\}\exp\frac{qV_{eb}}{kT}\,, \tag{3.37}$$

where $I_{po} = K_1 p_{no}$, $I_{no} = K_3 n_{po}$, $A_b = (A_T - A_{sn})/A_T$, $A_e = (A_T - A_{sp})/A_T$, $B_b = A_{sn}/A_T$, and $B_e = A_{sp}/A_T$.

The base current is

$$I_b = I_{ne} + I_r \equiv I_{ne} + \theta I_{pe}\,, \tag{3.38}$$

since I_r, the total recombination current (bulk and surface), is proportional to I_{pe}. Combining Eqs. (3.36), (3.37) and (3.38) gives for the emitter current, $I_e = I_{pe} + I_{ne}$; base current; and collector current, $I_c = I_e - I_b$:

$$I_e = \exp[\frac{qV_{eb}}{kT}]\{I_{po}[A_b + B_b\ \overline{\gamma}_\nu(e_b)] + I_{no}[A_e + B_e\ \overline{\gamma}_\nu(e_e)]\} \tag{3.39}$$

$$I_b = \exp[\frac{qV_{eb}}{kT}]\{\theta I_{po}[A_b + B_b\ \overline{\gamma}_\nu(e_b)] + I_{no}[A_e + B_e\ \overline{\gamma}_\nu(e_e)]\} \tag{3.40}$$

$$I_c = \exp[\frac{qV_{eb}}{kT}](1 - \theta)\ I_{po}[A_b + B_b\ \overline{\gamma}_\nu(e_b)] \tag{3.41}$$

The forward grounded base current gain α is

$$\alpha = (\frac{\partial I_c}{\partial I_e})_{V_{cb}} = \frac{1 - \theta}{1 + \frac{I_{no}}{I_{po}} \frac{A_e + B_e\ \overline{\gamma}_\nu(e_e)}{A_b + B_b\ \overline{\gamma}_\nu(e_b)}} \tag{3.42}$$

It has been assumed in the preceding equations that the emitter-base voltage is the same for the stressed and unstressed regions. If the stressed region is small compared with the total junction area there can be a significant base spreading resistance associated with the stressed area. In this case the equations becomes:

$$I_e = \{I_{po}[A_b + B_b\ \overline{\gamma}_\nu(e_b)\ \exp(-\frac{qRI_{bs}}{kT})] + I_{no}[A_e + B_e\ \overline{\gamma}_\nu(e_e)\ \exp(-\frac{qRI_{bs}}{kT})]\}\ \exp[\frac{qV_{eb}}{kT}]\ , \tag{3.43}$$

$$I_b = \{I_{no}[A_e + B_e \overline{\gamma}_\nu(e_s) \exp(-\frac{qRI_{bs}}{kT})] + \theta I_{po}[A_b + B_b \overline{\gamma}_\nu(e_b) \exp(-\frac{qRI_{bs}}{kT})]\} \exp[\frac{qV_{eb}}{kT}] , \quad (3.44)$$

$$I_c = I_{po}(1 - \theta)[A_b + B_b \overline{\gamma}_\nu(e_b) \exp(-\frac{qRI_{bs}}{kT})] \exp[\frac{qV_{eb}}{kT}] , \quad (3.45)$$

where R is the spreading resistance and I_{bs} is the base current flowing into the stressed area:

$$I_{bs} = I_{no} B_e \overline{\gamma}_\nu(e_s) \exp[\frac{qV_{eb} - qRI_{bs}}{kT}] . \quad (3.46)$$

The base resistance associated with the unstressed part of the emitter-base junction has been neglected. The inclusion of the spreading resistance term makes the analysis considerably more difficult since a transcendental equation must be solved for I_{bs}; however, the major features are the same as before. Changes in R have been neglected here. The effect of large strains on conductivity are discussed in Appendix D.

All of the equations developed for p-n-p transistors will hold for n-p-n transistors if n and p are interchanged each time they appear.

As an example of the transistor theory, consider a silicon p-n-p transistor with the following parameters:

$$A_T = 5 \times 10^{-5} \text{ cm}^2$$
$$I_{po} = 5 \times 10^{-15} \text{ amp}$$
$$I_{no}/I_{po} = 10^{-3}$$
$$\theta = 2 \times 10^{-2}$$
$$\rho_{base} = 2 \text{ ohm-cm}$$

Let the stress be applied over a circle of diameter $d = 3.56 \times 10^{-4}$ cm. The spreading resistance of a flat circular area is

$$R \approx \frac{\rho_{base}}{2d} = 2800 \text{ ohms} .$$

Case I. Let the stress be applied in the [111] direction to both sides of the emitter-base junction, $e_e = e_b$, $A_{sn} = A_{sp} = 10^{-7}$ cm^2. Figure 11 is a plot of base current I_b as a function of emitter-base voltage V_{eb} for several stress levels. Figure 12 is a plot of collector current as a function of V_{eb} for the same stress levels. As shown by the curves, both I_b and I_c are changed by several orders of magnitude for small changes in stress in the high stress region. The effect of spreading resistance is shown by the convergence of I_b and I_c toward their unstressed value for high applied voltages. The effect of stress on the spreading resistance has been neglected. It would reduce the resistance and thereby cut down on the rate at which the stressed curves converge to the unstressed curves. The larger the spreading resistance the more rapidly the currents converge to their unstressed values. Note that α is not affected by the stress when both sides of the emitter-base junction are stressed Eq. (3.42).

Case II. Assume the same conditions as before except that only the emitter side of the emitter-base junction is stressed $e_e \gg e_b$. Figure 13 is a plot of I_b and I_c as a function of V_{eb} for several stress conditions. Note that I_c is not changed by the stress while I_b is changed. This means that α is changed. In this case, where $\theta > I_{no}/I_{po}$, the base current is not as sensitive to stress as it was for the previous case.

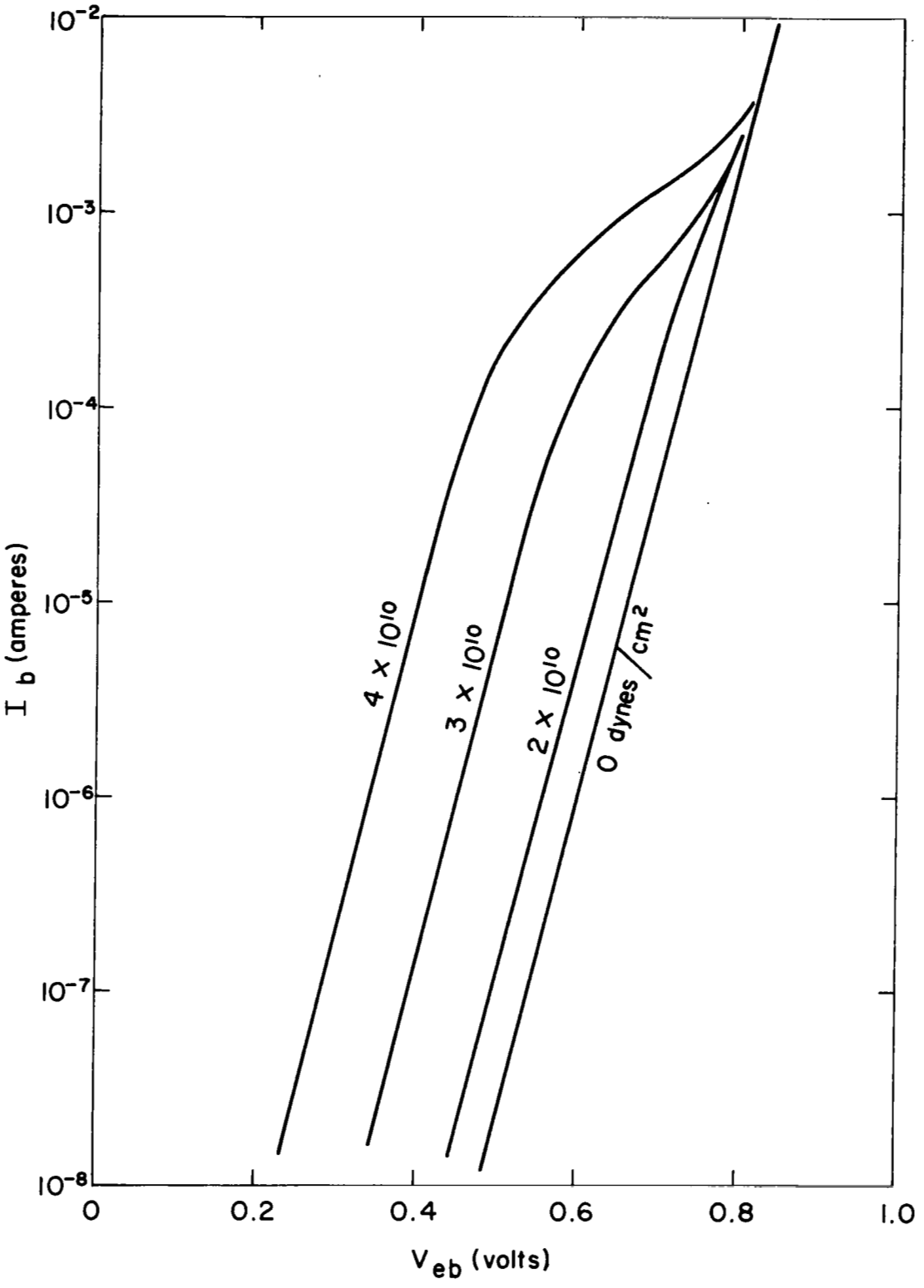

Fig. 11. Effect of Stress on Transistor Base Current for a Symmetrically Stressed Emitter-base Junction.

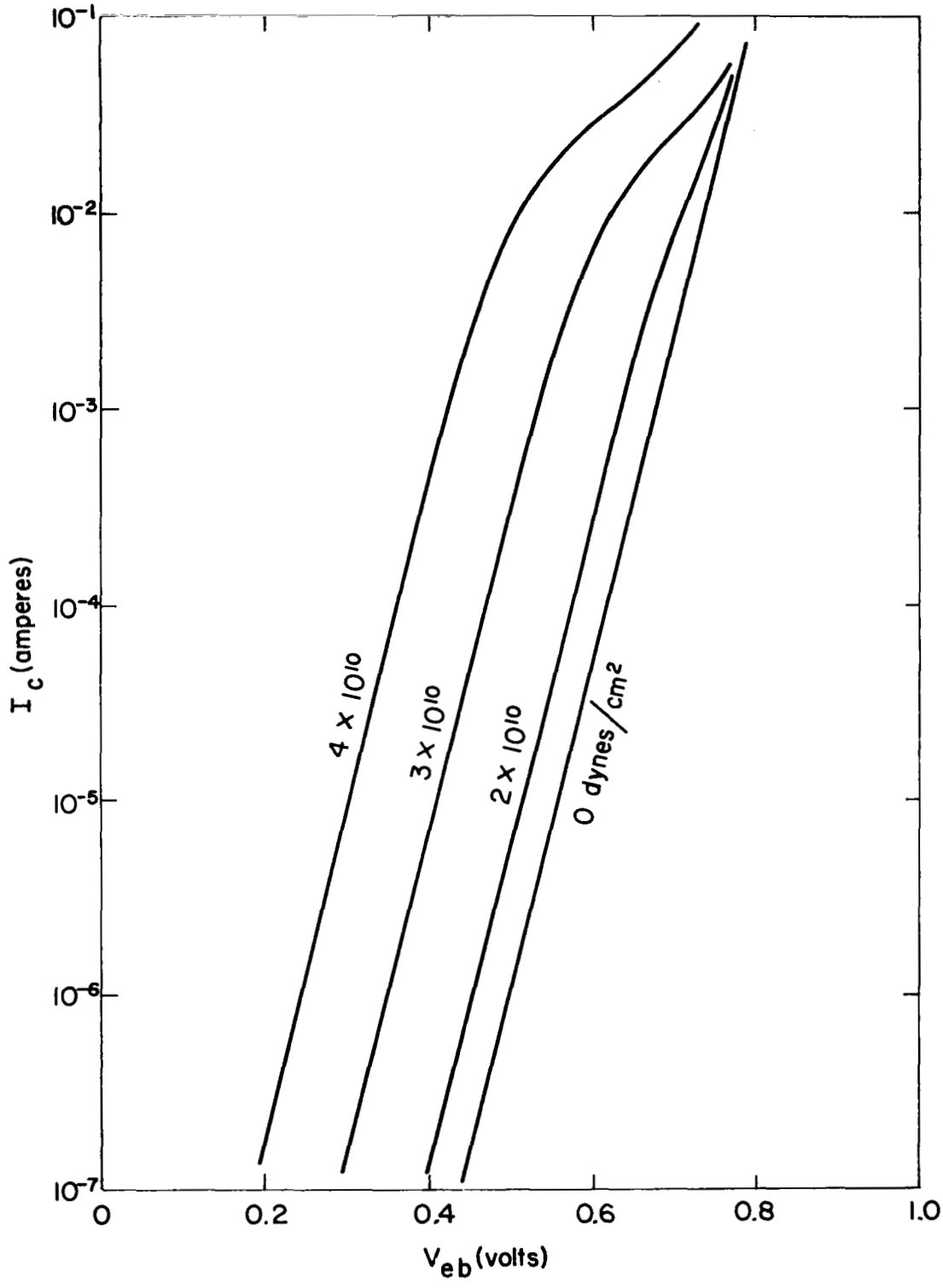

Fig. 12. Effect of Stress on Collector Current for a Symmetrically Stressed Emitter-base Junction.

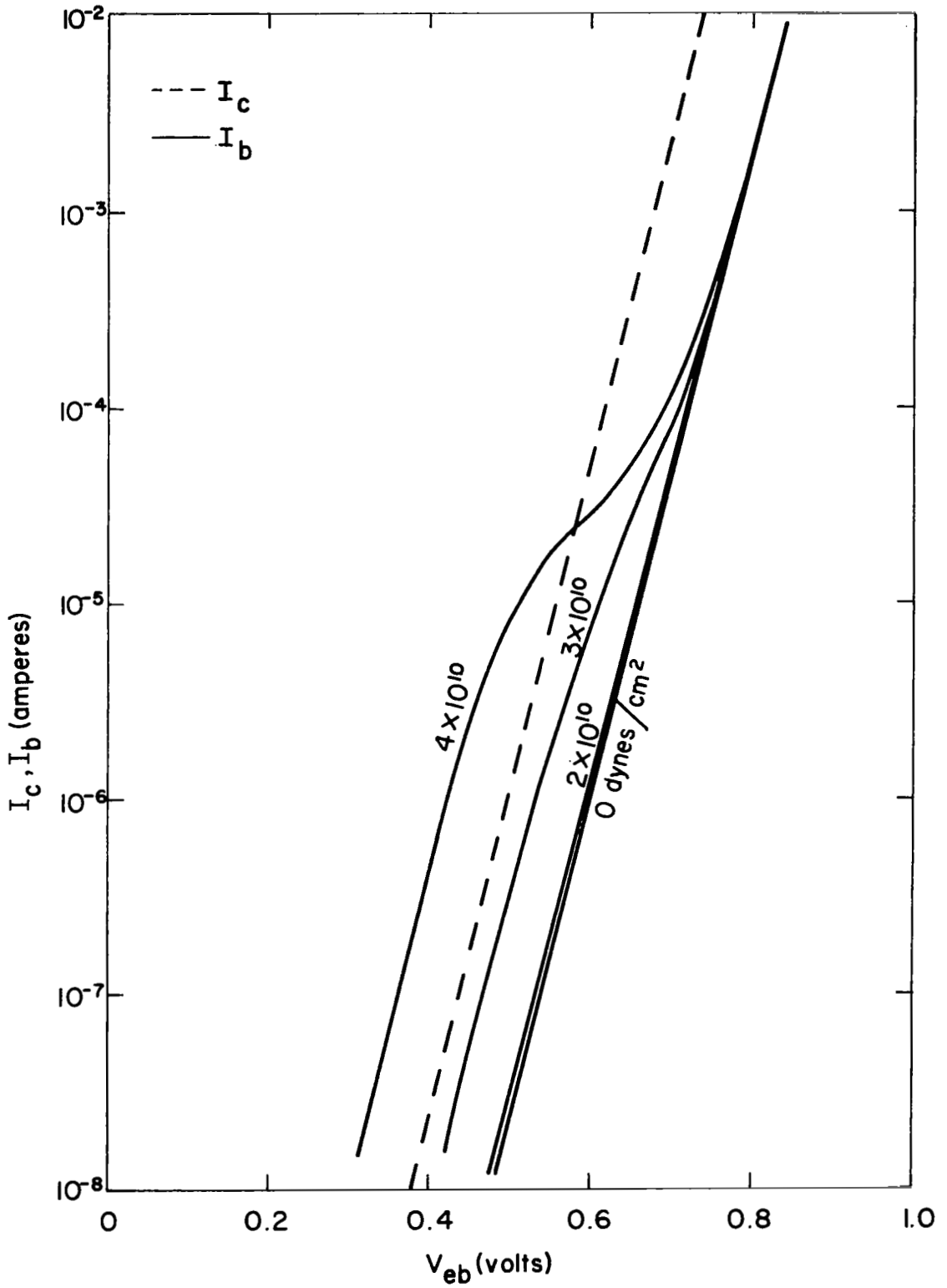

Fig. 13. Collector and Base Current as a Function of Emitter-base Voltage for Several Stress Levels in the Emitter Only.

In Fig. 14, I_c/I_{co} is plotted as a function of stress for constant emitter current and for constant base current, where I_{co} is the collector current with no stress. Spreading resistance was neglected in these calculations. As shown, changes in I_c/I_{co} are larger when the base current is held constant as compared to holding the emitter current constant.

Case III. Assume that the stress is applied only to the base side of the emitter-base junction ($e_e \ll e_b$). Using the assumed transistor parameters in Eqs. (3.42) and (3.44) it can be shown that α and I_b will remain approximately constant. However, in devices where θ is very small compared to I_{no}/I_{po} (Ge for example) the base current can change significantly depending upon the ratio of I_{no}/I_{po}. For constant base current, the collector current is constant.

These examples are not intended to be a complete analysis of the many implications of the preceding theory of stressed transistors but are intended to illustrate some of its salient features.

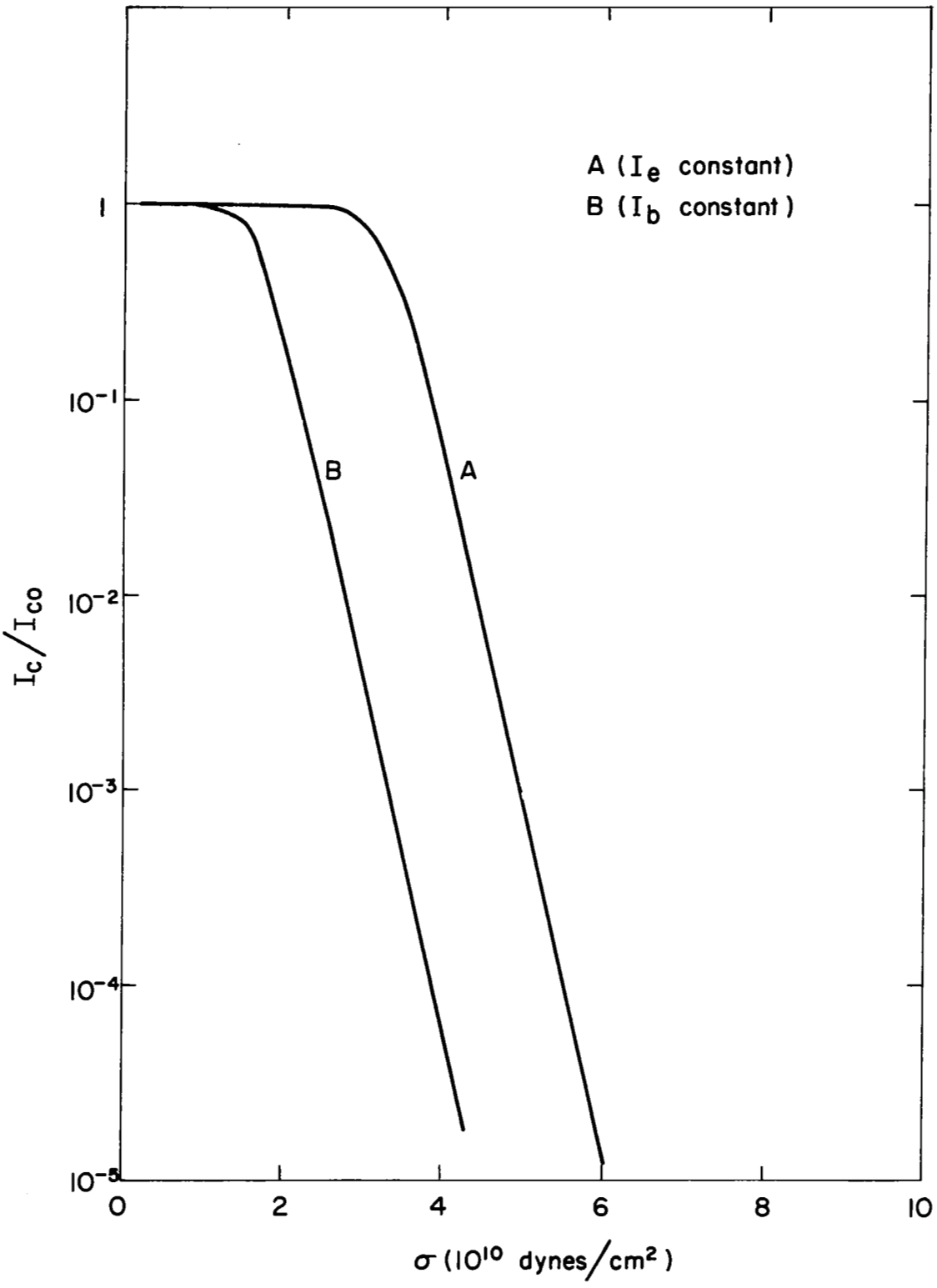

Fig. 14. Effect of Stress on Normalized Collector Current for Constant Emitter Current and for Constant Base Current. Stressed only in the emitter.

Chapter IV

EXPERIMENTAL

4.1 Introduction

A variety of experimental measurements have been made both on silicon diodes and silicon transistors in order to determine the effect of large anisotropic stresses on the electrical characteristics of the devices. While most of the test devices were fabricated in the laboratory, some were obtained from commercial sources. The devices fabricated in the laboratory were designed specifically to allow measurements to be made which would delineate the effect on the piezojunction phenomenon of such parameters as crystal orientation, junction depth, material resistivity. The object of the experimental work has been to understand the phenomenon better and to check the applicability of the theory.

4.2 Experimental Apparatus

An experimental test station was built and calibrated. The primary purpose of this apparatus was to apply a known mechanical stress to a semiconductor junction device and to measure the appropriate electrical parameters under various stress conditions. To obtain the large mechanical stress necessary to change the electrical characteristics of the devices,

it was necessary to restrict the stressed area to less than ten square mils in order to work with practical forces, 0 to 10^5 dynes. This was accomplished in all cases by using either a steel, sapphire or diamond phonograph needle.

Figure 15 is a schematic diagram of the stressing apparatus. Figure 16 is a photograph of the test station. The needle or indentor point which was used to apply the stress to the device was mounted near the end of a phonograph pick-up arm in much the same mannner as that normally used in a phonograph system. A dc solenoid was attached to the stationary part of the pick up arm a short distance from the pivot point of the arm. The plunger of the solenoid was attached to the arm. This arrangement permitted a continuous force range of 0 to 10^5 dynes by simply varying the current supplied to the solenoid. The force was calibrated in terms of the solenoid current. The device to be tested was mounted under the needle on a precision

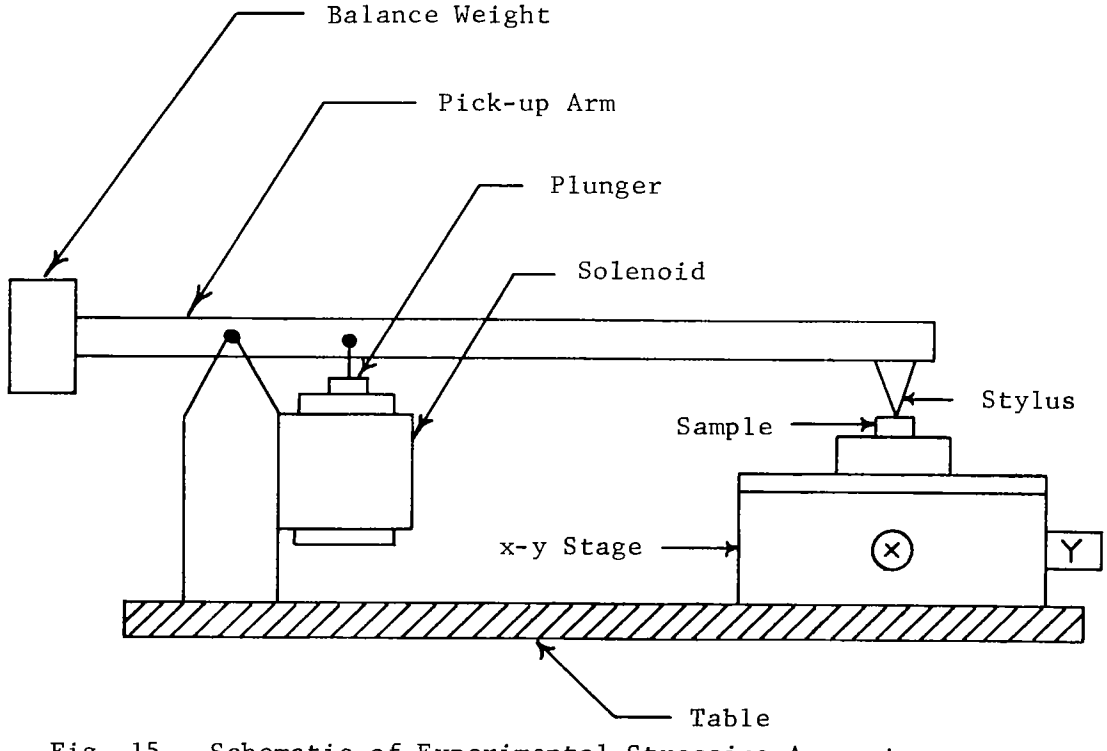

Fig. 15. Schematic of Experimental Stressing Apparatus.

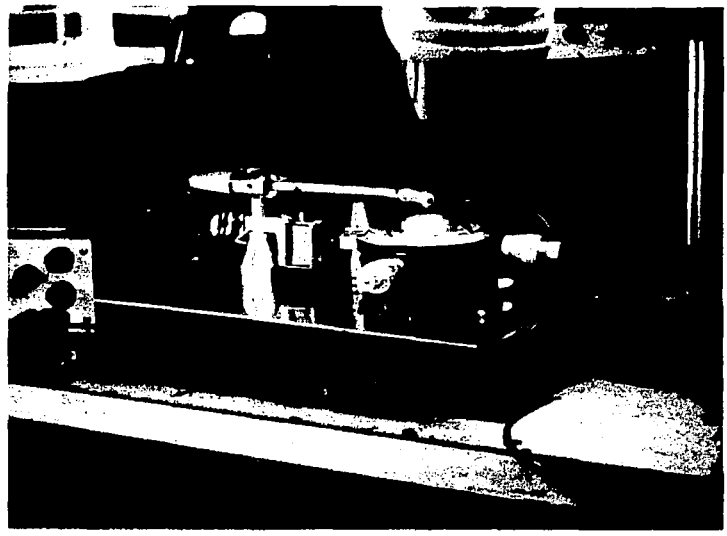

Fig. 16. Photograph of Experimental Stressing Device.

x-y stage. Due to the small size of the devices under test it was necessary to perform the alignment between the device and needle under a microscope.

The electrical current, voltage and current-voltage characteristics as a function of stress were the parameters of interest. The current range of interest covered about four to eight orders of magnitude. Most of the data taken on the devices were recorded directly on an x-y recorder. In order to cover the large current range a circuit was constructed which allowed the x-y recorder to plot the natural logarithm of current as a function of either voltage or solenoid current. An "ideal" diode (one in which the current through the device is proportional to the exponential of the voltage across the junction) was used as the logarithm element. The diode used was the emitter-base junction of a Texas Instrument 2N1711 planar transistor in which the base and collector leads were connected together. Figures 17 and 18 are schematic drawings of the test arrangement used for measuring the I-V characteristics of diodes and transistors under stressed conditions.

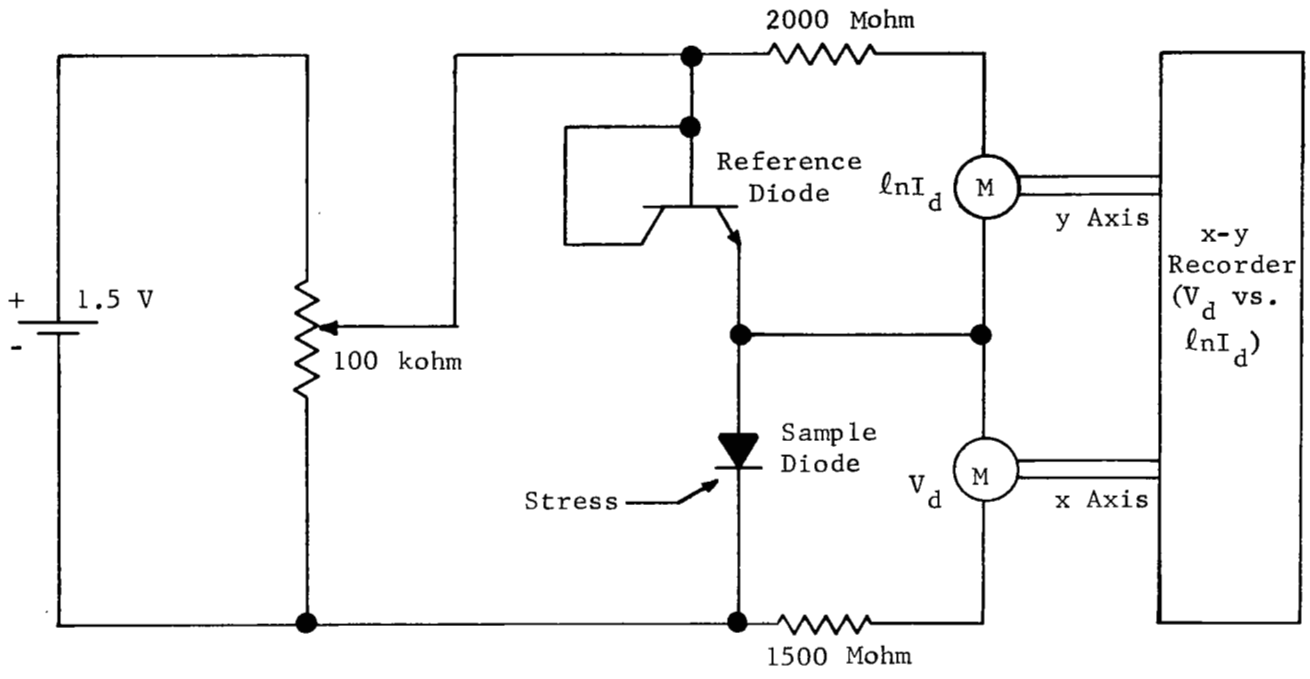

Fig. 17. Schematic of Diode Test Circuit.

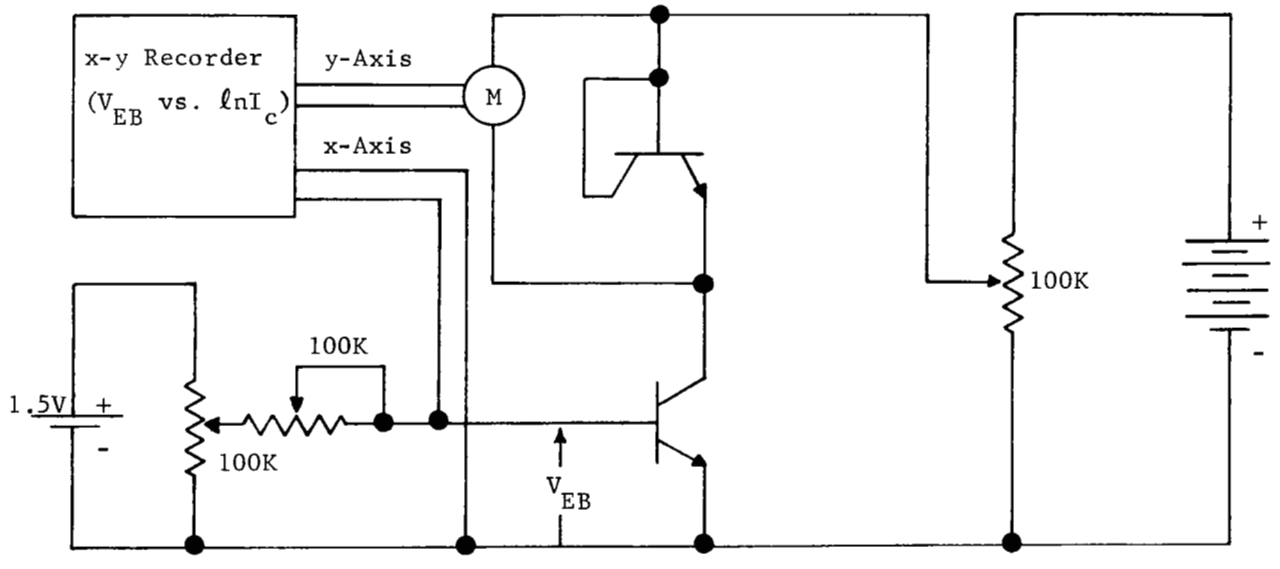

Fig. 18. Schematic of Transistor Test Circuit.

4.3 Mesa Diodes

Mesa diodes were fabricated in the laboratory by diffusion and photolithographic techniques. Figure 19 is a sketch of the mesa structure that was used. Diodes were formed on a variety of different silicon wafers in which the resistivity, junction depth and orientation were varied. Mechanical stress was applied to the diodes by a steel post (a needle whose radius of curvature was much greater than the diameter of the diode). The steel post was also used to make electrical contact to one side of the diode.

A typical set of forward biased current-voltage characteristics of a mesa diode for different stress levels is shown in Fig. 20. The diode was fabricated on a 0.01 ohm-cm crystal with a (100) orientation. The junction depth was approximately 3 microns and the diode diameter was 42 microns.

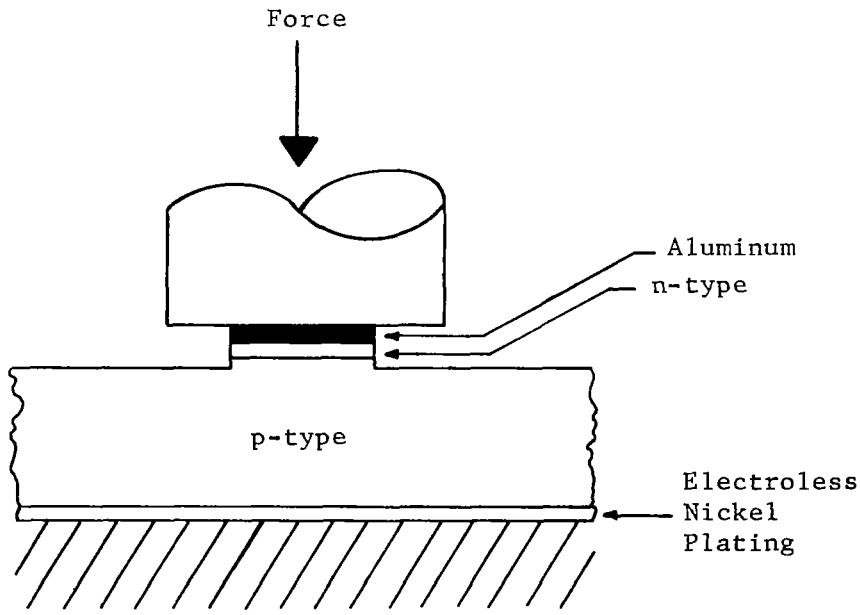

Fig. 19. Sketch of Mesa Diode Structure.

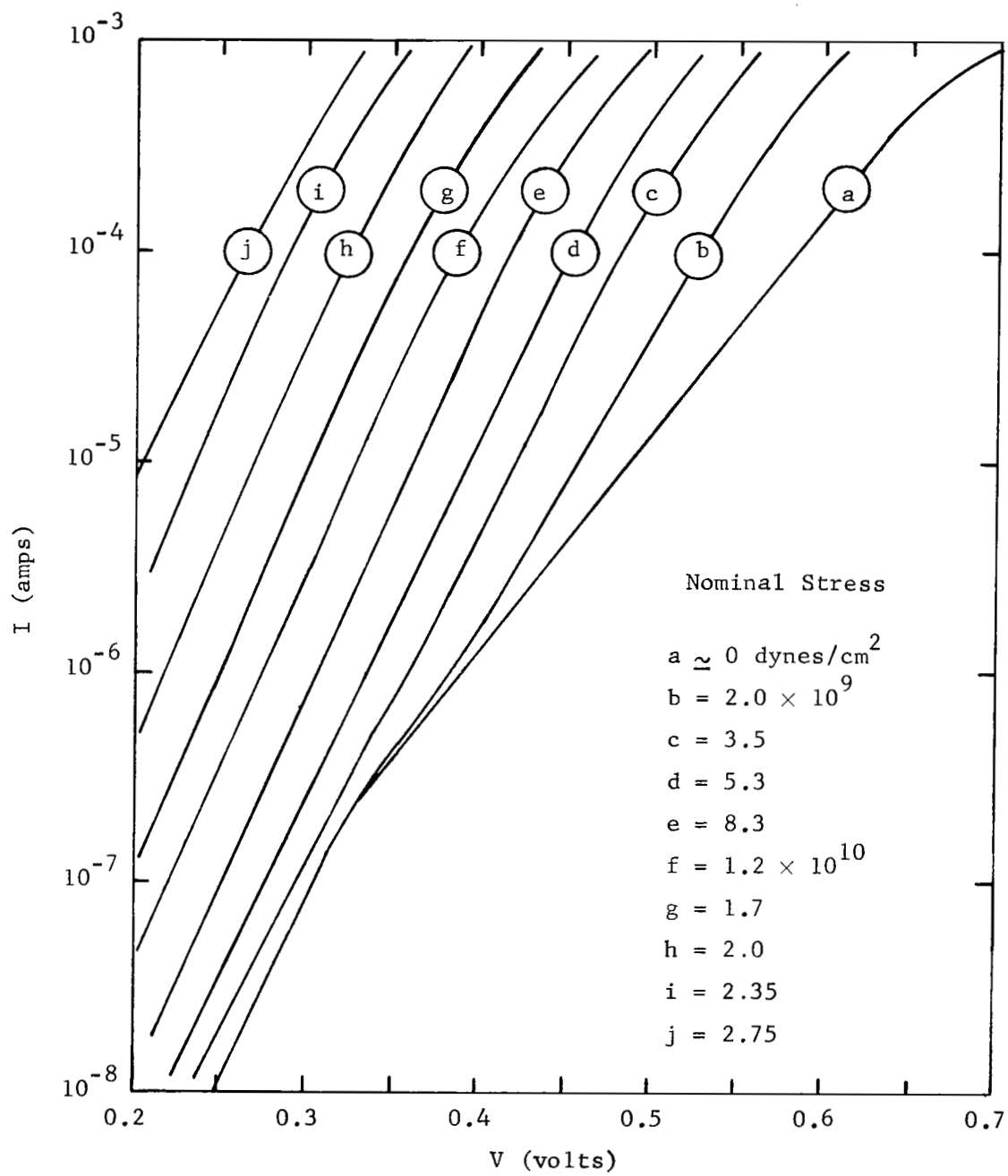

Fig. 20. Current vs Forward Voltage Characteristics of a Mesa Diode Under Various Stress Levels.

There are several significant features of the characteristics as shown in Fig. 20. For voltages below 0.3 volts, all of the curves have the same slope, qV/kT, where kT $\simeq$ 0.026 ev at room temperature. For low stress levels and voltages above 0.3 volts the slopes of the curves are functions of stress. In the latter case where the stress is zero, the slope is approximately qV/2kT. As stress is increased the slopes again approach a constant of qV/kT.

The change in the slope of the I-V characteristics can result from either the "ideal" or generation-recombination components or both. Considering first the "ideal" component, the slope of the I-V characteristics can change from qV/kT at low injection levels to a qV/2kT at high injection levels. The voltage at which high injection takes place for 0.01 ohm-cm crystal resistivity is approximately 0.65 volts. Since the slope change in the diode occurs at approximately 0.3 volts, high injection can be eliminated. Turning to the generation-recombination component of current it is seen from Eq. (3.25), neglecting the change in junction width as a function of voltage, the I_U can have a slope change from qV/kT at low voltages to a qV/2kT at higher voltages.

From Chapter III it is seen that the "ideal" component increases in magnitude in proportion to $\gamma_\nu(e)$ with increasing stress and that the generation-recombination component increases in proportion to $\sqrt{\gamma_\nu(e)}$ with increasing stress. Stress then has the effect of amplifying the "ideal" component more than the generation-recombination component. In light of the above discussion, if the unstressed current is essentially generation-recombination current, then as stress is increased the "ideal" component becomes increasingly important and at higher stress levels the "ideal" component dominates the total

current. The "ideal" component has the qV/kT slope. The theory is therefore consistent with the experimental data.

Current-stress characteristics of the diode just discussed for several voltages are shown in Fig. 21. These curves are essentially $\gamma_v(e)$ since $\gamma_v(e) \simeq I(e)/I(o)$. Comparing the data in Fig. 21 with that shown in Fig. 9 for $\gamma_v(e)$ which was calculated theoretically it is seen that there is excellent agreement. A large number of samples were tested in order to determine experimentally the parameter $\gamma_v(e)$ as a function of stress. Contrary to the above good agreement with the theoretical dependence of $\gamma_v(e)$ on stress, it was found experimentally that $\gamma_v(e)$ had the same general characteristics as the theoretical but in most cases the magnitude of the force required to give the same value of $\gamma_v(e)$ was lower than the theoretical value and varied from sample to sample. This variation was found with samples made on the same crystal at the same time and stressed with the same needle. Figure 22 shows an example of this variation for two diodes on the same crystal.

The large variation in $\gamma_v(e)$ as a function of stress is expected since $\gamma_v(e)$ is exponentially related to stress. The nominal stress in the present experiments was calculated from measurements of force and diode diameter. The data indicate that the actual or effective stress varies from sample to sample. This probably results from variations in the area over which the force acts. This is believed to result from a non-uniform or rough surface on the diode and from the non-linearity of $\gamma_v(e)$ vs e. Since the junctions are very close to the surface of the diode (0.5 - 10 microns), a rough diode surface would cause uneven stress to be set up in the junction.

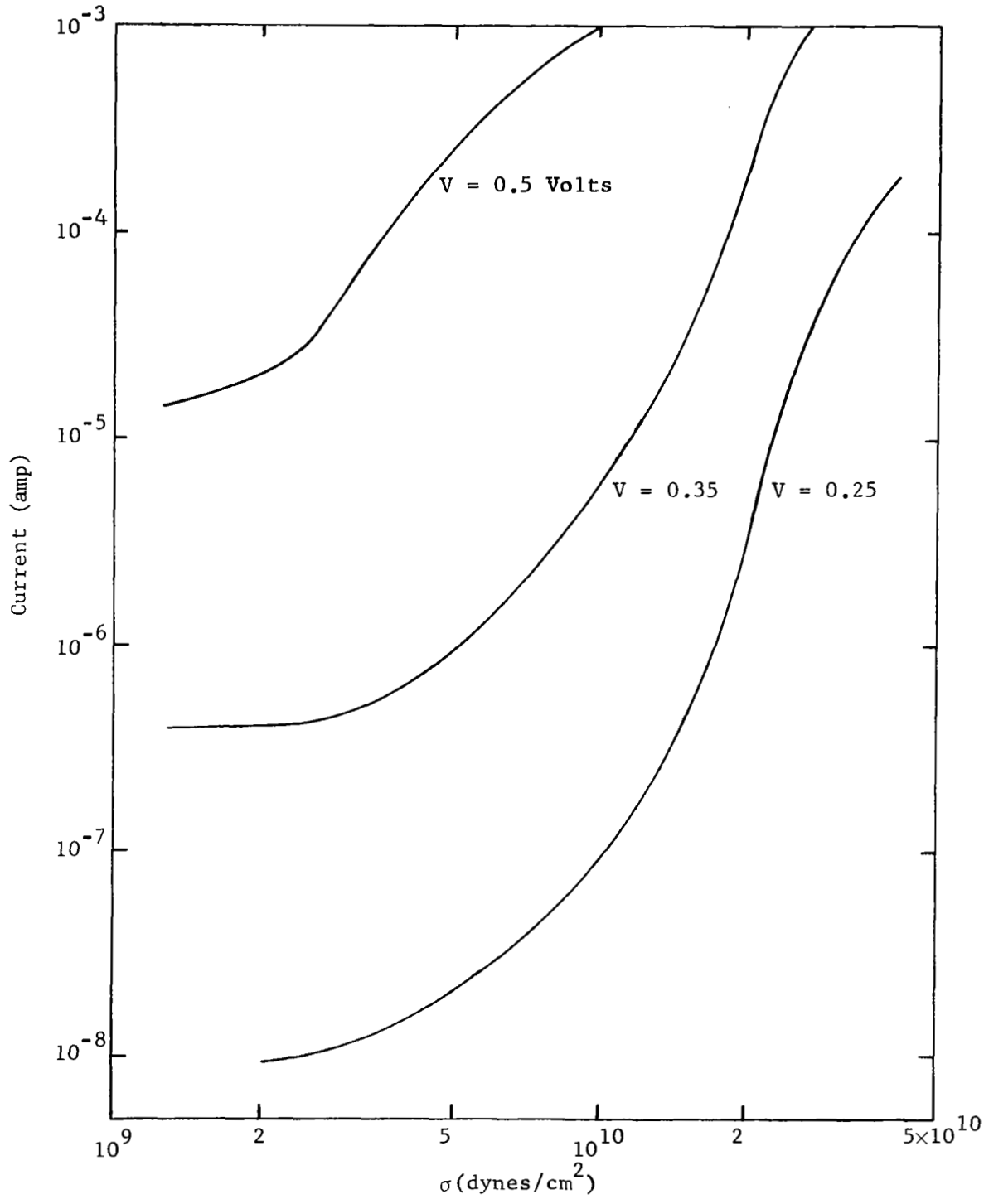

Fig. 21. Current as a Function of Stress at Several Voltage Levels for the Diode Characteristics Shown in Fig. 20.

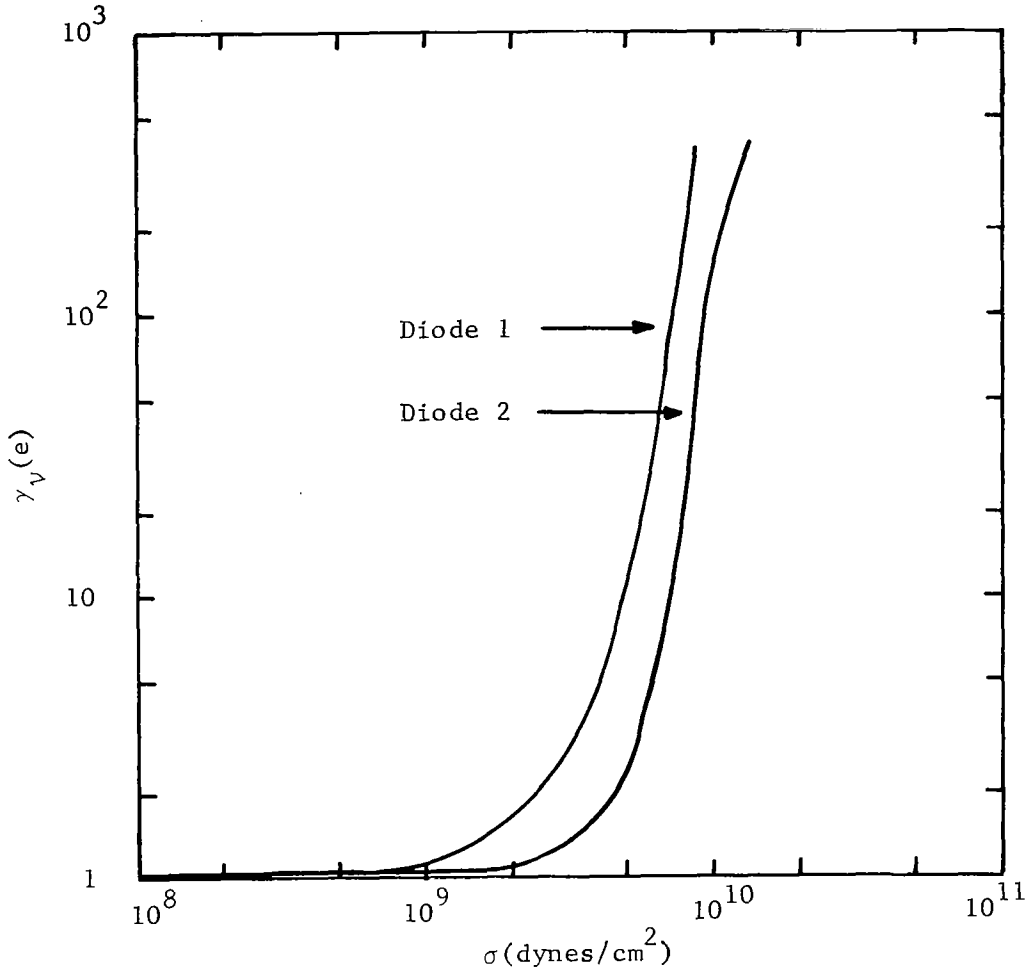

Fig. 22. γ_v(e) as a Function of Stress for Two Diodes Made on the Same (111) Wafer.

A series of tests was made to determine the effect of crystal orientation on the phenomenon. Figure 23 is a typical plot of γ_v(e) for three different crystal orientations. As shown in the figure, the orientations in order of decreasing sensitivity are <100>, <110>, and <111>. This is in agreement with the theory as shown in Fig. 9 in which the theoretical values of γ_v(e) are plotted.

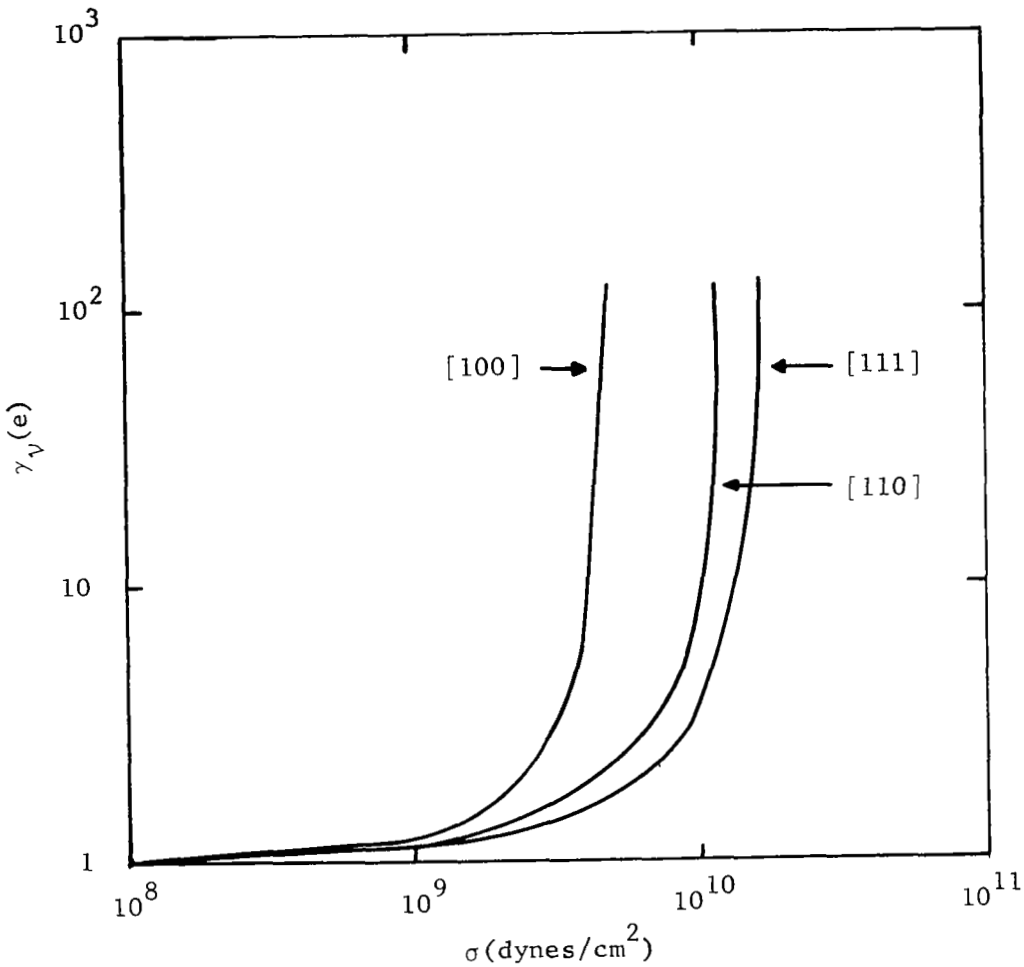

Fig. 23. $\gamma_\nu(e)$ as a Function of Stress for a [100], [110], and [111] Uniaxial Stress.

Experiments were performed to determine the effect of junction depth on the phenomenon. It was found that the shallower the junction depth the more sensitive the devices are to stress. Figures 24 and 25 show the

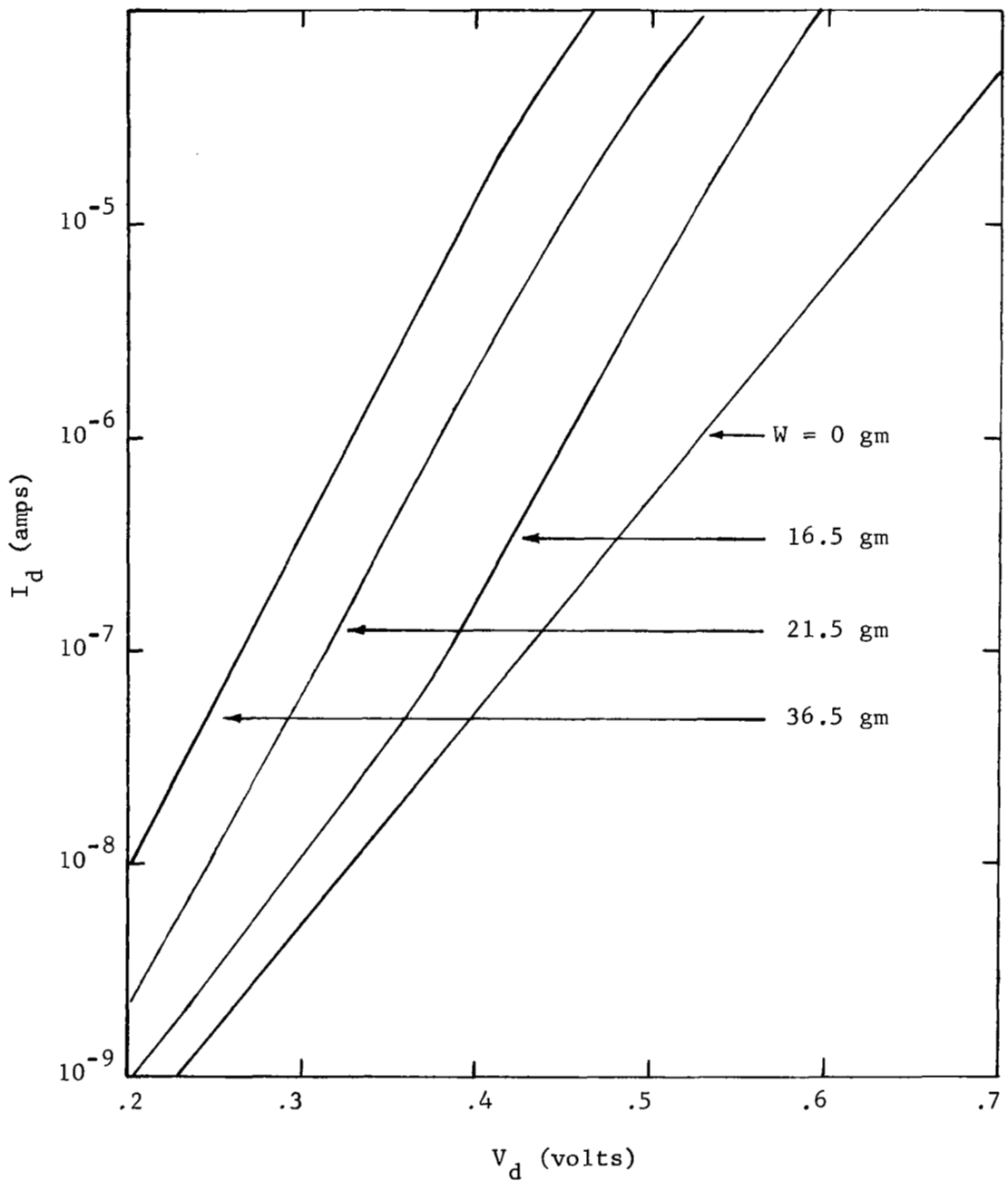

Fig. 24. I-V Characteristics of a Mesa Diode Under Varying Stress Conditions. The Junction Depth Was 0.6μ and the Orientation Was a (111) Plane.

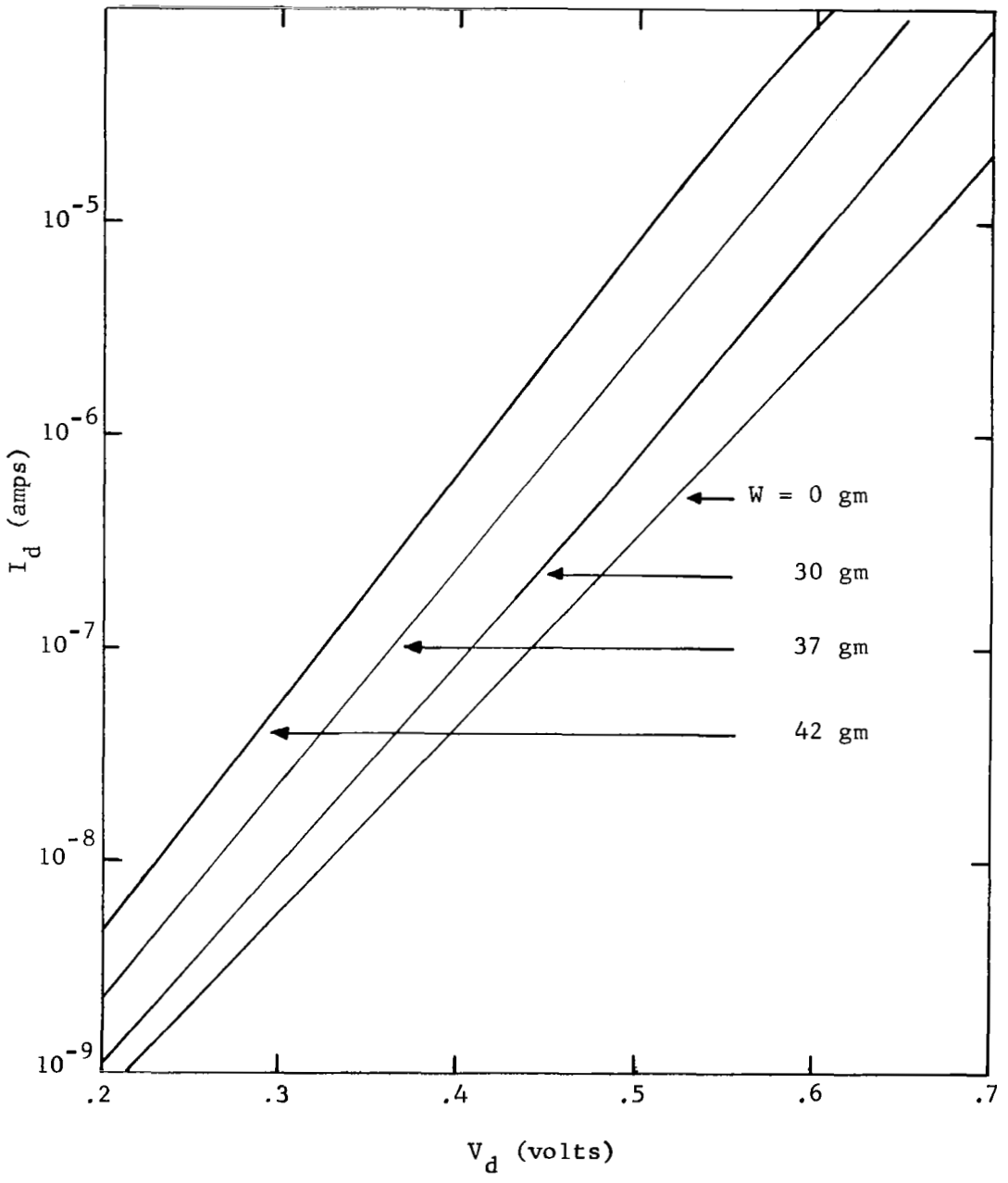

Fig. 25. I-V Characteristics of a Mesa Diode Under Varying Stress Conditions. The Junction Depth was 2.5μ and the Orientation Was a (111) Plane.

I-V characteristics at several stress levels for a 0.6 and a 2.5 micron junction respectively. There are two reasons why stress sensitivity increases with decreasing junction depth. First, for shallow junctions the "ideal" current component is larger than it is for deep junctions. This is due to larger minority carrier density gradients (see Eqs. (E.2) and (E.3) of Appendix E). The closer the junction is to the surface the steeper the gradient for the minority carriers near the surface. The second reason for increased stress sensitivity is that the closer the junction is to the surface the more nonuniform the stress is in the junction due to surface roughness of the diode.

4.4 Planar Diodes

Diodes of the planar type were fabricated. Figure 26 is a sketch of the planar structure. Again a steel needle was used to apply the mechanical stress and to make electrical contact to one side of the junction. Figure 27 is a typical plot of diode current versus forward voltage for several stress levels. The sample crystal was 1 ohm-cm with a (111) orientation. As was the case for mesa diodes, the slopes of the curves for planars are stress sensitive at low stress levels. It appears that the total diode current in this case is almost all "ideal" as evidenced by the slope of approximately qV/kT and the many orders of magnitude of current over which the slope is constant. The effect of spreading resistance can be seen by the turnover of the curves at the higher voltage levels. Figure 28 shows the current vs stress characteristics for several voltage levels. The characteristics are essentially the same as those for mesa diodes.

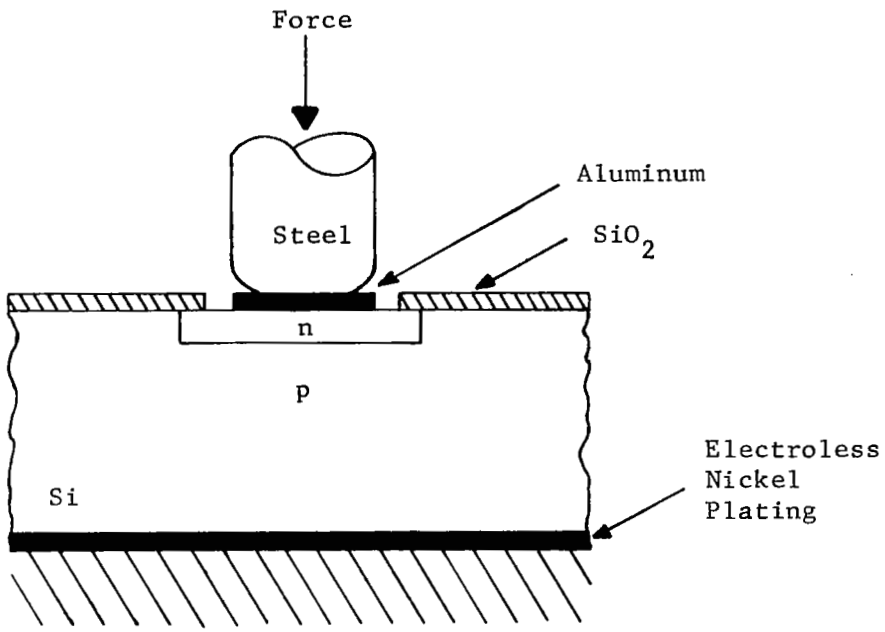

Fig. 26. Schematic of Planar Diode Structure.

4.5 Transistors

The transistors used in the present experiments have all been of the planar type. A variety of devices have been tested with the aim of exhibiting the many facets of the piezojunction phenomenon is multi-junction devices. No attempts were made to compare quantitatively the data on transistors with the theory due to the extreme difficulty of determining the stress and strain fields caused by spherical indentor points. The indentor point can be applied to a number of locations on the structure of planar transistor-emitter, emitter-base junction where the junction comes to the surface, base, base-collector junction where it comes to the surface, and the collector. In all of the locations the stress or strain field must be at or near a junction in order to alter the electrical characteristics.

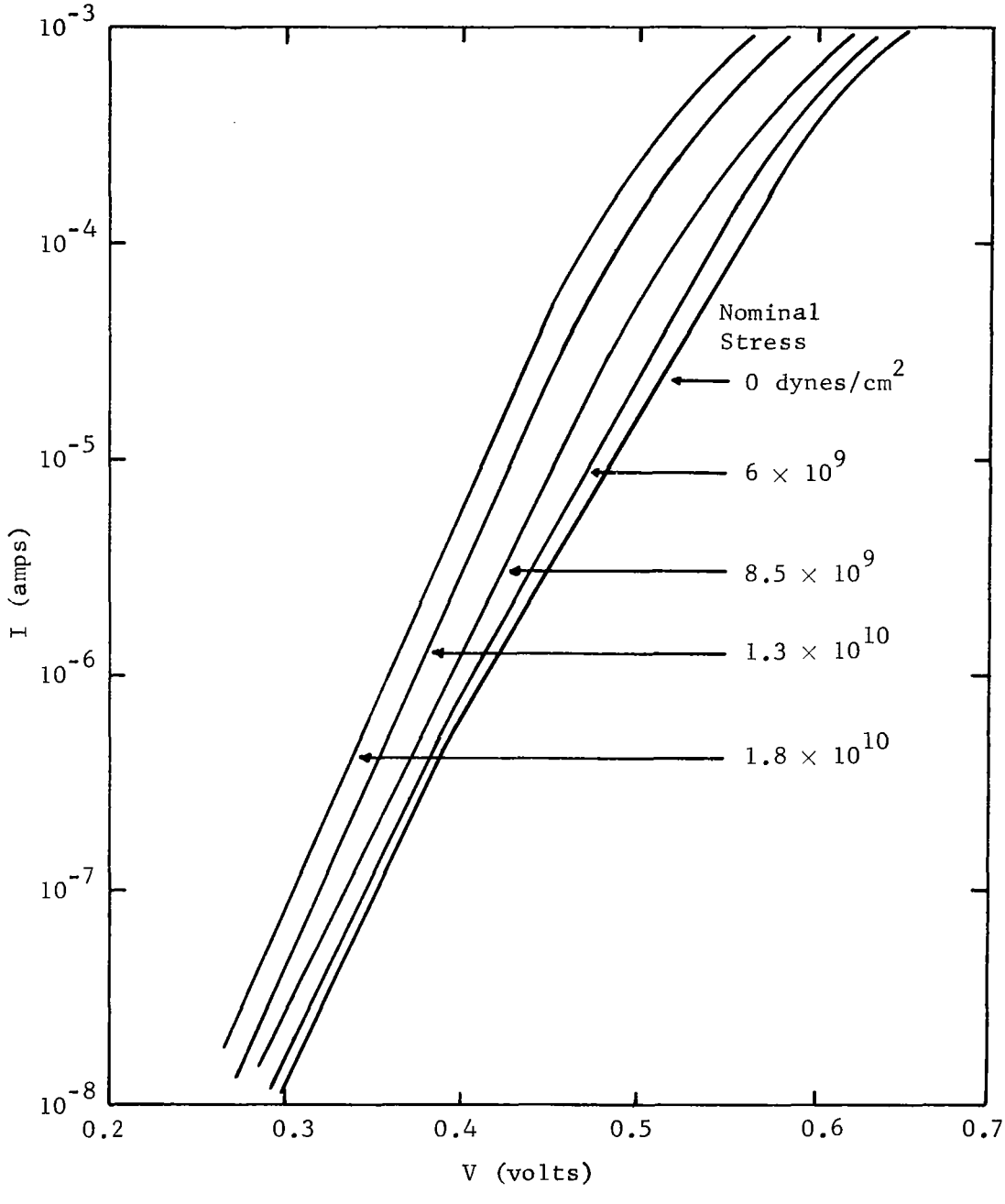

Fig. 27. I-V Characteristics of a Planar Diode Under Several Nominal Stress Conditions.

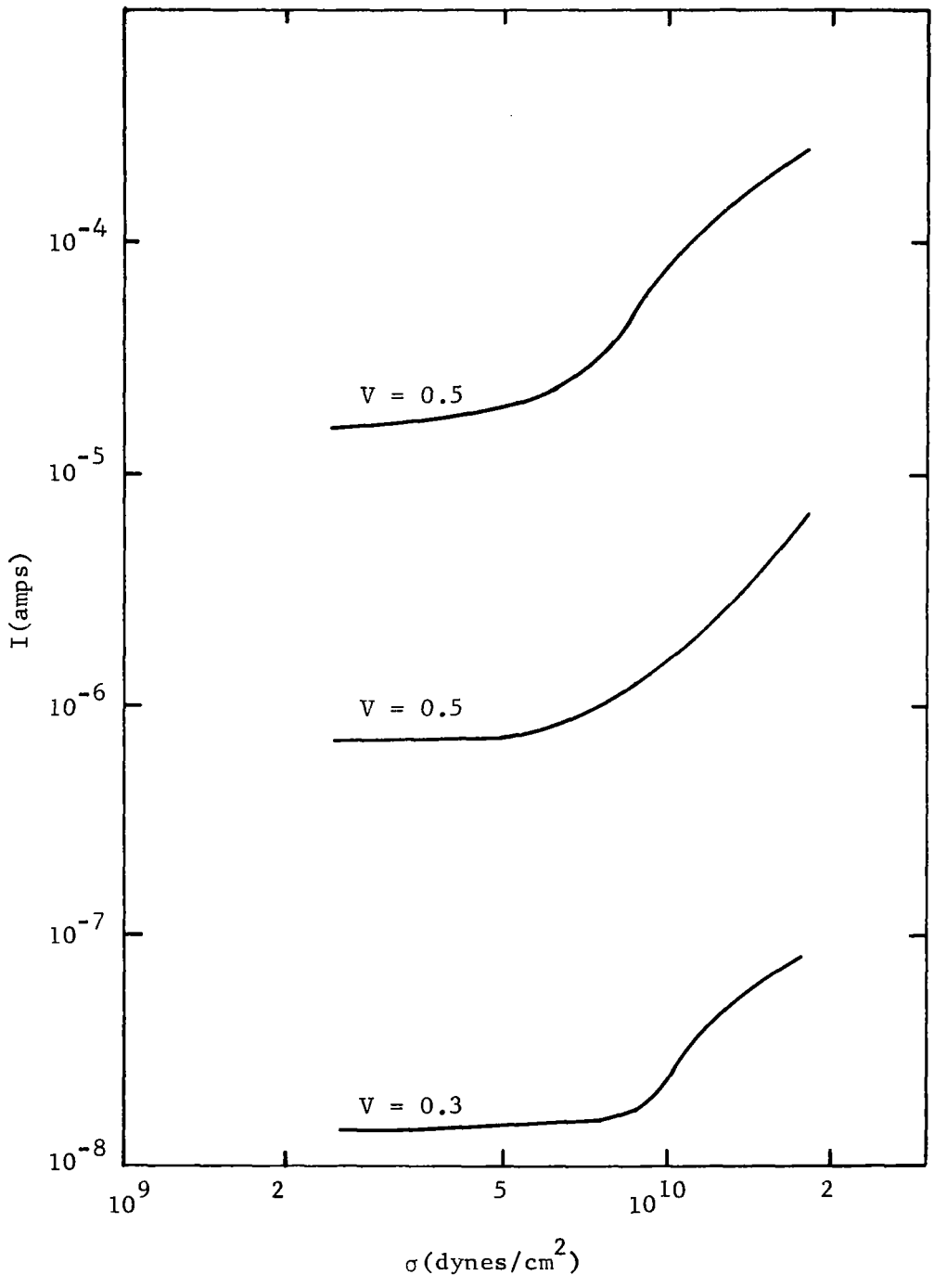

Fig. 28. Current vs Nominal Stress for a (111) Plane Planar Diode for Several Voltage Levels.

The most interesting results have been obtained on transistors in which stress was applied either directly on the emitter-base junction or near the emitter-base junction on the emitter side. The latter can be done in two ways. The first method is to place the indentor very close to the junction where the junction comes to the surface. The second is to apply the indentor anywhere in the emitter region. The stress produced by a spherical indentor point is attenuated very fast with distance underneath the indentor. When the indentor is placed on the emitter there is some stress on the base side of the junction; however, the stress on the emitter side of the junction is larger and essentially dominates the piezojunction effect.

The effect of stress on the collector current with either emitter current constant or base current constant for a 2N1958 n-p-n transistor is shown in Fig. 29. The stress was applied to the emitter by a 0.7 mil sapphire needle. As shown in Fig. 29 the collector current is more sensitive to stress with base current held constant than it is with emitter current held constant. By comparing Fig. 29 with Fig. 14 which was calculated theoretically it is seen that the experimental results are in good qualitative agreement with the theory.

Figure 30 is a plot of I_C as a function of V_{eb} for several stress levels with base current held constant in a laboratory n-p-n planar transistor. In this case the stress was applied to the emitter with a 3 mil steel needle. The effect of stress on the base current with collector current and emitter-base voltage held constant is shown in Fig. 31. The transistor was a 2N2102 n-p-n device with stress applied by a 0.7 mil sapphire needle. The base current of an n-p-n 2N2102 transistor as a function of emitter-base voltage

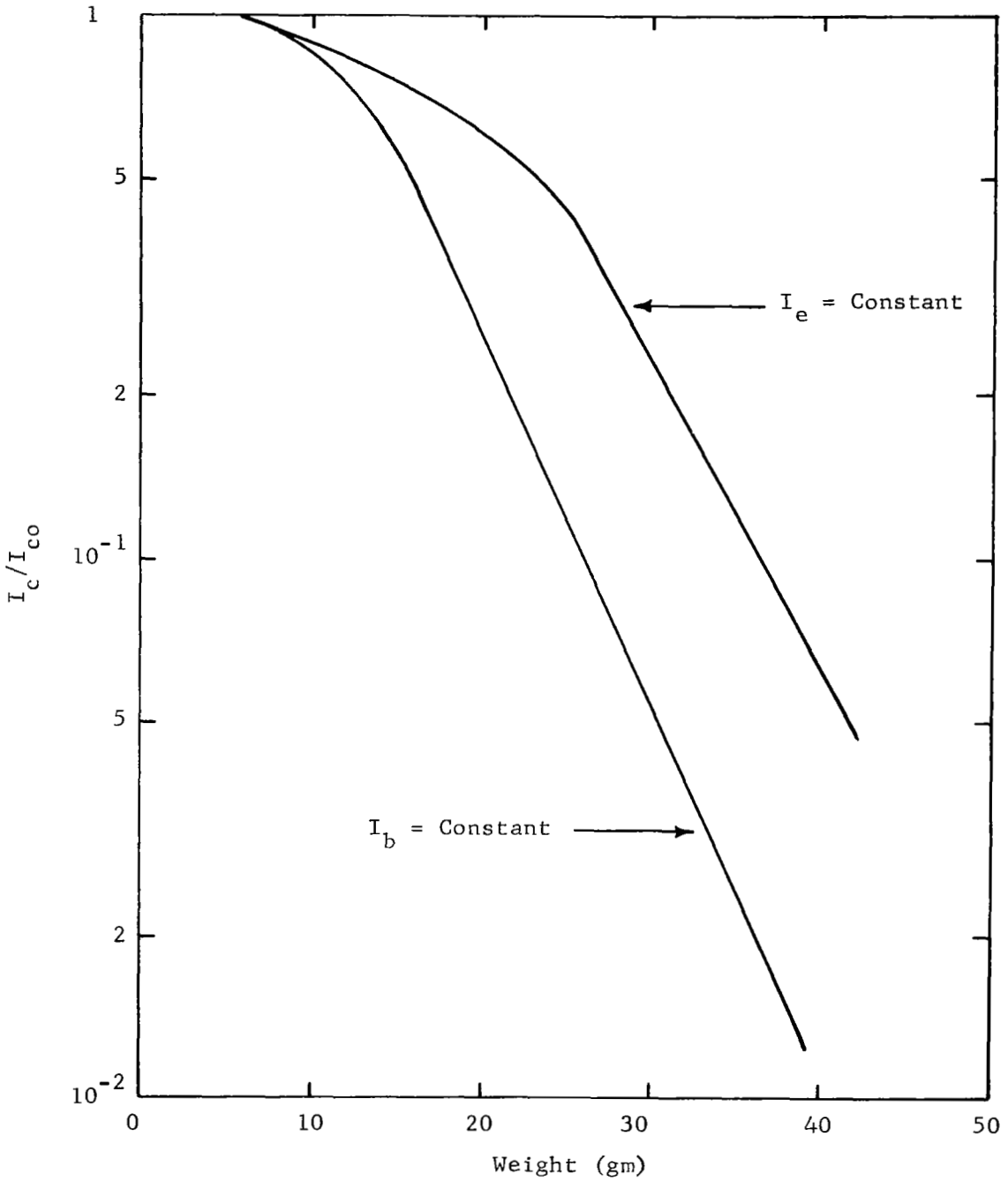

Fig. 29. Ratio of Stressed to Unstressed Collector Current of a 2N1958 n-p-n Transistor with Base Current Held Constant and with Emitter Current Held Constant.

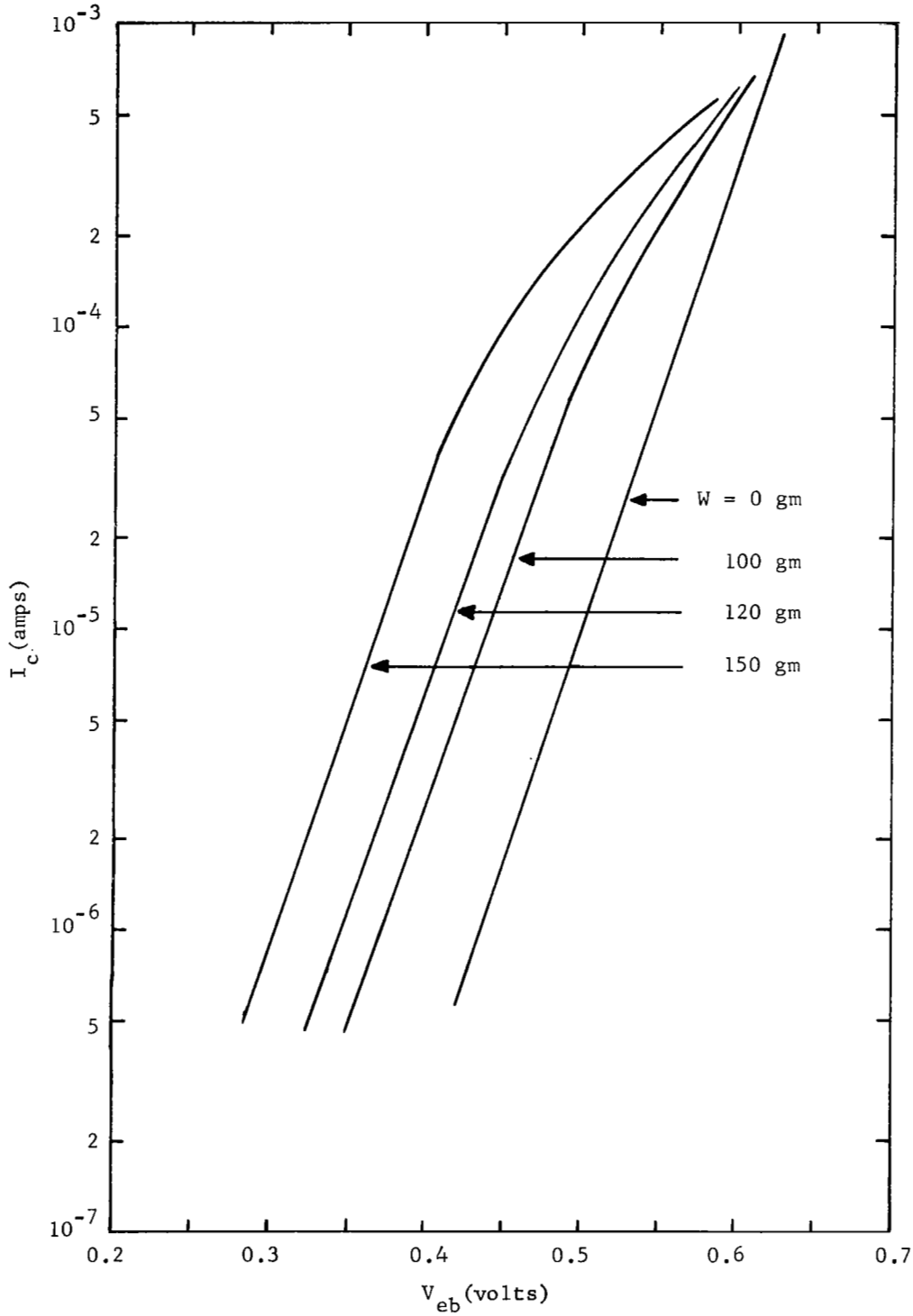

Fig. 30. Collector Current as a Function of Emitter Base Voltage for Constant Base Current and Several Stress Levels in an n-p-n Silicon Transistor Stressed in the Emitter Area with a Steel Needle.

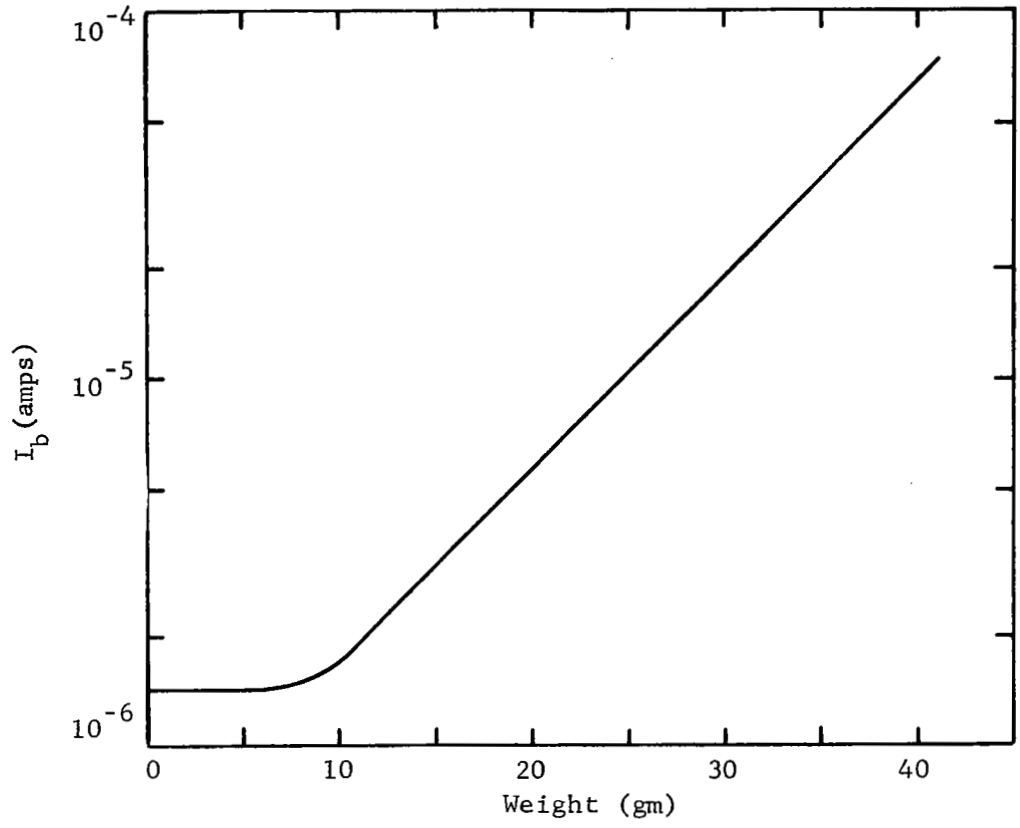

Fig. 31. Base Current as a Function of Stress with the Emitter-Base Voltage Held Constant for an n-p-n 2N2102 Transistor Stressed in the Emitter Area with a Sapphire Needle.

for several stress levels is shown in Fig. 32. In this case the emitter-base junction was stressed where it comes to the surface with a 3 mil sapphire needle. This particular device had an oxide over the junction and the stress was applied through the oxide.

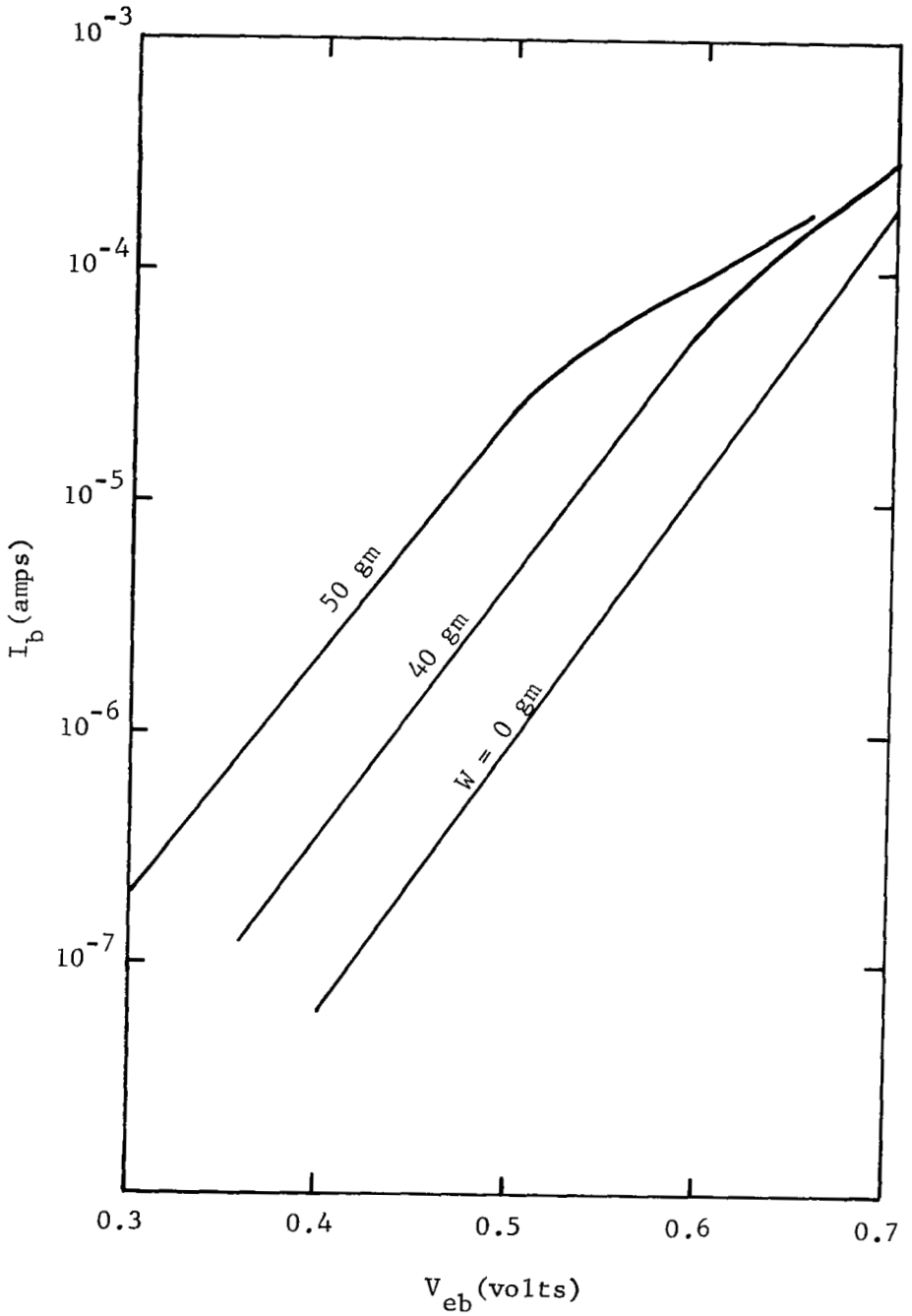

Fig. 32. Base Current as a Function of Emitter Base Voltage for Three Stress Levels in an n-p-n Silicon Transistor. The transistor was stressed on the emitter base junction with a 3 mil Sapphire needle.

Stress applied on the base side of the emitter-base junction has a much smaller effect on the electrical characteristics of most transistors. It was found however that in some power transistors a stress on the base side of the e-b junction causes the base current to decrease. Figure 33 is a plot of base current as a function of emitter-base voltage for constant emitter current and several stress levels. This device was an n-p-n power transistor manufactured by Solid State Products Inc. The stress was applied with a 0.7 mil sapphire needle near the emitter-base junction on the base side. As shown in the figure the base current can be made to decrease and go negative at low voltages and high stress levels. This means that the collector-base potential has been lowered by the stress to the point that the collector leakage is larger than the emitter current. Stress applied on the collector side of the base-collector junction was found to have little or no effect on transistor characteristics.

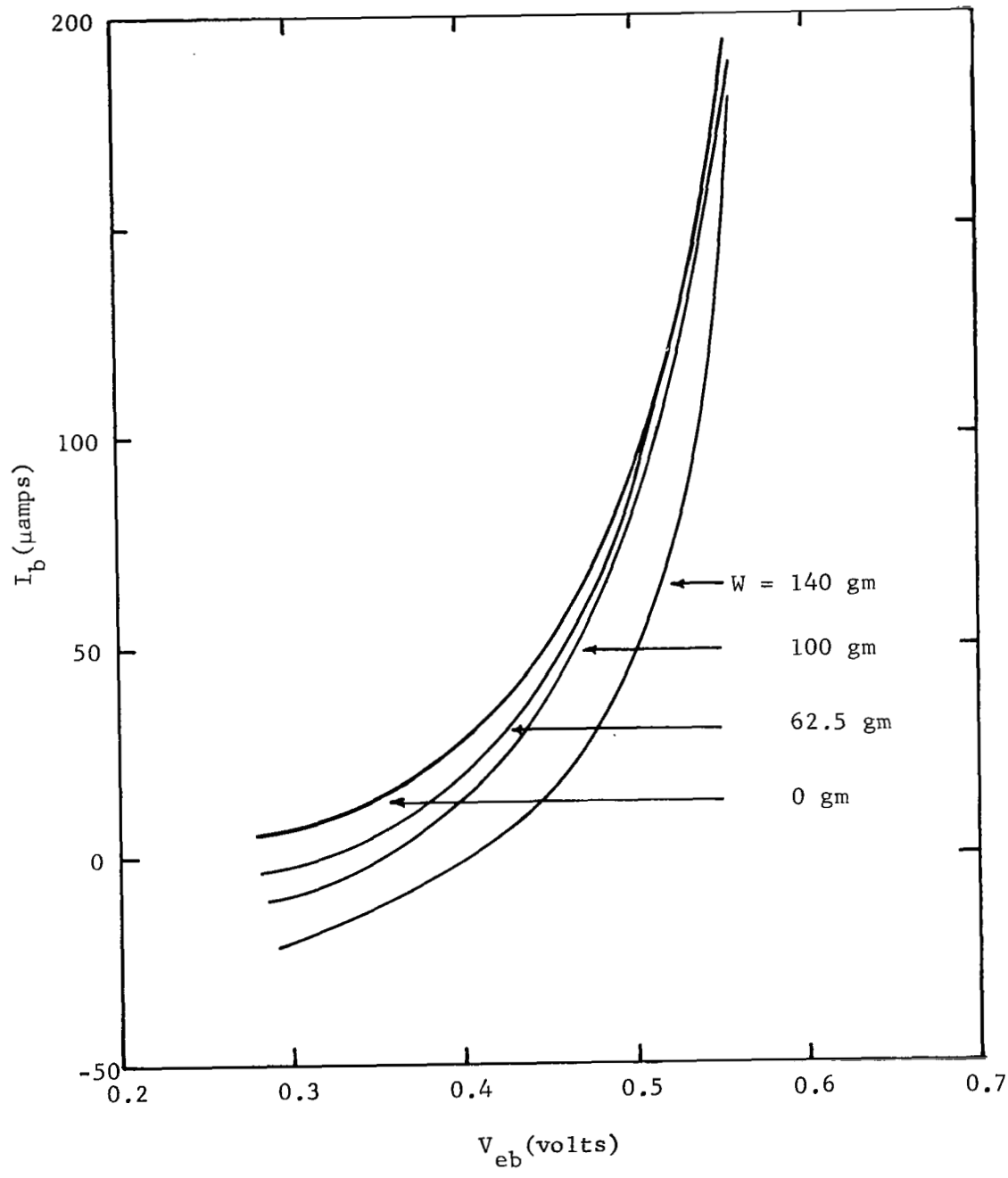

Fig. 33. Base Current of a Silicon Transistor as a Function of Emitter-Base Voltage with Constant Emitter Current and with Stress Applied to the Base with a 0.7 Mil Sapphire Needle.

Chapter V

DISCUSSION AND SUMMARY

A theory of the effect of a general strain on the electrical characteristics of p-n junctions is developed. The model is based on the deformation potential theory of semiconductors, i.e., the change in the energy band structure with strain. The energy band structure of germanium and silicon is reviewed and the necessary deformation potential theory is developed. Energy band changes with strain are incorporated into the current-voltage p-n junction equations. Equations are developed which describe the current-voltage characteristics of diodes and transistors under strain. The diode and transistor model as developed has neglected the effects of strain on such junction parameters as effective mass, mobility and carrier lifetime.

Comparing the theoretical model with experimental data it shows that there is good agreement. Quantitative comparisons have not been made in cases where the stress was applied by an indentor point. When stress is introduced in the junction by a spherical needle, the calculations for the strain tensor, in which accuracy is needed, is difficult if not impossible. This distributed strain problem has not been considered here. As demonstrated by the experimental data, the theory can be used to predict the electrical characteristics of diodes and transistors under strain. As an example, theory predicted that a [100] oriented junction in silicon would

be more sensitive to strain than a [110] or [111] orientation and a [110] orientation would be more sensitive than a [111] orientation. This was found to be correct experimentally. Theory predicts that a [111] orientation is more sensitive in germanium than a [110] or [100] orientation and a [110] is more sensitive than a [100] orientation. Rindner et al., [6] have found experimentally that this is the case.

The present theory explains the many facets of the piezojunction phenomenon as observed in silicon and germanium p-n junction devices. This theory should be useful in the design of semiconductor junction transducers. In addition, there are useful applications in evaluating and fabricating diodes and transistors. For example, if one wishes to determine whether the current in a diode is "ideal" or due to generation-recombination, a mechanical stress can be applied to the junction which will cause the "ideal" component to be amplified more than the generation-recombination component. Also it has been the practice to test semiconductor devices before lead attachment and encapsulation by placing small metal probes on the various contact areas. One of these areas is often a transistor emitter. It is very likely that device characteristics thus observed can be very different from those usually obtained, due to the strains introduced by the probes.

Appendix A

NOTATION USED TO REPRESENT STRESS AND STRAIN AND CALCULATIONS FOR SEVERAL CRYSTAL ORIENTATIONS

In all cases the stress and strain are referred to the crystal axes; x = 1,2,3 refer to the [100], [010] and [001] directions respectively. Tensional stresses and strains are positive and compressional are negative. The mechanical stress, σ, is represented as follows:

$\sigma_{\alpha\beta}$ = conventional stress ; $\alpha,\beta = x,y,z$

σ_{ij} = tensor stress ; $i,j = 1,2,3$

σ_{r} = engineering stress ; $r = 1,2,3,4,5,6$

where $\sigma_{\alpha\beta} = \sigma_{\beta\alpha}$ and $\sigma_{ij} = \sigma_{ji}$. The conventional, tensor and engineering stresses are related as follows:

Principal	Shear
$\sigma_{xx} = \sigma_{11} = \sigma_1$	$\sigma_{xy} = \sigma_{12} = \sigma_6$
$\sigma_{yy} = \sigma_{22} = \sigma_2$	$\sigma_{xz} = \sigma_{13} = \sigma_5$
$\sigma_{zz} = \sigma_{33} = \sigma_3$	$\sigma_{yz} = \sigma_{23} = \sigma_4$

The hydrostatic stress, P, is defined in terms of the principal stresses as

$$P = (\sigma_1 + \sigma_2 + \sigma_3)/3$$

The mechanical strain is represented as

$e_{\alpha\beta}$ = conventional strain ; $\alpha,\beta = z,y,z$

ϵ_{ij} = tensor strain ; $i,j = 1,2,3$

e_r = engineering strain ; $r = 1,2,3,4,5,6$

where $e_{\alpha\beta} = e_{\beta\alpha}$ and $\epsilon_{ij} = \epsilon_{ji}$. The conventional, tensor and engineering strains are related to each other in the following manner:

Principal	Shear
$e_{xx} = \epsilon_{11} = e_1$	$e_{xy} = 2\epsilon_{12} = e_6$
$e_{yy} = \epsilon_{22} = e_2$	$e_{xz} = 2\epsilon_{13} = e_5$
$e_{zz} = \epsilon_{33} = e_3$	$e_{yz} = 2\epsilon_{23} = e_4$

The hydrostatic strain, e, is defined as

$$e = e_1 + e_2 + e_3$$

For the case of cubic symmetry, the engineering stress is related to strain by Hook's generalized law

$$\begin{bmatrix} \sigma_1 \\ \sigma_2 \\ \sigma_3 \\ \sigma_4 \\ \sigma_5 \\ \sigma_6 \end{bmatrix} = \begin{bmatrix} c_{11} & c_{12} & c_{12} & 0 & 0 & 0 \\ c_{12} & c_{11} & c_{12} & 0 & 0 & 0 \\ c_{12} & c_{12} & c_{11} & 0 & 0 & 0 \\ 0 & 0 & 0 & c_{44} & 0 & 0 \\ 0 & 0 & 0 & 0 & c_{44} & 0 \\ 0 & 0 & 0 & 0 & 0 & c_{44} \end{bmatrix} \times \begin{bmatrix} e_1 \\ e_2 \\ e_3 \\ e_4 \\ e_5 \\ e_6 \end{bmatrix},$$

and

$$\begin{bmatrix} e_1 \\ e_2 \\ e_3 \\ e_4 \\ e_5 \\ e_6 \end{bmatrix} = \begin{bmatrix} s_{11} & s_{12} & s_{12} & 0 & 0 & 0 \\ s_{12} & s_{11} & s_{12} & 0 & 0 & 0 \\ s_{12} & s_{12} & s_{11} & 0 & 0 & 0 \\ 0 & 0 & 0 & s_{44} & 0 & 0 \\ 0 & 0 & 0 & 0 & s_{44} & 0 \\ 0 & 0 & 0 & 0 & 0 & s_{44} \end{bmatrix} \times \begin{bmatrix} \sigma_1 \\ \sigma_2 \\ \sigma_3 \\ \sigma_4 \\ \sigma_5 \\ \sigma_6 \end{bmatrix},$$

where the c's and s's are the stiffness and compliance coefficient for the crystal.

When a general stress is applied to a crystal, it is always possible to choose a rectangular coordinate system (not necessarily the crystal axes) such that there is zero shear stress and three principal stresses. Let the principal stress system have the coordinates x′, y′, z′, the shear stresses are then $\sigma_{x'y'} = \sigma_{x'z'} = \sigma_{y'z'} = 0$. The principal stresses are related to the crystal axes by the following equation.

$$\begin{aligned}
\sigma_{xx} &= \sigma_{x'x'}\, \ell_1^2 + \sigma_{y'y'}\, \ell_2^2 + \sigma_{z'z'}\, \ell_3^2 \\
\sigma_{yy} &= \sigma_{x'x'}\, m_1^2 + \sigma_{y'y'}\, m_2^2 + \sigma_{z'z'}\, m_3^2 \\
\sigma_{zz} &= \sigma_{x'x'}\, n_1^2 + \sigma_{y'y'}\, n_2^2 + \sigma_{z'z'}\, n_3^2 \\
\sigma_{xy} &= \sigma_{x'x'}\, \ell_1 m_1 + \sigma_{y'y'}\, \ell_2 m_2 + \sigma_{z'z'}\, \ell_3 m_3 \\
\sigma_{xz} &= \sigma_{x'x'}\, \ell_1 n_1 + \sigma_{y'y'}\, \ell_2 n_2 + \sigma_{z'z'}\, \ell_3 n_3 \\
\sigma_{rz} &= \sigma_{x'x'}\, m_1 n_1 + \sigma_{y'y'}\, m_2 n_2 + \sigma_{z'z'}\, m_3 n_3
\end{aligned}$$

where ℓ, m, n are the direction cosines defined by the following transformation.

$$\begin{bmatrix} x \\ y \\ z \end{bmatrix} = \begin{bmatrix} \ell_1 & m_1 & n_1 \\ \ell_2 & m_2 & n_2 \\ \ell_3 & m_3 & n_3 \end{bmatrix} \times \begin{bmatrix} x' \\ y' \\ z' \end{bmatrix}$$

It is of practical interest here to determine the strain components for hydrostatic, uniaxial [100], uniaxial [011] and uniaxial [111] stresses. For the hydrostatic case,

$$\sigma_1 = \sigma_2 = \sigma_3 = -P$$

and

$$\sigma_4 = \sigma_5 = \sigma_6 = 0 \ .$$

Solving for the strains yields

$$e_1 = e_2 = e_3 = -(s_{44} + 2s_{12})P \ ,$$
$$e_4 = e_5 = e_6 = 0 \ .$$

Consider a uniaxial compressional stress of magnitude T applied along the [111] direction. In this case $\ell_1 = m_1 = n_1 = 1/\sqrt{3}$, for which

$$\sigma_1 = \sigma_2 = \sigma_3 = \sigma_4 = \sigma_5 = \sigma_6 = -\ T/3 \ ,$$

and

$$e_1 = e_2 = e_3 = -\ T(s_{11} + 2s_{12})/3 \ ,$$
$$e_4 = e_5 = e_6 = -\ T\ s_{44}/3 \ .$$

Next consider a uniaxial compression stress of magnitude T applied along the [011] direction. In this case $\ell_1 = 0$, $m_1 = 1/\sqrt{2}$, $n_1 = 1/\sqrt{2}$ for which

$$\sigma_1 = 0 \ , \ \sigma_2 = \sigma_3 = -\ T/2 \ , \ \sigma_4 = -\ T/2 \ , \ \sigma_5 = \sigma_6 = 0 \ ,$$

and

$$e_1 = -s_{12}T \ , \ e_2 = e_3 = -\ T(s_{11} + s_{12})/2 \ ,$$

$$e_4 = - T s_{44}/2 , e_5 = e_6 = 0 .$$

Finally consider a uniaxial compression stress of magnitude T applied along the [100] direction. This gives $\ell_1 = 1$, $m_1 = 0$, $n_1 = 0$ for which

$$\sigma_1 = - T , \sigma_2 = \sigma_3 = \sigma_4 = \sigma_5 = \sigma_6 = 0 ,$$

and

$$e_1 = -s_{11} T , e_2 = e_3 = -s_{12} T ,$$
$$e_4 = e_5 = e_6 = 0 .$$

Appendix B

EFFECT OF STRAIN ON THE EFFECTIVE MASS

B.1 Introduction

There is little experimental information available on the effect of large strains ($e_s > 1\%$) on the effective mass. Cyclotron resonance measurements of the effective mass have been made on silicon subjected to uniaxial stress in which the strain levels were less than 1% [19,20,37]. In these experiments the effective mass was found to change only a few percent. Hasegawa [38] and Hensel and Hasegawa [19] have derived theoretical expressions for the effective mass of some of the energy levels in silicon as a function of some particular stresses. By using the results of their work it can be shown that strain in the range of interest here ($e_s < 5\%$) produces a negligible change in the effective mass of silicon when compared to changes in carrier concentration.

B.2 Effective Mass of Holes in Silicon

The shape of the energy bands at the band edge points determines the effective mass, i.e.,

$$m^*_{ij} = \frac{1}{\hbar^2}\left[\frac{\partial^2 E(k)}{\partial k_i \partial k_j}\right]^{-1} , \qquad (B.1)$$

where m^*_{ij} is the effective mass tensor and i and j are the $\bar{k}$-directions. In the case of spherical bands, $E \propto [k_x^2 + k_2^2 + k_3^2]/m^*$, the effective mass, m^*, is independent of direction. Such is the case for the split-off hole band (E_{v3}) in silicon and germanium. The light hole band (E_{v2}) can be approximated to within a few percent by a sphere [11]. The heavy hole band (E_{v1}) is a warped sphere. It can also be approximated with less accuracy as a sphere with a radius equal to the average radius of the warped sphere [11]

As discussed in Chapter II, when the crystal is mechanically strained the degeneracy of the $\Gamma'_{25}(j = 3/2)$ is removed. Strain causes the warped spheres to transform into ellipsoids similar to that encountered in the conduction bands of Si and Ge [38]. Hasegawa [38] has developed a theoretical expression for the energy of the heavy hole band as a function of $\bar{k}$ and the magnitude of a uniaxial compression stress applied along the <100> axes of the crystal:

$$E_{v1} = (A - \frac{1}{2} BZ)k_{\parallel}^2 + (A + BZ)k_{\perp}^2 \quad , \tag{B.2}$$

where $k_{\parallel}$ is parallel to the <100> direction and $k_{\perp}$ is perpendicular to the <100> direction, A and B are constants which can be determined experimentally and Z is the degree of mixing between the heavy hole band and the split-off band and is given by

$$Z = \frac{1}{2}\left(1 + \frac{1 - 9x}{(1 - 2x + 9x^2)^{1/2}}\right) \tag{B.3}$$

where

$$x = \frac{e_1 D_u}{\delta} \quad , \tag{B.4}$$

δ is the separation between the heavy hole band and the split-off band (see Fig. 3).

Solving Eqs. (B.1) and (B.2) for the components of the effective mass tensor gives

$$\frac{\hbar^2}{2m_{\parallel}} = A - \frac{1}{2} BZ \tag{B.5}$$

and

$$\frac{\hbar^2}{2m_{\perp}} = A + BZ \ . \tag{B.6}$$

A "density of states effective mass", m_c, can now be defined in the same manner as is done for the conduction band, i.e.

$$(m_c)^{3/2} = \sqrt{m_{\perp}^2 \, m_{\parallel}} \ . \tag{B.7}$$

Hensel and Feber [37] have determined experimental values of A, B, and D_u as follows:

$$\begin{aligned} A &= -4.28 \, \hbar^2/2m_o \ , \\ B &= -0.75 \, \hbar^2/2m_o \ , \\ D_u &= 2.04 \text{ ev} \ . \end{aligned} \tag{B.8}$$

Solving the above equations for the density of states effective mass as a function of strain shows that m_c changes less than 1% for stress levels as large as 6×10^{10} dyne/cm^2. This change is negligible when compared to changes in the carrier concentration for the same stress.

The effective mass can also be obtained from the theory of Hasegawa [38] as a function of other uniaxial stresses ([011] and [111]). Changes in the density of states effective mass for these directions are also found to be very small.

B.3 Effective Mass of Electrons in Silicon

The Hamiltonian for the conduction electrons has been discussed in Chapter II, Eq. (2.8). Diagonalizing the Hamiltonian gives

$$E(\bar{k}) = \frac{\hbar^2}{2m_{\parallel}} \kappa_x^2 + \frac{1}{2m_{\perp}}(k_y^2 + k_z^2) + []_d\, e + []_u\, e_1 \pm [\hbar^2 V^2 \kappa_x^2 + ([]'_u\, e_4 + N\, k_y\, k_z)^2]^{1/2} . \tag{B.9}$$

The band edge point along the [100] axis has already been shown to be located at

$$\hbar^2 (\kappa_x)^2_{min} = \hbar^2 \kappa_o^2 - \frac{([]'_u\, e_4)^2}{V^2} , \tag{B.10}$$

$$\hbar^2 k_y^2 = 0 ,$$
$$\hbar^2 k_z^2 = 0 .$$

It can be seen from Eq. (B.9) that constant energy surfaces are not ellipsoids or spheres in k-space when there is an applied strain. If one wants the density of states exactly, it would be necessary to use Eq. (B.9) for $E(\bar{k})$ in the density of states relationship. To do this would require considerable effort which is probably unwarranted. An approximate approach is to expand $E(\bar{k})$ in a Taylor series about the band edge point. Performing this expansion to second order powers in $\bar{k}$ yields;

$$E(\bar{k}) = \delta_e + \frac{\hbar V}{3\kappa_o}(\kappa_x)^2_{min}[\kappa_x - (\kappa_x)_{min}]^2 + \hbar^2\left(\frac{k_y^2 + k_z^2}{2m}\right) + \alpha\, e_4\, k_y\, k_z , \tag{B.11}$$

where δ_e represents the shift of the band edge and

$$\alpha = \frac{2N[\,]'_u}{-\Delta E} \cdot \tag{B.12}$$

This approach has been taken by Hensel and Hasegawa [19], and they find that α is given approximately by

$$\alpha \approx \frac{2[\,]'_u}{-\Delta E} \frac{1}{m_o}\left(\frac{m_o}{m_\perp} - 1\right) \tag{B.13}$$

An analysis of Eq. (B.10) shows that as $e_4 \longrightarrow \Delta E/2[\,]'_u$, $(\kappa_x)_{min} \longrightarrow 0$. This means that $E(\bar{k})$ becomes independent of κ_x to second order powers in κ_x for the strain level. Therefore one would not expect Eq. (B.11) to hold near this strain level. For strains below the above critical value Eq. (B.11) is expected to be a good approximation.

Taking the derivatives of Eq. (B.11) and solving for the components of the effective mass tensor yields:

$$\frac{1}{m^*_{ij}} = \begin{bmatrix} \frac{1}{m_{\|}}[1 - (2[\,]'_u/\Delta E)^2 e_4^2 & 0 & 0 \\ 0 & \frac{1}{m_\perp} & \alpha e_4 \\ 0 & \alpha e_4 & \frac{1}{m_\perp} \end{bmatrix} \tag{B.14}$$

as expected there are terms in the tensor which are non-zero for the off diagonal elements. This is handled in the usual manner (diagonalizing the tensor) which yields

$$\frac{1}{m^*_{kl}} = \begin{bmatrix} \frac{1}{m_1(e)} & 0 & 0 \\ 0 & \frac{1}{m_2(e)} & 0 \\ 0 & 0 & \frac{1}{m_3(e)} \end{bmatrix} = \begin{bmatrix} \frac{1}{m_{\|}}\left[1 - \left(\frac{2[\,]'_u}{\Delta E}\right)^2 e_4^2\right] & 0 & 0 \\ 0 & \frac{1}{m_\perp}(1+m_\perp \alpha e_4) & 0 \\ 0 & 0 & \frac{1}{m_\perp}(1-m_\perp \alpha e_4) \end{bmatrix} . \quad (B.15)$$

where k and l are different from i and j and are used to show that the new coordinate system is different from the old x, y, z system.

The inverse density of states effective mass is

$$\left(\frac{1}{m_c^*(e)}\right)^3 = \frac{1}{m_1(e)}\,\frac{1}{m_2(e)}\,\frac{1}{m_3(e)} . \quad (B.16)$$

Rewriting Eq. (B.16) in terms of the strain gives

$$\left(\frac{m_c^*(e)}{m_c^*(o)}\right)^3 = \frac{1}{\left[1 - (2[\,]'_u/\Delta E)^2 e_4^2\right]\left[1 - m^2\alpha^2 e_4^2\right]} , \quad (B.17)$$

where $m_c^*(o)$ is the unstrained effective mass. Using the experimental value [19] $\alpha m_o = 16.4$ and substituting into Eq. (B.17) the values of the other band parameter gives

$$\left(\frac{m_c^*(e)}{m_c(o)}\right)^3 = \frac{1}{(1 - 520\, e_4^2)\,(1 - 268\, e_4^2)} . \quad (B.18)$$

Referring to Eq. (B.17) it is seen that there are two singularities in the effective mass equation. This is not unexpected since the energy was expanded in a Taylor series and accounts only for second order power in $\bar{k}$. It is seen that, in fact, if the shear strain is less than about 2 percent,

there is a negligible effect on the effective mass. In the case of hydrostatic pressures the shear is zero and hence the effective mass is independent of strain.

B.4 Summary

The above treatment of the variation of effective mass with strain for silicon is by no means complete. It does however indicate that for strain levels below a few percent, effective mass changes are negligible. Although no treatment has been given for germanium, it is expected that germanium will behave similarly to silicon. More important than the preceding discussion is the fact that experimental measurements made on the electrical parameters of p-n junction devices subjected to mechanical stress indicate that effective mass variations are at least second order when compared to carrier density variations.

Appendix C

EFFECT OF STRAIN ON THE MINORITY CARRIER LIFETIME, CARRIER MOBILITIES, DIFFUSION CONSTANTS AND DIFFUSION LENGTHS

C.1 Minority Carrier Lifetime*

The minority carrier lifetime of a semiconductor, based on a single trap level located in the forbidden band [33], is given by [39]

$$\tau = \frac{\tau_{po}(n + n_1) + \tau_{no}(p + p_1)}{n + p} \tag{C.1}$$

where n and p are the respective electron and hole concentrations in the particular semiconductor. τ_{po} and τ_{no} are the lifetimes of holes and electrons in highly n- and p-type materials respectively. Both τ_{po} and τ_{no} are inversely proportional to the trap density [39]. n_1 and p_1 in Eq. (C.1) are given by [33].

$$n_1 = n_i \exp[(E_i - E_t)/kT] , \tag{C.2}$$

$$p_1 = n_i \exp[(E_t - E_i)/kT] , \tag{C.3}$$

where E_t is the energy of the trap level and E_i is the energy of the intrinsic Fermi level.

---

* The present treatment of minority carrier lifetime is closely related to the treatment of generation recombination current given in Appendix E.

It is seen from Eq. (C.1) that if the material is highly n- or p-type, the lifetime expression reduces to either τ_{po} or τ_{no}. Any changes in the latter two quantities can be neglected, based on the arguments presented in Sect. 3.3; namely, the density of generation-recombinations centers is not changed by strain. The capture cross section is assumed to remain constant. The lifetimes, τ_n and τ_p, which appear in the theory of the "ideal" junction current are the lifetimes of electrons at the edge of the depletion region on the p side of the junction and of the holes at the edge of the depletion region on the n side of the junction respectively. It will be assumed for the present purposes that the material at the edges of the depletion regions is doped heavily enough so that the lifetimes are independent of the carrier concentrations n, p, n_1 and p_1. The effects of strain induced changes in the lifetime of carriers inside the depletion region are accounted for in the theory of generation-recombination currents (see Appendix E and Sect. 3.3).

Matukura [40] has measured the lifetime of minority carriers in stressed and unstressed silicon p-n junctions. He found that the lifetime decreased 10 to 30 percent for the stressed diodes. In his experiments a diamond needle was used to introduce a high stress level over a small region of the p-n junction area. The lifetime was measured by first injecting minority carriers with a large forward biased current pulse. Following the current pulse, the decay time was measured. The unstrained lifetime was found to be 0.3 μ-seconds. Assuming that the change in the decay time with the application of strain is due to a change in the lifetime of carriers in the strained area only, it is found that the lifetime in the strained material is reduced to 10^{-13} μ-seconds! Physically, this

value is not acceptable. The results of this experiment can be explained by neglecting changes in lifetime in favor of energy band changes.

C.2 Mobility

Much work has been done on the piezoresistance properties of germanium and silicon [41,42,43,44,45,46]. This work, however, has been concerned mainly with low strain, i.e., strain levels low compared to the levels of interest here. The piezoresistance effect in many-valley semiconductors (n-type Ge and Si) is explained by the deformation potential theory [41,42]. The major effect has been found to result from the relative population and depopulation of the valleys in the conduction band with strain as discussed in Chapters II and III.

For low strain levels, the relative change in the resistivity of germanium and silicon has been found to be directly proportional to strain. The proportionality constant or elastoresistance coefficient is on the order of 175 for extrinsic silicon and -150 for extrinsic germanium [43] For silicon this gives

$$\frac{\Delta\mu}{\mu} \sim 175\ S \qquad (C.4)$$

where μ is the mobility of the majority carriers and S is the strain. The relative change in mobility is seen to have a small effect compared to that of minority carrier changes.

It is the minority carrier mobility that is of interest here. It will be assumed that changes in the minority carrier mobility are of the same order of magnitude as that for majority carriers. This is probably

a good assumption since the majority carrier mobility changes mainly due to relative changes in the density of carriers at the band edge points while for minority carriers the density of the carriers are small to begin with and therefore would have less influence on the mobility.

It should also be noted that the relative change in resistance tends to saturate below the strains of interest here. This comes about because relatively small changes in the energy levels cause all the majority carriers to occupy certain valleys while leaving the other valleys empty. Strains above those required to empty the valleys have little effect on the mobility.

C.3 Diffusion Coefficients

The minority carrier diffusion coefficients are directly proportional to the minority carrier mobilities ($D = \mu kT/q$). As discussed in Sect. C.2 above, the minority carrier mobility is expected to be relatively insensitive to strain--especially when compared to minority carrier density changes. Changes in the diffusion coefficients with strain are therefore expected to be negligible.

C.4 Diffusion Length

The diffusion lengths L_p and L_n are proportional to the square root of $\mu_p\tau_p$ and $\mu_n\tau_n$ respectively. Changes with strain of both mobility and lifetime have been discussed above and it was concluded that the changes were negligible compared to other parameter changes. Another effect arises due to the changing energy levels which produce a "quasielectric" field

acting on the minority carrier [47]. This means that an effective diffusion length must be used which includes the drift field effect. The "quasielectric" field will have an effect similar to a built-in electric field. The field is directly proportional to the band gap changes and thus directly proportional to strain. These linear changes will be neglected compared to the exponential changes of the minority carrier density.

Appendix D

EFFECT OF LARGE STRAINS ON CONDUCTIVITY

Most of the piezoresistance work which was cited in Appendix C has been concerned with conductivity and resistivity changes as a function of strain. Again this work has been for low strain levels in extrinsic material such that the carrier density was determined by the impurity density and was independent of strain. As pointed out in Chapter III, the minority carrier density in extrinsic material can change by several orders of magnitude for large strain levels. Also in intrinsic material both the hole and electron densities can change with strain.

For the present purposes it will be assumed that mobility is independent of strain. The conductivity is

$$\sigma = nq\mu_n + pq\mu_p \ . \tag{D.1}$$

For the case of intrinsic material ($n \simeq p$) the conductivity expression reduces to

$$\sigma = nq(\mu_n + \mu_p) \ . \tag{D.2}$$

From Eqs. (3.11) and (3.12)

$$pn = n_{io}^2 \ \gamma_v(e) = n^2 \ . \tag{D.3}$$

The conductivity then reduces to

$$\sigma(e) = n_{io} q \sqrt{\gamma_\nu(e)} \ , \tag{D.4}$$

or

$$\frac{\sigma(e)}{\sigma(o)} = \sqrt{\gamma_\nu(e)} \ . \tag{D.5}$$

Since $\gamma_\nu(e)$ can change by orders of magnitude with high strain levels, the conductivity of intrinsic material can also change by orders of magnitude.

In the case of extrinsic material, p-type for example, the hole density is approximately equal to N_A. Substituting this into Eqs. (D.1) and (D.3) gives

$$\sigma = \frac{n_{io}^2}{N_A} q\mu_n \gamma_\nu(e) + N_A q\mu_p \ . \tag{D.6}$$

The conductivity is then expected to change with strain in extrinsic material when $n_{io}^2 \gamma_\nu(e)$ approaches the same order of magnitude as N_A.

Large changes in the conductivity of near intrinsic germanium have been observed for large strain levels by Graham, Jones and Holland [48]. In their experiments very large strains were set up in the sample by shock waves.

Appendix E

SPACE CHARGE GENERATION-RECOMBINATION CURRENT IN P-N JUNCTIONS

Space charge generation-recombination current can be important in p-n junctions (particularly in silicon) [33]. This current adds to the "ideal" or diffusion current which is predicted by the Shockley theory. In a p-n junction in which there is a single trap level located in the forbidden band, the steady state recombination rate U for holes or electrons is [33].

$$U = \frac{pn - n_i^2}{\tau_{no}(p + p_1) + \tau_{po}(n + n_1)} \quad , \tag{E.1}$$

where p_1 is the density of holes in the valence band when the Fermi level falls at the trap level, n_1 is the density of electrons in the conduction band when the Fermi level falls at the trap level, τ_{no} is the lifetime for electrons injected into highly p-type material, and τ_{po} is the lifetime for holes injected into highly n-type material. Hauser [34,49] has treated this problem and has obtained an approximate solution for the generation-recombination current. The discussion to follow is a review of his work.

The hole and electron currents are given by

$$J_p = q\mu_p pE - qD_p dp/dx \tag{E.2}$$

and

$$J_n = q\mu_n nE + qD_n dn/dx \ , \tag{E.3}$$

where E is the electric field at x. The continuity equations for steady state are

$$0 = -U - \frac{1}{q}\frac{dJ_p}{dx} \tag{E.4}$$

and

$$0 = -U + \frac{1}{q}\frac{dJ_n}{dx} \tag{E.5}$$

Figure 34 is a sketch of the junction which shows the two regions (n and p) and the space charge region where the width of the space charge region is W. Integrating Eqs. (E.4) and (E.5) over the space charge region gives

$$J_p(W) = J_p(0) - q\int_o^W U\,dx \tag{E.6}$$

and

$$J_n(0) = J_n(W) + q\int_o^W U\,dx \tag{E.7}$$

The total current density is obtained by adding the hole current density and the electron current density at any point x, for example x = 0. This gives

$$J = J_n(0) + J_p(0) = J_n(0) + J_p(W) + q\int_o^W U\,dx \tag{E.8}$$

or

$$J = J_I + J_U \ , \tag{E.9}$$

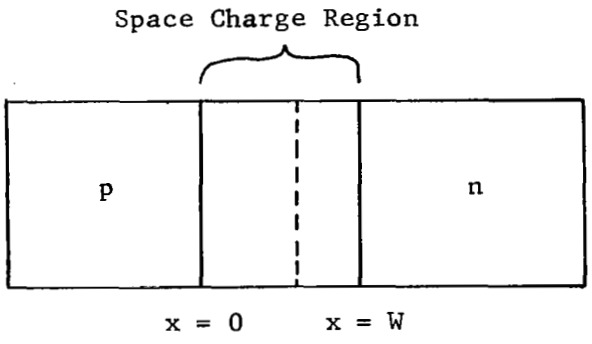

Fig. 34. Generation-Recombination Junction Model.

where J_I is the "ideal" or diffusion current density and J_U is the generation-recombination current density given by

$$J_U = q \int_o^W U \, dx \qquad (E.10)$$

In the space charge region J_p and J_n are small compared to the drift and diffusion terms which reduces Eqs. (E.2) and (E.3) to:

$$\mu_p pE \simeq D_p dp/dx \qquad (E.11)$$

and

$$-\mu_n nE \simeq D_n dn/dx \ . \tag{E.12}$$

Using Einstein's relation ($D = \mu kT/q$) and solving Eqs. (E.11) and (E.12) for the hole and electron densities gives

$$p \approx C_1 \exp[-qV/kT] \tag{E.13}$$

and

$$n \approx C_2 \exp[qV/kt] \ . \tag{E.14}$$

It can be shown that [49]

$$pn \approx n_i^2 \exp[qV_a/kT] \ , \tag{E.15}$$

where V_a is the applied junction voltage.

Substituting Eqs. (E.1) and (E.15) into Eq. (E.10) gives

$$J_U = q\, n_i^2[\exp\{qV_a/kT\} - 1] \int_o^W \frac{dx}{\tau_{no}(p + p_1) + \tau_{po}(n + n_1)} \cdot \tag{E.16}$$

An explicit evaluation of the integral is not possible because the hole and electron densities are a function of the applied voltage. Several important cases can be analyzed however. First, consider the case for large reverse bias such that $qV_a/kT \ll 1$. In this case $p \ll p_1$ and $n \ll n_1$. Integrating Eq. (E.16) gives

$$J_U = \frac{-q\, n_i^2\, W}{\tau_{no}\, p_1 + \tau_{po}\, n_1} \cdot \tag{E.17}$$

The width of the space charge region W in Eq. (E.17) is a function of the applied voltage V_a.

For the case of a step junction

$$W = W_o(1 - V_a/V_o)^{1/2} , \tag{E.18}$$

where W_o is the width of the space charge region with zero applied voltage and V_o is the built-in junction potential.

A second case of interest is for large forward bias such that $qV_a/kT \gg 1$, for which

$$p \approx n = n_i \exp\{qV_a/2kT\} , \tag{E.19}$$

where $p \gg p_1$ and $n \gg n_1$. Under these conditions the generation-recombination current density becomes

$$J_U = \frac{q\, n_i}{\tau_{no} + \tau_{po}} W \exp\{qV_a/2kT\} . \tag{E.20}$$

Again W is a function of the applied voltage.

The third case which can be solved is the small forward bias case such that $p \ll p_1$ and $n \ll n_1$ for which

$$J_U = \frac{q\, n_i^2\, W}{\tau_{no}\, p_1 + \tau_{po}\, n_1} [\exp\{qV_a/kT\} - 1] . \tag{E.21}$$

The above three special cases are of particular interest; however, it would be desirable to obtain a solution which is valid for all values of applied voltage. Although Eq. (E.16) cannot be solved in general, limits can be established on the current density. Consider the denominator of the integral term of Eq. (E.16)

$$f(V) = \tau_{no}(p + p_1) + \tau_{po}(n + n_1) , \tag{E.22}$$

where

$$p = p_n \exp\{qV/kT\} \tag{E.23}$$

and

$$n = n_n \exp\{-qV/kT\} \tag{E.24}$$

where p and n are the hole and electron densities in the junction at the point where the voltage is V and p_n and n_n are the densities on the n-side of the junction. The function f(V) has a minimum value for some value of voltage V. The minimum can be found in the usual manner, i.e.

$$\frac{\partial f(V)}{\partial V} = 0 = \tau_{no}\, p_n \frac{q}{kT} \exp\{qV/kT\} - \tau_{po}\, n_n \frac{q}{kT} \exp\{-qV/kT\} \tag{E.25}$$

or

$$\exp\{qV/kT\} = \left(\frac{\tau_{po}}{\tau_{no}} \cdot \frac{n_n}{p_n}\right)^{1/2} . \tag{E.26}$$

Therefore

$$f(V) \geq \tau_{no}\{\sqrt{n_n p_n}\sqrt{\tau_{po}/\tau_{no}} + p_1\} + \tau_{po}\{\sqrt{n_n p_n}\sqrt{\tau_{no}/\tau_{po}} + n_1\} \tag{E.27}$$

or

$$f(V) \geq (\tau_{no}p_1 + \tau_{po}n_1) + \sqrt{\tau_{po}\tau_{no}}\, n_i \exp\{qV_a/2kT\} \tag{E.28}$$

Substituting Eq. (E.27) into (E.16) and integrating gives

$$J_U \leq \frac{q\, n_i^2\, W}{(\tau_{no}p_1 + \tau_{po}n_1)} \frac{[\exp\{qV_a/kT\} - 1]}{1 + \dfrac{\sqrt{\tau_{po}\tau_{no}}\, n_i \exp\{qV_a/2kT\}}{(\tau_{no}p_1 + \tau_{po}n_1)}} \tag{E.29}$$

An inspection of Eq. (E.29) shows that for large reverse bias the limit is, in fact, equal to the exact value found earlier, Eq. (E.17). For large forward bias Eq. (E.29) becomes

$$J_U \leq \frac{q\, n_i W \exp\{qV_a/2kT\}}{\sqrt{\tau_{po}\tau_{no}}} \quad . \tag{E.30}$$

By comparing Eq. (E.29) with the exact value given in Eq. (E.20), it is found that if $\sqrt{\tau_{po}\tau_{no}}$ is replaced by $(\tau_{po} + \tau_{no})$ then the two equations give the same value. As an approximation the recombination-generation current density is equal to the limiting value given in Eq. (E.29) with $\sqrt{\tau_{no}\tau_{po}}$ replaced by $(\tau_{po} + \tau_{no})$,

$$J_U \simeq \frac{q\, n_i^2 W[\exp\{qV_a/kT\} - 1]}{(\tau_{no}p_1 + \tau_{po}n_1)\left(1 + \dfrac{(\tau_{no} + \tau_{po})\, n_i \exp\{qV_a/2kT\}}{[\tau_{no}p_1 + \tau_{po}n_1]}\right)} \quad . \tag{E.31}$$

Comparing the ratio $(\tau_{po} + \tau_{no})/(\tau_{po}\tau_{no})^{1/2}$ we see that if $\tau_{po} = \tau_{no}$ then the ratio is equal to 2. If however $\tau_{no} = 10\tau_{po}$ the ratio is equal to $11/\sqrt{10} \approx 3$. The error introduced by making the substitution in Eq. (E.30) is then expected to be less than a factor of 2 for $\tau_{po} = \tau_{no}$ and less than 3 for $\tau_{no} = 10\tau_{po}$.

LIST OF REFERENCES

[1] H. Hall, J. Bardeen and G. Pearson, "The Effects of Pressure and Temperature on the Resistance of p-n Junctions in Germanium", Phys. Rev. 84, October 1951, pp. 129-132.

[2] W. Rindner, "Anisotropic Strain Effects in p-n Junctions", Bull. Am. Phys. Soc. 7, January 1962, pp. 65-66.

[3] W. Rindner and I. Braun, "Effects of Elastic and Plastic Deformations in p-n Junctions", Bull. Am. Phys. Soc. 7, April 1962, p. 331.

[4] W. Rindner and I. Braun, "On the Effects of Elastic and Plastic Deformation on p-n Junctions in Semiconductors", Report of the International Conference on the Physics of Semiconductors-Exeter, England, July 1962, The Institute of Physics and the Physical Society, London, 1962, p. 167.

[5] W. Rindner, "Resistance of Elastically Deformed Shallow p-n Junctions", J. Appl. Phys. 33, August 1962, pp. 2479-2480.

[6] W. Rindner and I. Braun, "Resistance of Elastically Deformed Shallow p-n Junctions. II.", J. Appl. Phys. 34, July 1963, pp. 1958-1970.

[7] Y. Matukura, "Some Factors Influencing on the Anisotropic Stress Effect of pn Junctions", Japanese J. Appl. Phys. 3, September 1964, pp. 516-520.

[8] R. Edwards, "Some Effects of Localized Stress on Silicon Planar Transistors", IEEE Transactions on Electron Devices ED-11, June 1964, pp. 286-294.

[9] W. G. Pfann, "Improvements of Semiconductor Devices by Elastic Strain", Solid-State Electronics 3, November-December 1961, pp. 261-267.

[10] M. E. Sikorski, et al., "Transistor Microphone", Rev. Sci. Instr. 33, October 1962, pp. 1130-1131.

[11] F. Herman, "The Electronic Energy Band Structure of Silicon and Germanium", Proc. IRE 43, December 1955, pp. 1703-1732.

[12] See reference 1.

[13] See, for example, L. Mariot, Group Theory and Solid State Physics, Prentice-Hall, Inc., Englewood Cliffs, New Jersey, 1962.

[14] W. P. Mason and T. B. Bateman, "Ultrasonic Wave Propagation in Doped n-Germanium and p-Silicon", Phys. Rev. 134, June 1964, pp. A1387-A1396.

[15] J. Bardeen and W. Shockley, "Deformation Potentials and Mobilities in Non-Polar Crystals", Phys. Rev. 80, October 1950, pp. 72-80.

[16] C. Herring and E. Vogt, "Transport and Deformation-Potential Theory for Many-Valley Semiconductors with Anisotropic Scattering", Phys. Rev. 101, February 1956, pp. 944-961.

[17] W. H. Kleiner and L. M. Roth, "Deformation Potential in Germanium from Optical Absorption Lines for Exciton Formation", Phys. Rev. Letters 2, April 1959, pp. 334-336.

[18] L. I. Schiff, Quantum Mechanics, McGraw-Hill Book Company, Inc., New York, New York, 1949, p. 144.

[19] J. C. Hensel and H. Hasegawa, "Cyclotron Resonance of Electrons in Uniaxially Stressed Silicon: Energy Bands Near X in the Diamond Structure", (paper presented at the International Conference on the Physics of Semiconductors, Paris, July 1964).

[20] J. C. Hensel, H. Hasegawa and M. Nakayama, "Cyclotron Resonance in Uniaxially Stressed Silicon II: Nature of the Covalent Bond", (to be published).

[21] L. Kleinman, "Deformation Potentials in Silicon. I. Uniaxial Strain", Phys. Rev. 128, December 1962, pp. 2614-2621.

[22] L. Kleinman, "Deformation Potentials in Silicon. II. Hydrostatic Strain and the Electron-Phonon Interaction", Phys. Rev. 130, June 1963, pp. 2283-2289.

[23] I. Goroff and L. Kleinman, "Deformation Potentials in Silicon. III. Effects of a General Strain on Conduction and Valence Levels", Phys. Rev. 132, November 1963, pp. 1080-1084.

[24] W. P. Mason and T. B. Bateman, "Ultrasonic Attenuation and Velocity Changes in Doped n-type Germanium and p-type Silicon and their use in Determining an Intrinsic Electron and Hole Scattering Time", Phys. Rev. Letters 10, March 1963, pp. 151-154.

[25] See reference 14.

[26] P. Csavinsky and N. G. Einspruch, "Effect of Doping on the Elastic Constants of Silicon", Phys. Rev. 132, December 1963, pp. 2434-2440.

[27] J. S. Blakemore, Semiconductor Statistics, Pergamon Press, Inc., New York, New York, 1962, Chaps. 1 and 2.

[28] W. Paul and D. M. Warschauer, Solids Under Pressure, McGraw-Hill Book Company, Inc., New York, New York, 1963, Chap. 8, p. 188.

[29] J. J. Hall, "Long-Strain Dependence of the Acceptor Binding Energy in Germanium", Phys. Rev. 128, October 1962, pp. 68-75.

[30] W. Kohn, Solid State Physics, Volume 5, F. Seitz and D. Turnbull, eds., Academic Press Inc., New York, New York, 1957.

[31] See reference 1.

[32] See, for example, A. Phillips, Transistor Engineering, McGraw-Hill Book Company, Inc., New York, New York, 1962, Chap. 3, p. 51.

[33] C. Sah, R. Noyce and W. Shockley, "Carrier Generation and Recombination in P-N Junctions and P-N Junction Characteristics", Proc. IRE 45, September 1957, pp. 1228-1243.

[34] W. Rindner and R. F. Tramposch, "Plastic Deformation of Germanium at and Below Room Temperature", J. Appl. Phys. 34, April 1963, pp. 758-759.

[35] J. V. Craig and E. N. Pugh, "Indentation of Germanium at Room Temperature", J. Appl. Phys. 35, November 1964, pp. 3417-3418.

[36] J. R. Hauser (private communications).

[37] J. C. Hensel and G. Feher, "Cyclotron Resonance Experiments in Uniaxially Stressed Silicon: Valence Band Inverse Mass Parameters and Deformation Potentials", Phys. Rev. 129, February 1963, pp. 1041-1062.

[38] H. Hasegawa, "Theory of Cyclotron Resonance in Strained Silicon Crystals", Phys. Rev. 129, February 1963, pp. 1029-1040.

[39] Alvin B. Phillips, Transistor Engineering, McGraw-Hill Book Company, Inc., New York, New York, 1962, Chap. 4, p. 83.

[40] Y. Matukura, "Anisotropic Stress Effect of Silicon pn Junctions", Japanese J. Appl. Phys. 3, May 1964, pp. 256-261.

[41] R. W. Keyes, "The Effects of Elastic Deformation on the Electrical Conductivity of Semiconductors", Solid State Physics, Academic Press Inc., New York, New York, 1962, pp. 149-221.

[42] C. Herring and E. Vogt, "Transport and Deformation-Potential Theory for Many-Valley Semiconductors with Anisotropic Scattering", Phys. Rev. 101, February 1956, pp. 944-961.

[43] C. S. Smith, "Piezoresistance in Silicon and Germanium", Phys. Rev. 94, April 1954, pp. 42-49.

[44] D N. Tufte and E. L. Stelzer, "Piezoresistance Properties of Heavily Doped n-Type Silicon", Phys. Rev. 133, March 1964, pp. A1705-A1716.

[45] W. P. Mason and R. N. Thurston, "Use of Piezoresistive Materials in the Measurement of Displacement, Force and Torque", J. Acoust. Soc. An. 29, October 1957, pp. 1096-1101.

[46] M. Pollack, "Piezoresistance in Heavily Doped n-Type Germanium", Phys. Rev. 111, August 1958, pp. 798-802.

[47] H. Kroemer, "Quasi-Electric and Quasi-Magnetic Fields in Nonuniform Semiconductors", RCA Rev. 18, September 1957, pp. 332-342.

[48] R. A. Graham, O. E. Jones and J. R. Holland, "Electrical Resistivity and Stress-Volume Measurements on Shock-Loaded Germanium", (to be published).

[49] J. R. Hauser, "A Study of Interactions in Silicon Multi-Junction Devices", Ph.D. Dissertation, Duke University, 1964.